

Master Thesis
IB-FT-BS-2021-92

**Development and Optimization of
Motion Cueing for Flight Simulation
of Maritime Helicopter Operations**

Daniel Greiwe

DLR German Aerospace Center
Institute of Flight Systems
Rotorcraft
Braunschweig



DLR

**Deutsches Zentrum
für Luft- und Raumfahrt**
German Aerospace Center

Institutsbericht
DLR-IB-FT-BS-2021-92

Development and Optimization of Motion Cueing for Flight Simulation of Maritime Helicopter Operations

Daniel Greiwe

139 Seiten
71 Abbildungen
20 Tabellen
47 Referenzen

Deutsches Zentrum für Luft- und Raumfahrt e.V.
Institut für Flugsystemtechnik
Abteilung Hubschrauber

Zugänglichkeitsstufe I: öffentlich zugänglich

Braunschweig, 10. Mai 2021

Institutsdirektor: Prof. Dr.-Ing. S. Levedag
Abteilungsleiter: Dipl.-Ing. M. Höfinger
Betreuer: M. Maibach
Verfasser: D. Greiwe

Unterschriften:

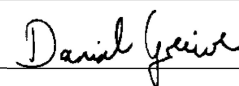


Marc Hoefinger

Digital Signiert von Marc Hoefinger
DN: C=DE, O=Deutsches Zentrum fuer Luft- und Raumfahrt e.V., OU=DLR, CN=Marc Hoefinger
Grund: Ich genehmige dieses Dokument
Cm: Signierungsort hier eingeben
Datum: 2021.07.26 14:41:10+0200
Fax# PDF: Erste Version: 11.0.0



Digital Signiert von Malte-Jörn Maibach
DN: C=DE, OU=FT-HUB, O=Deutsches Zentrum für Luft- und Raumfahrt e.V., CN=Malte-Jörn Maibach, E=malte.joern.maibach@dlr.de
Grund: Ich bin der Verfasser dieses Dokuments
Ort: Braunschweig
Datum: 2021.07.26 08:27:22+0200
Fax# PDF: Reader Version: 11.0.0



DLR German Aerospace Center

Institute of Flight Systems

Rotorcraft

Dr.-Ing. Klausdieter Pahlke and Dipl.-Ing. Marc Höfing

Lilienthalplatz 7

38108 Braunschweig

Germany

Tel: +49 531 295-2691

Fax: +49 531 295-2641

Web: <http://www.dlr.de/ft/en/hub>

Daniel Greiwe

Tel: +49 531 295-3372

Fax: +49 531 295-2641

Mail: daniel.greiwe@dlr.de

Document Identification:

Report number	IB-FT-BS-2021-92
Title	Development and Optimization of Motion Cueing for Flight Simulation of Maritime Helicopter Operations
Subject	Master Thesis
Author(s)	Daniel Greiwe
Filename	Masterthesis_DG.tex
Last saved on	10th May 2021



DLR e. V. Institut für Flugsystemtechnik
Lilienthalplatz 7, 38108 Braunschweig

An die
Fakultät Maschinenbau
der Technischen Universität Braunschweig

Name Prof. Dr.-Ing. Stefan Levedag

Telefon +49 (0)531 295 2600

Telefax +49 (0)531 295 2864

E-Mail Stefan.Levedag@dlr.de

07.05.2021

Master thesis task description for Mr. Daniel Greiwe

Student number.: 4275097 Degree: Luft- und Raumfahrttechnik

Mail: d.greiwe@tu-braunschweig.de

Language: English

Title:

- o Development and Optimization of Motion Cueing for Flight Simulation of Maritime Helicopter Operations

Introduction:

Specific challenges are encountered during helicopter offshore operational scenarios. Helicopter ship deck landings for example usually require lengthy and expensive flight test campaigns to determine operative limits. Using an optimized and realistic simulation environment for ship deck landing can save time and cost and minimize risks. The German Aerospace Center (DLR) is continuously developing such a simulation environment in their Air Vehicle Simulator (AVES). Therefore, the ship dynamics, the airwake, the graphics and motion model and the flight model have to be developed and modified. At the current state, only preliminary steps have been undertaken to modify the motion model parameters for use in the maritime environment. Due to the influence of wind, waves and the resulting ship movements and its airwake for this scenario a highly dynamic motion model is necessary. For a realistic simulation environment, adjustment is required to motion parameters.

Within the scope of this Master thesis, a tuning setting for the highly dynamic ship environment simulation shall be developed. To achieve this, a motion filter algorithm will be developed. After extensive testing and offline tuning on a desktop computer a simulation campaign will be planned and executed for acquiring a tuning setting either for the own developed filter algorithm or the MOOG Motion Cueing model. Finally, the identified tuning setting shall be compared with results published as scientific papers or literature.

Scope and tasks of the thesis:

- Literature research concerning motion cueing algorithms, motion platform tuning and methods for assessment
- Comparison of mission task elements (MTE) with special regard to the suitability for motion tuning and similarity with maritime mission elements
- Modification of the available MTE scenarios in the AVES simulation for usage in simulation campaigns with pilots
- Development of a Classical Washout Filter (CWA) algorithm in MATLAB/Simulink
- Offline tuning of the developed filter algorithm to archive results comparable with published results in literature
- *Optional: Development of a toolchain for implementing the developed filter algorithm on the MOOG motion platform at the AVES simulator*
- Planning of a simulation campaign for the tuning of the filter algorithm in the AVES simulator
- *Optional: Executing of the planned simulation campaign with internal or external helicopter pilots*
- Execution of Objective Motion Cueing Tests (OMCT) and comparison of the results with published results in literature
- Preparation of a documentation with an extensive description of the above-mentioned points
- Discussion of the results from the simulation campaign

Literature:

- [1] H. Duda, T. Gerlach, S. Advani, and M. Potter, "Design of the DLR AVES Research Flight Simulator," in Proceedings of the AIAA Modeling and Simulation Technologies (MST) Conference, Boston, MA, USA, 2013.
- [2] Jones, M. (2018): Enhancing motion cueing using an optimisation technique. In: Aeronaut. j. 122 (1249), S. 487–518. DOI: 10.1017/aer.2017.141.
- [3] Jones, Michael (2019): The Suitability of Objective Motion Criteria for Rotorcraft Manoeuvres. In: AIAA Scitech 2019 Forum. AIAA Scitech 2019 Forum. San Diego, California, 07.01.2019. Reston, Virginia: American Institute of Aeronautics and Astronautics.
- [4] Jones, Michael; White, Mark; Fell, Thomas; Barnett, Miles (2017): Analysis of Motion Parameter Variations for Rotorcraft Flight Simulators. In: American Helicopter Society 73rd Annual Forum & Technology Display. Fort Worth, Texas, US, 09.-11.05.2017.
- [5] S. J.R.P. Carignan, A. W. Gubbels, and K. Ellis, "Assessment of Handling Qualities for the Shipborne Recovery Task - ADS-33 (Maritime)," in American Helicopter Society 56th Annual Forum.
- [6] P. R. Grant and L. D. Reid, "Motion Washout Filter Tuning: Rules and Requirements," Journal of Aircraft, vol. 34, no. 2, pp. 145–151, 1997, doi: 10.2514/2.2158.
- [7] S. J. Hodge, P. Perfect, G. D. Padfield, and M. D. White, "Optimising the vestibular cues available from a short stroke hexapod motion platform," Aeronaut. j., vol. 119, no. 1211, pp. 1–21, 2015, doi: 10.1017/S0001924000010228.
- [8] Moog Inc., "Motion Cueing Model Description," 2010.
- [9] L. D. Reid and M. A. Nahon, "Flight Simulation Motion-Base Drive Algorithms: Part 1. Developing and Testing Equations," UTIAS Report, No. 296, Dec. 1985.



General Regulations:

Start: 15.10.2020
End: 15.04.2021

The work on the master thesis will be done at the German Aerospace Center / Deutsches Zentrum für Luft- und Raumfahrt e.V. (DLR). All information accessible during the thesis must be handled confidential.

Working time: 3 Months (Bachelor) 6 Months (Master)
 Projektarbeit (Bachelor) (2 Months) Studienarbeit (Master) (3-4 Months)

Tutors:


Malte-Jörn Maibach, Michael Jones
Institut für Flugsystemtechnik / Abteilung Hubschrauber
Deutsches Zentrum für Luft- und Raumfahrt e.V.
Lilienthalplatz 7
38108 Braunschweig

First Examiner:

Professor Dr.-Ing. Levedag
Deutsches Zentrum für Luft- und Raumfahrt e.V.
Institut für Flugsystemtechnik
Lilienthalplatz 7
38108 Braunschweig

Second Examiner:

Professor Dr.-Ing. P. Hecker
Technische Universität Braunschweig
Institut für Flugführung
Hermann-Blenk-Straße 27
38108 Braunschweig



Prof. Dr.-Ing. Levedag

Declaration of Authorship

I hereby declare that this master thesis "Development and Optimization of Motion Cueing for Flight Simulation of Maritime Helicopter Operations" is my own work and that I have not used any sources other than those listed in the bibliography. Content from published or unpublished works that has been quoted directly or indirectly or paraphrased is indicated as such. The thesis has not been submitted in the same or similar form for any other academic award.

Braunschweig, 10th May 2021



Daniel Greive

Kurzfassung

Der Einsatz von Helikoptern in maritimen Szenarien wie zum Beispiel einer Helikopterschiffsdecklandung sind sowohl für den Piloten als auch für den Helikopter sehr anspruchsvoll. Da in einem Simulator viele mögliche Sicherheitsrisiken einer Offshoremission entfallen, ist die Entwicklung einer maritimen Simulationsumgebung sinnvoll. Diese könnte für das Training von Piloten oder zur Entwicklung neuer Systeme oder Verfahren verwendet werden. Für eine maritime Simulationsumgebung ist allerdings auch ein speziell optimiertes Bewegungssystem notwendig. In den letzten Jahren wurden neue Verfahren entwickelt, um Bewegungssysteme einfacher, schneller und objektiv zu optimieren. Diese Methoden sind allerdings noch nicht ausreichend validiert, da es auch an geeigneten Standards zur Validierung fehlt.

In dieser Arbeit wird eine Methodik zur Implementierung eines Classical Washout Algorithmus (CWA) in den Simulator vorgestellt. Zur Entwicklung geeigneter Parameter für eine Helikopterschiffsdecklandung wird die Fitness Function als neues Optimierungsverfahren angewendet. Zur Validierung des gesamten Systems werden pilotierte Versuche im Simulator geplant und durchgeführt. Im Vergleich dazu wird eine unpilotierte Validierung mittels des Objective Motion Cueing Test (OMCT) durchgeführt.

Abstract

Maritime helicopter operations such as helicopter ship deck landings are highly demanding for both the pilot and the helicopter. In the absence of potential safety risks during an offshore mission a maritime simulation environment offers a benefit for pilot training and development of new systems and procedures. Such a maritime simulation environment requires a specific optimized motion system. In the recent past years new methods have been developed to tune the motion system in an easier, faster and objective way. Unfortunately, these methods are not sufficiently validated because however suitable validation methods are still missing.

This master thesis presents a methodology to implement a Classical Washout Algorithm (CWA) in the simulator. To develop suitable motion parameter sets for a helicopter ship deck landing procedure the fitness function is used as a novel optimization method. The validation is conducted with piloted simulator flight test trials that are newly developed. Additionally, an unpiloted validation is carried out with the Objective Motion Cueing Test (OMCT). The results of both validation methods are compared to each other.

Contents

Declaration of Authorship	V
Kurzfassung	VII
Abstract	IX
Nomenclature	XIX
Abbreviations	XXIII
1. Introduction	1
1.1. Motivation	1
1.1.1. Helicopter Ship Deck Landing	1
1.1.2. Motion Simulator Platforms	2
1.2. Literature Review	2
1.2.1. Procedures of a Helicopter Ship Deck Landing	3
1.2.2. Mission Task Elements	4
1.3. Thesis Objective and Structure	5
2. Theory of Motion Simulators	7
2.1. Human Motion Perception	7
2.2. Motion Drive Algorithm MDA	9
2.3. Tuning Methods	14
2.3.1. Piloted Tuning Procedure	14
2.3.2. Fitness Function	15
2.3.3. Vestibular Motion Perception Error VMPE	18
2.4. Evaluation Methods	21
2.4.1. Objective Methods	21
2.4.2. Subjective Methods	24
2.5. AVES Research Facility	27
2.5.1. Motion Platform	28
2.5.2. Helicopter Flight Model	29
2.5.3. Ship Dynamic Model	30

3. Development of a Simulator Campaign for a Helicopter Ship Deck Landing	33
3.1. Definition of the Flight Task	34
3.2. Set up of the Test Environment	35
3.3. Design of the Test Matrix	40
4. Methodology of an MDA Implementation and Optimization	45
4.1. Construction and Pre-Validation of an MDA	46
4.2. Adaptation and Installation into the Simulator Environment	51
4.3. Offline Tuning with a Genetic Algorithm	53
4.3.1. Construction of the Genetic Algorithm	54
4.3.2. Execution of the GA	57
4.3.3. Processing and Evaluation of the Results	59
4.4. Validation of the Optimized Motion Settings	69
4.4.1. Objective Motion Cueing Test	70
4.4.2. Piloted Simulator Campaign	70
5. Analysis and Discussion of the Results	73
5.1. Objective Motion Cueing Test	73
5.2. Piloted Simulator Campaign	78
5.3. Comparison of the Results	88
6. Conclusions and Future Work	89
A. Test Cards of the Simulator Flight Test Trials	A
B. Outputs of easy Test Signals of the Pre-Validation	E
C. Comparison of the Prediction and the Results of the OMCT	M

List of Figures

2.1. Frequency Response of the Vestibular System	8
2.2. Reference Frames according to [1]	10
2.3. Classical Washout Algorithm according to [1]	12
2.4. Typical 3rd-order Motion Filter Response according to [2]	17
2.5. VMPE Technique Architecture according to [3]	19
2.6. Schroeder Boundaries at 1 rad/s	22
2.7. OMCT Boundaries for Roll Output to Roll Input	23
2.8. Motion Rating Scale by Jones [2]	25
2.9. Motion Rating Scale by Hodge [4]	26
2.10. DLR's ACT/FHS	27
2.11. AVES Motion Platform	28
2.12. ACP in HeliWorX [5]	30
2.13. Maritime Simulation Environment [5]	31
2.14. Example of the Ship Dynamics	32
3.1. Superslide Task - Side View	36
3.2. Desired/Adequate Target Boundaries	36
3.3. Superslide Task - geometric Correlations	37
3.4. Superslide Task - Top View	38
3.5. Unsteady Airwake of a F124 "Sachsen class" Frigate	39
3.6. Bedford Workload Rating according to [6]	42
4.1. Developed Methodology of an MDA Implementation and Optimization	45
4.2. Phase I - Development & Pre-Validation	46
4.3. Pulse Input of a longitudinal Acceleration	47
4.4. CWA Output according to a Pulse Input of a longitudinal Acceleration	48
4.5. Ramp Input of a longitudinal Acceleration	49
4.6. CWA Output according to a Ramp Input of a longitudinal Acceleration	50
4.7. Phase II - Adaptation & Installation	51
4.8. Example: Flight Test Trial - Roll Axis	53
4.9. Phase III - Offline Tuning	54
4.10. Structure and Information within a Chromosome	55

4.11. Evolution Process of a Genetic Algorithm	55
4.12. Crossover	56
4.13. Mutation	56
4.14. Characterization of used Flight Test Data	58
4.15. PSD of an unsteady airwake at a WT	59
4.16. Characterization of used Database of Flight Test Data	60
4.17. Frequency Response of the Motion Sets	62
4.18. Final Motion Settings against Schroeder Boundaries at 1 rad/s	63
4.19. Final Motion Settings - Break Frequencies	63
4.20. Predicted Motion Envelope of each Motion Set	65
4.21. Comparison of VMPE against Fitness Function - ST	67
4.22. Comparison of VMPE against Fitness Function - TRA	68
4.23. Comparison of VMPE against Fitness Function - ROT	68
4.24. Comparison of VMPE against Fitness Function - OP	69
4.25. Phase IV - Validation	70
5.1. OMCT Results of the Motion Sets: On-Axis	74
5.2. OMCT Results of the Motion Sets: Off-Axis	75
5.3. Prediction and Results of the OMCT for motion set OP	77
5.4. Bedford Workload Rating given by the Pilots	78
5.5. Motion Rating given by the Pilots	79
5.6. Flightpath - Pilot A, SS0	80
5.7. Flightpath - Pilot B, SS0	80
5.8. Control Input- SS0	81
5.9. Desired Performance for the Hover Task	81
5.10. Time Plot of the translational Accelerations	82
5.11. Time Plot of the rotational Accelerations	83
5.12. Input/Output of the FCS	84
5.13. Comparison of used Flight Test Data and recorded Flight Data	86
5.14. Comparison of the different Airwakes used during the offline Tuning and recorded during the Simulator Flight Test Trials	87
A.1. Test Card Page 1: Preparation	B
A.2. Test Card Page 2: Documentation of the Runs carried out for one Test Point	C
A.3. Test Card Page 3: Pilot Questionnaire	D
B.1. Output according to Pulse Input at sway axis	F
B.2. Output according to Pulse Input at heave axis	G
B.3. Output according to Pulse Input at roll axis	H
B.4. Output according to Pulse Input at pitch axis	I
B.5. Output according to Pulse Input at yaw axis	J

B.6. Output according to Ramp Input at sway axis	K
C.1. Prediction and Results of the OMCT for motion set ST	N
C.2. Prediction and Results of the OMCT for motion set TRA	O
C.3. Prediction and Results of the OMCT for motion set ROT	P

List of Tables

2.1. Motion Perception Thresholds [7]	9
2.2. Coefficient Adjustments according to [8]	16
2.3. OMCT Test Matrix according to [9]	23
2.4. Frequencies and Amplitudes for each Test Point according to [9]	24
2.5. AVES motion platform limits [10]	28
3.1. Desired/Adequate Boundaries of the Superslide Task	34
3.2. Desired/Adequate Boundaries of the adapted Superslide Task	35
3.3. Distances of the adapted Superslide Task	37
3.4. Sea State Code from the World Meteorological Organization (WMO) [11]	39
3.5. Test Matrix including Number of the Test Points	41
3.6. Turbulent Air Scale	41
4.1. Motion Set A according to [1]	47
4.2. Interface of the MOOG Motion System	52
4.3. Motion Set B	52
4.4. Variance Factors	57
4.5. Evolution Parameter	57
4.6. Fixed Motion Parameter	59
4.7. Final Motion Sets	61
4.8. Fitness and mean VMPE of the Motion Sets	67
4.9. Overview of Pilot Experience	71

Nomenclature

Roman Symbols

A	aircraft-fixed reference frame at a reference point
\vec{a}_b	linear body accelerations at CG, m/s^2
a_x, a_y, a_z	linear body accelerations in x, y, z direction at CG, m/s^2
B	aircraft-fixed reference frame at CG
C	fictitious forces, N
D	damping forces, N
d	characteristic body dimension, m
dx, dy	longitudinal and lateral separation distance of the pylons, m
F	fitness of the motion response, -
F_i	fitness of the motion response of the i-th axes, -
$F_{weighted}$	weighted fitness of the motion response, -
\vec{f}	specific force, m/s^2
\vec{f}_{AA}	specific force of the aircraft in the aircraft-fixed reference frame, m/s^2
f_w	wake shedding frequency, Hz
f_x, f_y, f_z	specific forces in x, y, z directions at CG, m/s^2
G_i	gain of the motion filter of the i-th axis, -
\vec{g}	gravitation vector, m/s^2
g	gravitational constant, $9.81 m/s^2$
g_x, g_y, g_z	acceleration due to gravity, body reference frame, m/s^2
H_i	frequency-dependent amplitude response in the i-th axis, -
$\angle H_i$	frequency-dependent phase response in the i-th axis, $^\circ$
h_1, h_2, h_{31}, h_{32}	vertical distances, m
I	inertial reference frame
i	response in the i-th axis
K_{LP}, K_{HP}	motion drive algorithm filter gain of the low-pass and high-pass filter
K_1, K_2, K_3	constant weighting factors, -
L_{IS}	transformation matrix from simulator to inertial coordinate system
M	mass matrix
m	total number of discrete data points

N	number of considered axes
\vec{P}_A	position vector from aircraft CG to aircraft reference point, m
PA	aircraft-fixed reference frame at pilot position
PS	simulator-fixed reference frame at pilot position
p, q, r	roll, pitch, yaw angular velocities, $^{\circ}/s$
$p_{dot}, q_{dot}, r_{dot}$	roll, pitch, yaw angular accelerations, $^{\circ}/s^2$
\vec{R}_A	position vector from aircraft reference point to pilot position, m
\vec{R}_S	position vector from simulator reference point to pilot position, m
$RMSE_{norm,fi}$	normalized root-mean-squared error of the perceived specific force
$RMSE_{norm,\omega}$	normalized root-mean-squared error of the perceived angular rate
$RMSE_{VMPE,fi}$	root-mean-squared error of the perceived specific force between aircraft and simulator, m/s^2
$RMSE_{VMPE,\omega}$	root-mean-squared error of the perceived angular rate between aircraft and simulator, $^{\circ}/s$
S	simulator-fixed reference frame at a reference point
S_I	platform displacements, m
S_t	Strouhal number
T_S	transformation matrix to Euler angle accelerations
t	time, s
u, v, w	linear velocities in x, y, z direction, m/s
$V_{E,HUB}$	local wind speed in earth-fixed reference frame at rotor hub, m/s
$V_{W,G}$	global wind speed, m/s
$V_{W,L}$	local wind speed, m/s
$V_{W,T}$	total wind speed, m/s
VAR_F	variance of the fitness values of the considered axes, -
$VMPE_{NO}$	VMPE of simulation model's input
$VMPE_{norm}$	normalized VMPE, -
$VMPE_{norm,f}$	normalized VMPE of the specific forces, -
$VMPE_{norm,\omega}$	normalized VMPE of the angular velocity, -
$VMPE_{RMSE-MTS-f}$	mean specific forces perception root-mean-squared error between aircraft and simulator, m/s^2
$VMPE_{RMSE-MTS-\omega}$	mean angular velocity perception root-mean-squared error between aircraft and simulator, $^{\circ}/s$
x_1, x_2	longitudinal distances, m
x, y, z	linear displacements in x, y and z direction, m
x_N, x_E, x_D	linear displacements in north, east and down direction, m
y_a, y_b	lateral distances, m

Greek Symbols

β	side slip angle, °
$\vec{\beta}$	Euler angle, °
$\vec{\beta}_S$	simulator angle displacements, °
ζ	damping ratio of motion filter, -
θ_x, θ_y	longitudinal and lateral control input, %
τ_{ctrl}	control forces, N
τ_{env}	environmental forces, N
Φ_i	phase of the motion response of the i-th axis, °
ϕ, θ, ψ	roll, pitch and yaw angle, °
$\vec{\omega}$	angular accelerations, °/s ²
ω, ω_2	break frequency of motion filter, °/s
$\vec{\omega}_{AA}$	aircraft angular accelerations in the aircraft reference frame, °/s ²

Abbreviations

ACP	Airload Computation Point	LP	Low-Pass
ACT/FHS	Active Control Technology Demonstrator and Flying Helicopter Simulator	MDA	Motion Drive Algorithm
API	Application Programming Interface	MSS	Marine Systems Simulator
AVES	Air Vehicle Simulator	MTE	Mission Task Element
BWR	Bedford Workload Rating	NATO	North Atlantic Treaty Organization
CFD	Computational Fluid Dynamics	OMCT	Objective Motion Cueing Test
CG	Centre of Gravity	OTO	Otolith Organs
CLS	Control Loading System	PIO	Pilot-Induced-Oscillation
CWA	Classical Washout Algorithm	PSD	Power Spectral Density
DLR	German Aerospace Center	RMSE	Root-Mean-Squared Error
DoF	Degree of Freedom	RORO	Roll-On/Roll-Off
EFS	Emergency Floatation System	RTO	Research and Technology Organization
FCS	Flight Control System	RTOS	Real Time Operating System
FoV	Field of View	SAS	Stability Augmentation System
GA	Genetic Algorithm	SCC	Semicircular Canals
GVE	Good Visual Environment	SS	Sea State
HOSTAC	Helicopter Operations from Ships other than Aircraft Carrier	VMPE	Vestibular Motion Perception Error
HP	High-Pass	WMO	World Meteorological Organization
HQR	Handling Quality Rating	WT	Wind Turbine
IC	Interface Computer		

1. Introduction

1.1. Motivation

Helicopter operations in a maritime environment such as helicopter ship deck landings can be highly demanding for the pilot and the helicopter. As stated out in [5] weather conditions are often challenging in comparison to onshore operations. Sudden development of low visibility, precipitation and turbulence, to name a few, characterize the dynamic nature of the offshore environment. To successfully complete missions pilots are often required to fly within such dynamic environments. During onshore operations such conditions would normally be avoided. The development of a maritime environment in a simulator can offer a huge benefit. The associated safety risk of offshore missions are absent in the simulator. This allows for new operational techniques, adverse or emergency scenarios to be tested and trained in a maritime simulation environment. New systems can be developed in the simulator without lengthy certification and implementation efforts. The dynamic environment of the simulator is particularly suitable for the development process through the loop of pilot feedback and subsequent modification of the system. The cost of operating a simulation environment is also much lower than that of a real helicopter during an equivalent mission. The German Aerospace Center (DLR) is developing such a maritime environment at the Air Vehicle Simulator (AVES) in Braunschweig [5].

1.1.1. Helicopter Ship Deck Landing

There are defined procedures for helicopter ship deck landings and according limits. Each combination of ship and helicopter has to be certified separately, due to their unique characteristics [12]. Accordingly the certification process is quite expensive. A simulation environment would have many advantages if it is used during training, certification and development along real equivalent flight missions. But as of now are no standards that define criteria for such a simulator environment. In [13] Hodge et al. specify major requirements for such a simulator environment. Those are defined according to the challenges

the pilot faces during a helicopter ship deck landing. Sea fog or sea spray can generate a degraded visual environment, giving pilots only a few visual references. Ship superstructures in combination with wind can produce high-frequency turbulences on the ship deck. Waves can lead to ship movements, that prove to be difficult to predict. [14] Although no current standards for a maritime simulation environment exist yet [13], a simulation environment has to fulfil all the requirements derived from challenges a maritime environment has to offer to be as realistic as possible. Some of these aspects are subject research or already implemented [5] whereas other are not, for example the optimization of the motion system. The following thesis contributes in refining the motion system for simulating ship deck landings.

1.1.2. Motion Simulator Platforms

The vestibular feedback can be helpful to generate a more realistic environment in a simulator. Due to the physical and mechanical limitations of motion platforms it is however not possible to deliver the same accelerations as in a real helicopter. Motion Drive Algorithms (MDAs) are used to translate the accelerations of a real helicopter into motion platform demands. These consist of many parameters that have to be independently tuned for each flight regime of the helicopter [2]. Current research work on different offline tuning procedures (see [10],[14]). Current tuning procedures rely on inputs from a pilot and a motion expert [15]. This procedure is cost and time expensive. However, none of these novel tuning methods is established. One reason is the missing of a standard evaluation method. The measurement and quantification of motion fidelity is subject of current research as well. The only standard evaluation is the Objective Motion Cueing Test (OMCT) that was validated following standards of fixed wing simulators [9]. Recent evaluations with helicopter simulators have shown that the results are only transferable to a certain limit (see [16], [17]). More research has thus to be done for the offline tuning methods as well.

1.2. Literature Review

In this section standards of helicopter ship deck landing procedures and abstracted flight tasks are summarized based on a literature review.

1.2.1. Procedures of a Helicopter Ship Deck Landing

The MPP-02, Volume I [18] is a publication of the "Helicopter Operations from Ships other than Aircraft Carrier" (HOSTAC) program that provides standardized information for successful transnational ship-helicopter operations. It includes approach, landing and deck handling procedures. The given information are not ship or aircraft specific. Within this documentation five different landing procedures are described based on the according wind conditions, deck motion limits and the procedure itself. These are

- 1) Port lateral & 45 Degree
- 2) Starboard lateral & 45 Degree
- 3) Straight-In
- 4) Starboard to Port Oblique
- 5) Port to Starboard Oblique

The Research and Technology Organization (RTO) of the North Atlantic Treaty Organization (NATO) published a document for standardization of Helicopter/Ship Qualification Testing in [12]. Within part 1 of this document, which is about the dutch/british clearance process, six standardized take-off and landing procedures are described. These are

- 1) Fore/aft or forward facing procedure
- 2) Relative-wind or into wind procedure
- 3) Cross-deck procedure
- 4) Aft/Fore or facing astern procedure
- 5) Astern procedure
- 6) Oblique procedures

By comparing both standards some of the presented landing procedures are equivalent. As an example the "Port lateral & 45 Degree" procedure (see [18]) or the "Fore/aft or forward facing procedure" (see [12]) is described as follows. The helicopter has to be aligned with

the ship's centre-line at the port side of the ship landing deck. After this the helicopter is translated laterally to the hover position of the flight deck. During a quiescent period of the ship movement the pilot lands the helicopter. At day time with a skidded helicopter the limits for this procedure are as follows. The pitch and roll movement of the landing deck has to be within $\pm 1^\circ$ and $\pm 3^\circ$. The minimum relative wind conditions are 10 kts from ship's head to 30° to the port side of the ship. The maximum relative wind conditions are 35 kts from ship's head to 20° to the port side of the ship and 30 kts up to 30° to the port side.

1.2.2. Mission Task Elements

In the Aeronautical Design Standard [19] over 20 Mission Task Elements (MTEs) are defined. According to [13] any mission can be constructed as a contiguous sequence of MTEs. The port lateral manoeuvre of a helicopter ship deck landing can be described as a sidestep manoeuvre followed by a hover task and a vertical manoeuvre. Those are going to be described in more detail within this section according to [19].

The sidestep manoeuvre is started from a stabilized hover. After a rapid and aggressive lateral acceleration the target velocity and the altitude should be constant for 5 seconds before an aggressive deceleration to hover. After maintaining hover for 5 seconds the manoeuvre is repeated in the opposite direction. Most important visual reference is a reference line on the ground that indicates the desired track and tolerances. The objectives of this MTE are the lateral-directional handling qualities for aggressive manoeuvring near the rotorcraft limits and moreover the ability to coordinate bank angle and collective to hold constant altitude. (see [19], section 3.11.12)

The hover task starts at a ground speed of 6 to 10 knots at an altitude less than 20 ft. The target hover point is placed 45 degrees relative to the heading of the rotorcraft and marked by a ground-referenced point. After the pilot reaches the hover point and decelerates the helicopter the position should be maintained within the given limits of this MTE for about 30 seconds. The transition to hover should be a smooth manoeuvre. Objectives of the task are to check the ability to transition from translating flight to a stabilized hover. For this both precision and a reasonable amount of aggressiveness are to be used. Another objective is to check the ability to maintain precise position, heading and altitude. (see [19], section 3.11.1)

The vertical manoeuvre starts from a stabilized hover at an altitude to 15 feet. After a vertical ascent of the rotorcraft of 25 feet, the position is maintained for 2 seconds before descending back to the initial hover position. The test course is based on the course of the

hover MTE. In addition, a second reference symbol for the high- and low-hover position is added. The objectives of this MTE are to check for an adequate heave damping, vertical control power and an undesirable coupling between collective and the pitch, roll and yaw axis. Also the general characteristics of the heave axis controller should be checked with this MTE. (see [19], section 3.11.6)

1.3. Thesis Objective and Structure

The objective of this thesis is to develop a methodology for an implementation and optimization of an MDA in a maritime simulation environment. Furthermore the developed process is validated. Simulator flight test trials and OMCTs are carried out and evaluated. A simulator campaign is developed for the flight test trials.

After the introduction an overview of the theory of motion simulators is given. This includes an introduction into the human motion perception and the MDA. Different tuning and evaluation methods are presented. At the end of this chapter an overview over the AVES research facility is given. In the next chapter a simulator campaign for a helicopter ship deck landing is developed. This includes the definition of the flight task, setup of the test environment and the design of the test matrix. In the next chapter the methodology of an MDA implementation and optimization is carried out. The MDA is constructed and pre-validated before it is adapted and installed into the simulator environment. Afterwards an offline tuning with a genetic algorithm (GA) is carried out. The chapter closes with the execution of the final validation. The analysis and discussion of the results are presented in the next chapter. Afterwards both methods are compared at the end of this chapter. The thesis closes with a summarization and conclusions are drawn. Considerations for future work will also be discussed.

2. Theory of Motion Simulators

2.1. Human Motion Perception

This section gives a general overview of human motion perception. The participating sensory systems are described. Afterwards the vestibular system is characterized in more detail. Examples for mathematical models are given before the perception threshold is discussed.

The visual and the vestibular system are used for human motion perception. Both of these systems are able to sense motion, but in a statically and dynamically different way. The vestibular system can be considered as a strap down navigation platform. It is limited due to an increasing inaccuracy over longer periods of time. The visual system is important to do relative navigation to surrounding objects and to reset the vestibular sensation. In order to perceive sharp images, the vestibular system needs to be stabilized when moving around. The bandwidth of the visual system is limited and therefore the perception is slower than the vestibular system. The visual system has a maximum frequency of 0.5 to 1.0 Hz, whereas the vestibular system has a bandwidth of up to 5 to 10 Hz. The cooperation of both is important for the human motion perception to work. [20]

The vestibular system is placed in the inner ear. It consists of the semicircular canals (SCC) and the otolith organs (OTO). The SCC are responsible to sense angular acceleration $\vec{\omega}$, whereas the OTO are relevant for the perception of specific forces \vec{f} . In [21] Telban et al. give an overview of mathematical models describing the vestibular system. They derive two transfer functions for the SCC and the OTO that are shown in equations 2.1 and 2.2 and in Fig. 2.1.

$$H_{SCC}(s) = 5.73 \frac{80s^2}{(1 + 80s)(1 + 5.73s)} \quad (2.1)$$

$$H_{OTO}(s) = 0.4 \frac{10s + 1}{(5s + 1)(0.016s + 1)} \quad (2.2)$$

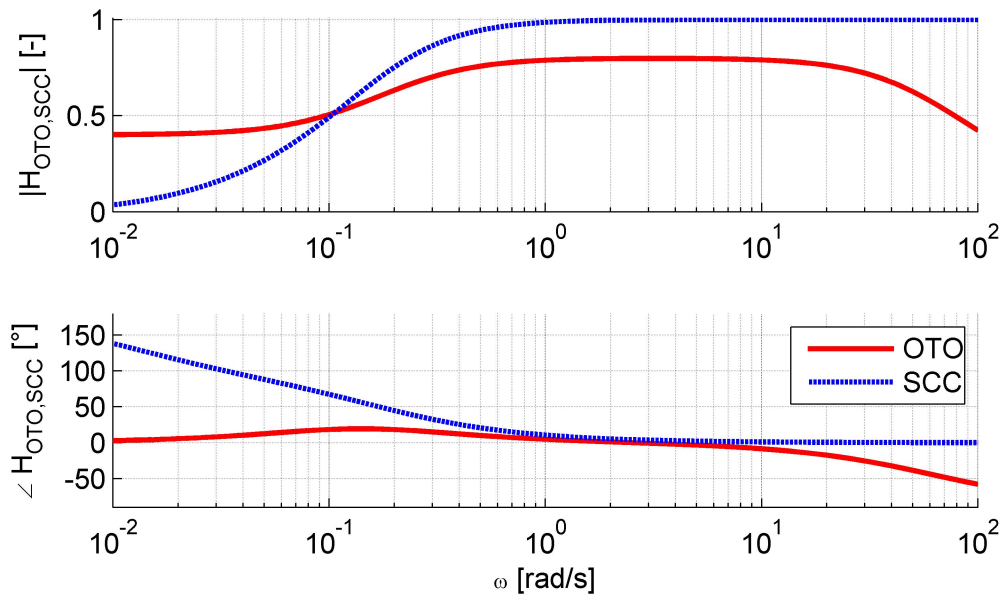


Figure 2.1.: **Frequency Response of the Vestibular System**

In addition to the transfer function of the vestibular system in equations 2.1 and 2.2 the motion perception model by Groen et al. [7] consists of perception thresholds. To implement frequency-dependent thresholds a constant threshold can be placed after the sensor's transfer function. This would be the simplest way of implementation. According to [7] there are three types of perception thresholds. A physical stimulus has to surpass all three to be actively perceived.

- 1) Sensory threshold: minimum stimulus energy that excites the peripheral sensor
- 2) Detection threshold: minimum stimulus that can be detected by the subject
- 3) Indifference threshold: determines whether or how a stimulus is perceived and interpreted by the brain

In [7] Groen et al. stated out that perception thresholds are strongly context dependent. Pilots may even perceive motion cues of the simulator when there is none. The perception

thresholds also vary depending on the task and the workload of the pilot. In table 2.1 motion perception for each axis are listed that are derived in [7] from an earlier simulator study in [22].

Table 2.1.: **Motion Perception Thresholds [7]**

Sensor	Axis	Threshold
OTO	x - Surge	$7.42 \cdot 10^{-2} \text{ m/s}^2$
	y - Sway	$7.43 \cdot 10^{-2} \text{ m/s}^2$
	z - Heave	$1.23 \cdot 10^{-1} \text{ m/s}^2$
SCC	x - Roll	$5.21 \cdot 10^{-3} \text{ rad/s}$
	y - Pitch	$7.34 \cdot 10^{-3} \text{ rad/s}$
	z - Yaw	$1.66 \cdot 10^{-2} \text{ rad/s}$

2.2. Motion Drive Algorithm MDA

To generate motion cues in a simulator, robotic mechanisms called motion platforms are used. According to Casas-Yrurzum et al. [15] there exist many different motion platforms, but the six degree of freedom (DoF) hexapod platform called Stewart-Gough platform [23] has become a standard for flight simulation. The motion platform is able to perform controlled movements that are controlled by an MDA. According to Casas-Yrurzum et al. [15] many MDAs have been proposed, but the most common is the Classical Washout Algorithm (CWA) introduced in [1] by Reid and Nahon. The MDA translates the translational and rotational accelerations of a vehicle model into simulator demands. Due to physical limitations of motion platform capabilities, the MDA has to be designed in such a way as to cope with the constraints of the physical simulator limits. [15]

As shown in Fig. 2.2 following reference frames at the simulator, the aircraft and the environment have to be considered according to [1]. All axes and angles of such reference frames are aligned as right-handed coordinate systems. The reference frames with the indices "B", "A" and "PA" are all aircraft-fixed with the x-axis pointing forward and the z-axis pointing downward, with different origins. The aircraft reference frame "A" has its origin located at a reference point that is attached to the aircraft. Reference frame "B" has its origin located at the aircraft's centre of gravity (CG). The reference frame "PA" is attached to the pilot's head with its origin located at a point midway between the vestibular system. It will be assumed that the reference frame "PA" is parallel to

the aircraft reference frame "A". \vec{P}_A is the location vector between the reference frames "B" and "A". \vec{R}_A is the location vector between the reference frames "A" and "PA". The reference frames with the indices "S" and "PS" are body-fixed reference frames of the simulator with the x-axis pointing forward and the z-axis pointing downward. The simulator reference frame "S" has its origin located at a reference point that is attached to the simulator. It has the same relative cockpit position as the aircraft reference point. The reference frame "PS" is attached to the pilot's head with its origin located at a point midway between the vestibular system. Again, it is assumed that the reference frame "PS" lies parallel to the simulator reference frame "S". \vec{R}_S is the location vector between the reference frames "S" and "PS". The inertial reference frame "I" is earth-fixed with the z-axis aligned with the gravity vector \vec{g} . As an example, the Euler angles $\vec{\beta} = (\phi, \theta, \psi)^T$ are marked in Fig. 2.2 in the inertial reference frame "I".

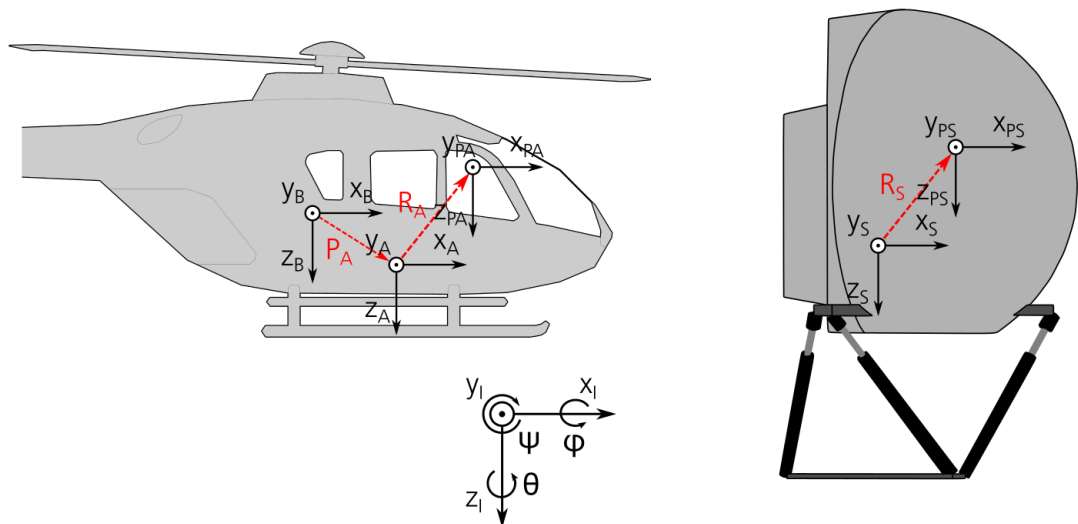


Figure 2.2.: Reference Frames according to [1]

According to [1] the basic task of the CWA is to recreate the specific force and angular acceleration of an aircraft in a simulator as shown in equations 2.3 and 2.4.

$$\vec{f}_{PS} \approx \vec{f}_{PA} \quad (2.3)$$

$$\vec{\omega}_{PS} \approx \vec{\omega}_{PA} \quad (2.4)$$

The equations 2.3 and 2.4 are defined in the reference frames "PS" and "PA" that are attached to the pilots' head. Because the location of this reference frames can differ due to several aircrew members it is convenient to designate a reference point as the location for which the CWA applies. This leads to the reference frames "S" and "A" at the simulator and the aircraft. Thus the CWA attempt to achieve the new relationships in equation 2.5 and 2.6. [1]

$$\vec{f}_{SS} \approx \vec{f}_{AA} \quad (2.5)$$

$$\vec{\omega}_{SS} \approx \vec{\omega}_{AA} \quad (2.6)$$

As shown in Fig. 2.3 the CWA by Reid and Nahon [1] features three different channels with high-pass (HP) and low-pass (LP) filtering elements. The two HP channels of specific forces \vec{f}_{AA} and angular accelerations $\vec{\omega}_{AA}$ are supposed to provide high frequency motion cues as sustained low frequency motion cues would cause violations against the motion travel limits. The specific forces \vec{f}_{AA} get LP filtered and the low frequency motion cues are then simulated by tilting relative to the gravitation vector \vec{g} . This is supposed to provide the perception of sustaining low frequency accelerations to the pilot.

As input for the CWA the angular accelerations $\vec{\omega}_{AA}$ and the specific forces \vec{f}_{AA} of the simulation model are used. To obtain g-less specific forces \vec{f}_{AA} from body accelerations \vec{a}_b equation 2.7 is used [14].

$$\begin{aligned} \vec{f}_{AA} &= \begin{pmatrix} f_{xAA} \\ f_{yAA} \\ f_{zAA} \end{pmatrix} = \begin{pmatrix} a_x \\ a_y \\ a_z \end{pmatrix} - \begin{pmatrix} g_x \\ g_y \\ g_z \end{pmatrix} \\ &= \begin{pmatrix} \dot{u} \\ \dot{v} \\ \dot{w} \end{pmatrix} - \begin{pmatrix} r \\ p \\ q \end{pmatrix} \begin{pmatrix} v \\ w \\ u \end{pmatrix} + \begin{pmatrix} q \\ r \\ p \end{pmatrix} \begin{pmatrix} w \\ u \\ v \end{pmatrix} - g \begin{pmatrix} -\sin \theta \\ \sin \phi \cos \theta \\ \cos \phi \cos \theta \end{pmatrix} \end{aligned} \quad (2.7)$$

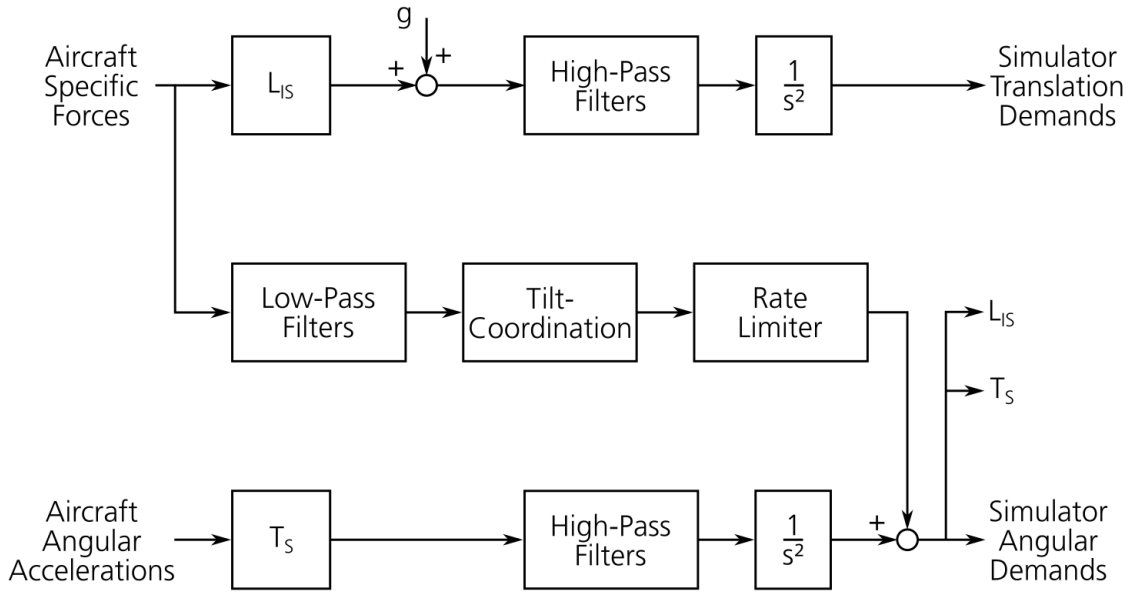


Figure 2.3.: **Classical Washout Algorithm according to [1]**

In the first channel the specific forces $\vec{r}_{AA}^{\rightarrow}$ are HP filtered. For this the input is transformed from the body frame to the inertial frame with L_{IS} in equation 2.8. Afterwards the gravitational constant g is added before the specific forces are transmitted to the HP filter. According to [24] for rotorcraft simulation third-order HP filters are required. As shown in equation 2.9 those third-order HP filters consist of a second-order HP filter multiplied with a first-order HP filter. They contain a motion gain K , a damping ratio ζ and two break frequencies ω , ω_2 . After filtering, the received motion accelerations are integrated twice to obtain the platform displacements S_I .

$$L_{IS} = \begin{pmatrix} \cos \theta \cos \psi & \sin \phi \sin \theta \cos \psi & \cos \phi \sin \theta \cos \psi \\ \cos \theta \sin \psi & \sin \phi \sin \theta \sin \psi & \cos \phi \sin \theta \sin \psi \\ -\sin \theta & \sin \phi \cos \theta & \cos \phi \cos \theta \end{pmatrix} \quad (2.8)$$

$$H_{HP,3rd}(s) = \frac{Ks^2}{s^2 + 2\zeta\omega s + \omega^2} \cdot \frac{s}{s + \omega_2} \quad (2.9)$$

$$H_{LP,2nd}(s) = \frac{K\omega^2}{s^2 + 2\zeta\omega s + \omega^2} \quad (2.10)$$

The second channel is the specific forces LP channel. As a first step the specific forces \vec{f}_{AA} get LP filtered with a second-order LP filter as shown in equation 2.10. To translate these into tilt angles of the dome, equation 2.13 is used. This equation is an approximation of equation 2.11 that is built up on the assumption of a low performance aircraft in equation 2.12. Those tilt angles get added to the Euler angles $\vec{\beta}_S$ of the third channel. They cause an additional movement of the simulator dome, that has to be below the motion perception threshold of the pilot. Otherwise it would lead to a distorted motion perception. The rate of the tilt angles has to be limited around 2-3 deg/s according to [24]. Note that the human motion perception thresholds in Tab. 2.1 according to [7] are smaller. However a rate limitation around 2-3 deg/s has become standard according to [24],[2] and [14].

$$\phi_{S,LP} = \tan^{-1} \left(\frac{f_{y,LP}}{f_{z,LP}} \right) \quad \theta_{S,LP} = -\tan^{-1} \left(\frac{f_{x,LP}}{f_{z,LP}} \cdot \cos \phi_{S,LP} \right) \quad \psi_{S,LP} = 0 \quad (2.11)$$

$$f_{LP,z} \approx -g \quad \sin x \approx x \quad \cos x \approx 1 \quad (2.12)$$

$$\phi_{S,LP} = -\frac{f_{LP,y}}{g} \quad \theta_{S,LP} = \frac{f_{LP,x}}{g} \quad \psi_{S,LP} = 0 \quad (2.13)$$

The third channel angular accelerations $\vec{\omega}_{AA}$ are HP filtered. This happens in a similar way to the HP filtering of the specific forces \vec{f}_{AA} . The only difference is the transformation in the beginning, where the rotational accelerations $\vec{\omega}_{AA}$ are converted to Euler angle accelerations $\vec{\omega}_S$ with T_S in equation 2.14. The final simulator angle demands $\vec{\beta}_S$ also get led back to the transformation matrices L_{IS} and T_S .

$$T_S = \begin{pmatrix} 1 & \sin \phi \tan \theta & \cos \phi \tan \theta \\ 0 & \cos \phi & -\sin \phi \\ 0 & \sin \phi \sec \theta & \cos \phi \sec \theta \end{pmatrix} \quad (2.14)$$

2.3. Tuning Methods

The tuning of motion parameters as mentioned in [15] aims first and foremost at correctly simulating motion and secondarily at increasing the motion fidelity. Motion fidelity summarizes the quality of the motion in a more general way and has to be divided in several aspects. The physical fidelity describes the capability of the simulator to provide the motion cues of the simulated vehicle. Whereas the perceptual fidelity describes the human perception of self-motion compared to the real situation. When there is a consistency between the behaviour of the pilot and the real situation, the simulation offers a good behavioural fidelity. Finally, if a fitness for purpose is reached and the simulator hits the goals set beforehand, a functional fidelity is reached.

After the typical tuning procedure for simulator commissioning the fitness function and the vestibular motion perception error (VMPE) are presented as methods for an offline tuning. During an offline tuning the improvement of the motion fidelity is conducted at a computer. No lengthy sessions at the simulator or pilots are needed ideally.

2.3.1. Piloted Tuning Procedure

During a piloted tuning procedure the MDA gets tuned in a feedback loop between an evaluation pilot and a washout filter expert. After each flight the washout filter expert adjusts the filter coefficients according to the impressions of the pilot. [25] This tuning method improves the motion fidelity in a perceptual way.

After a definition of motion cue errors by Grant and Reid in [25] a specific set of problem types were defined in [8]. Those are connected with derived coefficient adjustments for the CWA as shown in Tab. 2.2. In general three categories of motion cue errors should be considered: false cues, scaling or missing cue errors and phase errors. The correlating problem types are false cues, motion jerkiness, motion amplitude, motion duration, motion lag and unknown problems.

The pilot should state false cues if he detects a distinct unexpected motion cue. This includes cues when none was expected as well as cues that are opposite to expected cues. This problem type is consistent to the description of the motion cue error. Motion jerkiness is a high frequency motion cue error and a natural way to describe those. High frequency distortion of low frequencies are often described as jerkiness. When initial, transient or sustained cues are missing it is a motion amplitude problem. In general, motion duration

problems are caused due to missing or scaled transient cues. In case of missing high-frequency transient cues, the duration may be perceived as too short. Otherwise if low-frequency transient cues are missing, they may be perceived as too long. This can be caused due to the tilt coordination. In case of a phase error the pilot should state a motion lag problem. This can be traced back to the low-frequency tilt-coordination of specific forces due to missing transient cues. This leads to a temporary motion response from the initial and high-frequency transient cues, followed by a delay until the sustained cues are available. If none of the defined problems fits to the pilot's perception, an unknown problem is found. This term is used to sum up all other problems that do not fit in any of the previous terms. [8]

As described in [8], a stepwise appliance of pilot feedback and parameter adjustment can lead to an improved motion tuning within the physical limits of the motion platform. The main disadvantage of this tuning method is its subjectivity. But due to a lack of more satisfying mathematical methods this tuning procedure is still the preferred one. [25]

2.3.2. Fitness Function

The fitness function proposed by Jones was introduced in [10] and optimized in [2]. The purpose of this function is an improvement of the motion cueing's balance. A value hereinafter referred to as "fitness" is determined by the response of the motion system. To evaluate the fitness F , the motion response is considered in the typical frequency range of closed-loop pilot controls from 1 to 10 rad/s. Firstly, in accordance to Fig. 2.4 a fitness F_i for each axis is calculated in equation 2.16 before an overall fitness F is determined in equation 2.17. The number of axes that are considered in the fitness calculation is dependent on the user. For a six DoF system tuning would be conducted for the axes in equation 2.15.

Table 2.2.: Coefficient Adjustments according to [8]

Motion error	DoF	Coefficients	Likelihood	
False cue	Heave, yaw	$\uparrow \zeta_{HPz,HP\psi}, \downarrow K_{HPz,HP\psi}$	1	
	Surge, sway	$\uparrow \omega_{HP\phi,HP\theta}, \downarrow K_{HP\phi,HP\theta}, \uparrow \omega_{LPx,LPy},$	1	
		$\downarrow K_{HPx,HPy}, \uparrow \dot{\phi}_{lim}, \dot{\theta}_{lim}$	2	
		$\downarrow \omega_{HPx,HPy}$	3	
		$\uparrow \zeta_{HPx,HPy}$	4	
	Motion jerkiness	Roll, pitch	$\downarrow \omega_{LPx,LPy}, \downarrow \dot{\phi}_{lim}, \dot{\theta}_{lim}, \downarrow K_{HPx,HPy}$	1
		Heave, yaw	$\downarrow \omega_{HPz,HP\psi}$	1
		Surge, sway	$\downarrow \zeta_{HPz,HP\psi}$	2
			$\downarrow \omega_{LPx,LPy}, \downarrow \omega_{HPx,HPy}, \downarrow K_{HPx,HPy}$	1
		Pitch, roll	$\downarrow \zeta_{HPx,HPy}$	2
Motion amplitude	Roll, pitch, yaw	$\uparrow \omega_{HP\phi,HP\theta,HP\psi}, \downarrow K_{HP\phi,HP\theta,HP\psi}$	1	
	Surge, sway, heave	$\uparrow \omega_{HPx,HPy,HPz}, \downarrow K_{HPx,HPy,HPz}$	1	
		$\downarrow \omega_{LPx,LPy}$	2	
Motion duration (too short)	Heave, pitch	$\downarrow \omega_{HPz,HP\phi,HP\theta,HP\psi}$	1	
	Roll, yaw	$\downarrow \zeta_{HPz,HP\phi,HP\theta,HP\psi}$	2	
	Surge, sway	$\downarrow \omega_{HPx,HPy}$	1	
$\downarrow \zeta_{HPx,HPy}$		2		
Motion duration (too long)	Surge, sway	$\uparrow \omega_{LPx,LPy}, \downarrow K_{HPx,HPy}, \uparrow \dot{\phi}_{lim}, \dot{\theta}_{lim}$	1	
Motion lag	Surge, sway	$\uparrow \omega_{LPx,LPy}, \uparrow \dot{\phi}_{lim}, \dot{\theta}_{lim}$	1	
Unknown	Heave, yaw	$\downarrow K_{HPz,HP\psi}, \downarrow \omega_{HPz,HP\psi}, \downarrow \zeta_{HPz,HP\psi}$	1	
	Surge, sway	$\downarrow K_{HPx,HPy}, \downarrow \omega_{HPx,HPy}, \downarrow \omega_{LPx,LPy},$		
		$\zeta_{HPx,HPy}, \downarrow \dot{\phi}_{lim}, \dot{\theta}_{lim}$	1	
Pitch, roll	$\downarrow K_{HP\phi,HP\theta}, \downarrow \omega_{HP\phi,HP\theta}, \downarrow \zeta_{HP\phi,HP\theta}$	1		

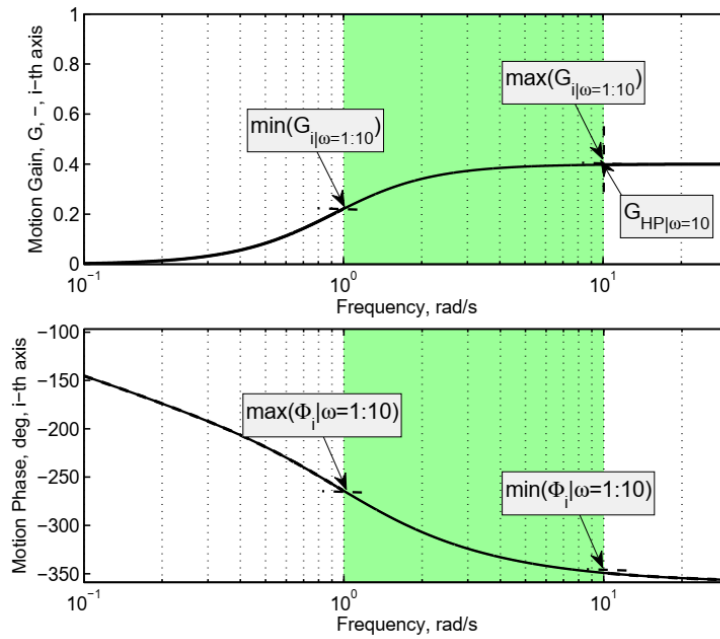


Figure 2.4.: Typical 3rd-order Motion Filter Response according to [2]

$$i = \{p, q, r, f_x, f_y, f_z\} \quad (2.15)$$

$$F_i = K_2 G_i|_{\omega=10} e^{-K_3 G_i|_{\omega=10} (\Delta G_i + \Delta \Phi_i)} \quad (2.16)$$

$$F = \frac{1}{1 + K_1 \text{var}(G_i|_{\omega=10}) \overline{\Delta \Phi}} \sum_{i=1}^N F_i \quad (2.17)$$

F is the overall fitness of the motion configuration. F_i is the fitness of the i -th axis. G_i and Φ_i are gain and phase of the motion response of the i -th axis. $\overline{\Delta \Phi}$ is the mean over the frequency range of the change in phase of the motion response. Subscript $\omega = j$ refers to the value at j rad/s. ΔG_i and $\Delta \Phi_i$ are defined as,

$$\Delta G_i = \max |G_i|_{\omega=1:10} - \min |G_i|_{\omega=1:10} \quad (2.18)$$

$$\Delta\Phi_i = \frac{\max |\Phi_i|_{\omega=1:10} - \min |\Phi_i|_{\omega=1:10}}{360} \quad (2.19)$$

K_1 , K_2 and K_3 are constants to scale specific elements of the fitness function (see equations 2.17 and 2.16). N is the number of axes considered in the fitness calculation.

As stated in [2] this optimized fitness function includes elements to determine the fitness of the complete motion set and of individual motion axis. Because it is an offline tuning method it improves the physical fidelity of the motion system. During the offline tuning many parameters have to be tuned independently. For an optimization problem with many unknowns several algorithms exist. Jones use a GA in combination with the fitness function in [16] because it was appropriate and simple to implement. Nevertheless he stated out, that another method may be more suitable. Simulator flight test trials with the tuned motion parameter were conducted for evaluation. The results were encouraging according to the author.

2.3.3. Vestibular Motion Perception Error VMPE

In [3] Memon et al. introduce the VMPE. This approach is based on minimizing the estimated error between the vestibular motion perceived by the pilot and the simulated vehicle. It is an objective method that attempts to reach perceptual fidelity through tuning the motion parameters with a human motion perception model. The architecture of this technique is shown in Fig. 2.5.

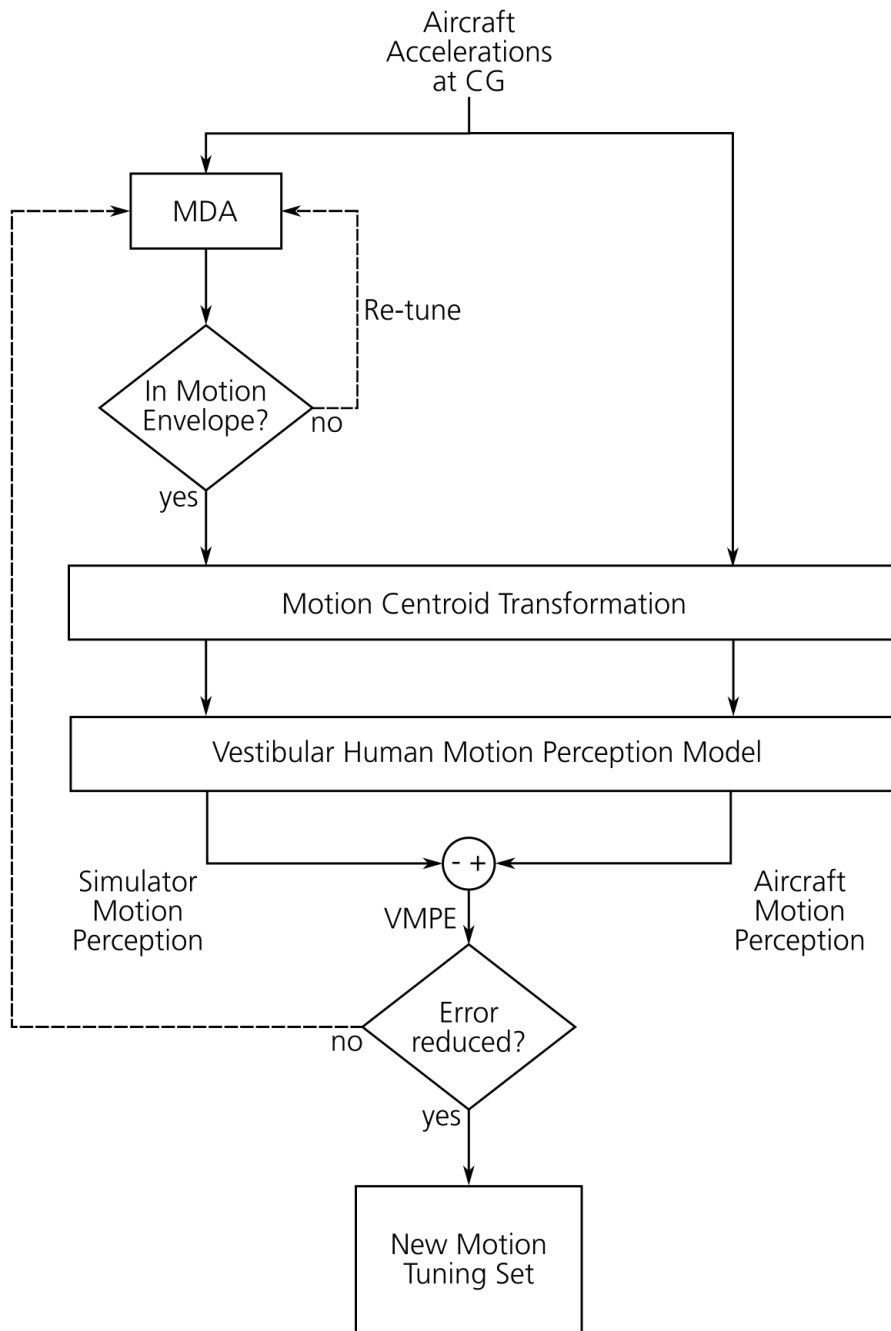


Figure 2.5.: **VMPE Technique Architecture according to [3]**

The aircraft accelerations in the form of the specific forces \vec{f}_{AA} and the angular accelerations $\vec{\omega}_{AA}$ are fed into the MDA. The resulting simulator translation and angular demands \vec{S}_I and $\vec{\beta}_S$ are checked whether they are within the motion envelope. Afterwards they are transformed back to the simulator reference frame "S" with equation 2.20 and differentiated twice to obtain the simulator accelerations in the form of the specific forces \vec{f}_S and the angular accelerations $\vec{\omega}_S$. These are transformed in the motion centroid transformation to the reference frame "PS" with equation 2.21. Likewise the aircraft accelerations are transformed to the reference frame "PA" with equation 2.22.

$$\vec{S}_S = L_{IS}^{-1} \cdot S_I \quad (2.20)$$

$$\vec{f}_{PS} = \vec{f}_S + \vec{\omega}_S \times (\vec{\omega}_S \times \vec{R}_S) + \vec{\omega}_S \times \vec{R}_S \quad (2.21)$$

$$\vec{f}_{PA} = \vec{f}_{AA} + \vec{\omega}_{AA} \times (\vec{\omega}_{AA} \times \vec{R}_A) + \vec{\omega}_{AA} \times \vec{R}_A \quad (2.22)$$

Afterwards the aircraft and simulator states at the pilot's vestibular centre run through the vestibular human motion perception model. Within this model the previously presented transfer function by [21] for the OTO (see equation 2.2) and the SCC (see equation 2.1) are used. This leads to the aircraft and simulator motion perception. The VMPE is calculated by comparison of the aircraft and the simulator motion perception. A new motion tuning set is found when the VMPE is smaller than before.

The calculation of the VMPE is carried out as follows. First the root-mean-squared error (RMSE) has to be calculated for each axis according to the equations 2.23 and 2.24. i stands for a specific translation or rotational axis and m for the total number of discrete data points of the acceleration. The aircraft motion perception is indicated by the index "Ai,Per". Accordingly, the simulator motion perception has the index "Si,Per". Afterwards the VMPE is calculated for the translational axis in equation 2.25 and for the rotational axis in 2.26, where N is the total number of axes that are dominant.

$$RMSE_{VMPE,fi} = \sqrt{\frac{\sum_{k=1}^m (f_{Ai,Per} - f_{Si,Per})^2}{m}} \quad (2.23)$$

$$RMSE_{VMPE,wi} = \sqrt{\frac{\sum_{k=1}^m (\omega_{Ai,Per} - \omega_{Si,Per})^2}{m}} \quad (2.24)$$

$$VMPE_{RMSE-MTS-f} = \frac{\sum_{k=1}^N (RMSE_{VMPE,fi})}{N} \quad (2.25)$$

$$VMPE_{RMSE-MTS-\omega} = \frac{\sum_{k=1}^N (RMSE_{VMPE,\omega i})}{N} \quad (2.26)$$

In [3] simulator flight test trials have been conducted with a VMPE tuned motion system. The results were promising. During the offline tuning no GA or another algorithm was used.

2.4. Evaluation Methods

In this section the evaluation methods are going to be presented. This methods must be divided into objective and subjective criteria. For the subjective methods only rating scales are presented.

2.4.1. Objective Methods

One objective method is proposed by Sinacori in [26] and later refined by Schroeder in [27]. According to [10] this criteria is one of the most used, applied and accepted methods to determine motion fidelity. In this method the motion fidelity is characterized from measured gain and phase shift at 1 rad/s. The frequency was chosen because the semicircular canals have the highest sensitivity [28]. The boundaries shown in Fig. 2.6 are determined in [27] and are based on subjective and objective evaluations. This leads to a characterization of the motion sets with "high", "medium" or "low" fidelity.

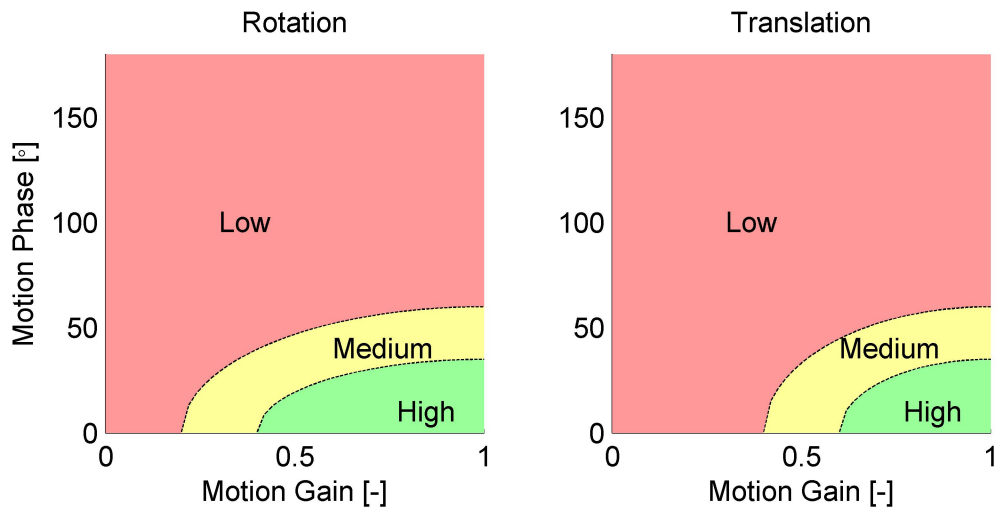
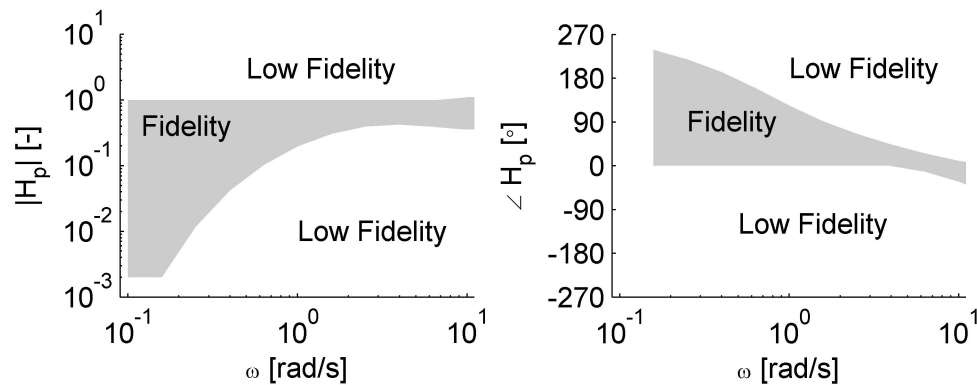


Figure 2.6.: **Schroeder Boundaries at 1 rad/s**

Another objective method is the OMCT introduced in [29] that is part of the ICAO Manual 9625 [9]. In comparison to the Sinacori/Schroeder criterion it does not focus on one frequency and also provides test procedures for cross-coupling between the axes. For this the OMCT contains ten different test cases (see Tab. 2.3). Within those test cases twelve different frequencies were observed according to Tab. 2.4 in a range between 0.1 rad/s and 15.849 rad/s. Each test case is defined by the input's axis and the observed output according to Tab. 2.3. As the OMCT is carried out a sinusoid input is generated. Afterwards the input is compared to the observed output in terms of magnitude and phase distortion. According to [30] a Fourier transformation should be used within the analysis. For the evaluation of the OMCT ten different simulators have been used with an optimized motion cueing system for optimum motion feedback [29]. After the combination of all test data boundaries, between a high and low motion fidelity were derived for each test case. Those are proposed in detail in [9]. As an example Fig. 2.7 shows the fidelity boundaries for the test case "Roll Output to Roll Input". The grey shaded area is the area with an optimal motion fidelity whereas the rest is the area with a low motion fidelity.

Figure 2.7.: **OMCT Boundaries for Roll Output to Roll Input**Table 2.3.: **OMCT Test Matrix according to [9]**

Input Signal/Response Output	Pitch	Roll	Yaw	Surge	Sway	Heave
Pitch	1			2		
Roll		3			4	
Yaw			5			
Surge	7			6		
Sway		9			8	
Heave						10

Although the OMCT is part of the ICAO Standard, especially the postulated motion fidelity boundaries are still part of current research. Zaal et al. refined them in [31]. The authors carried out test trials with three flight tasks and four different motion configurations per flight task. The refined boundaries of the OMCT were determined according to the task performance. Another subject of research was the question of applicability of the OMCT for rotorcraft. According to Dalmeijer et al. [17] the OMCT is representative for heave motion. For surge and pitch motion characteristics the results were different. A large sensitivity of the rate limiter in the tilt coordination was found. In [16] Jones has the same findings, that there are differences between the boundaries of the OMCT based on fixed-wing and rotorcraft requirements. He compared the pilots' subjective ratings of simulator flight test trials to the OMCTs of four different motion sets. The motion set with the best motion ratings was furthest from OMCT boundaries. The motion set with the poorest motion ratings was the only one within the OMCT boundaries.

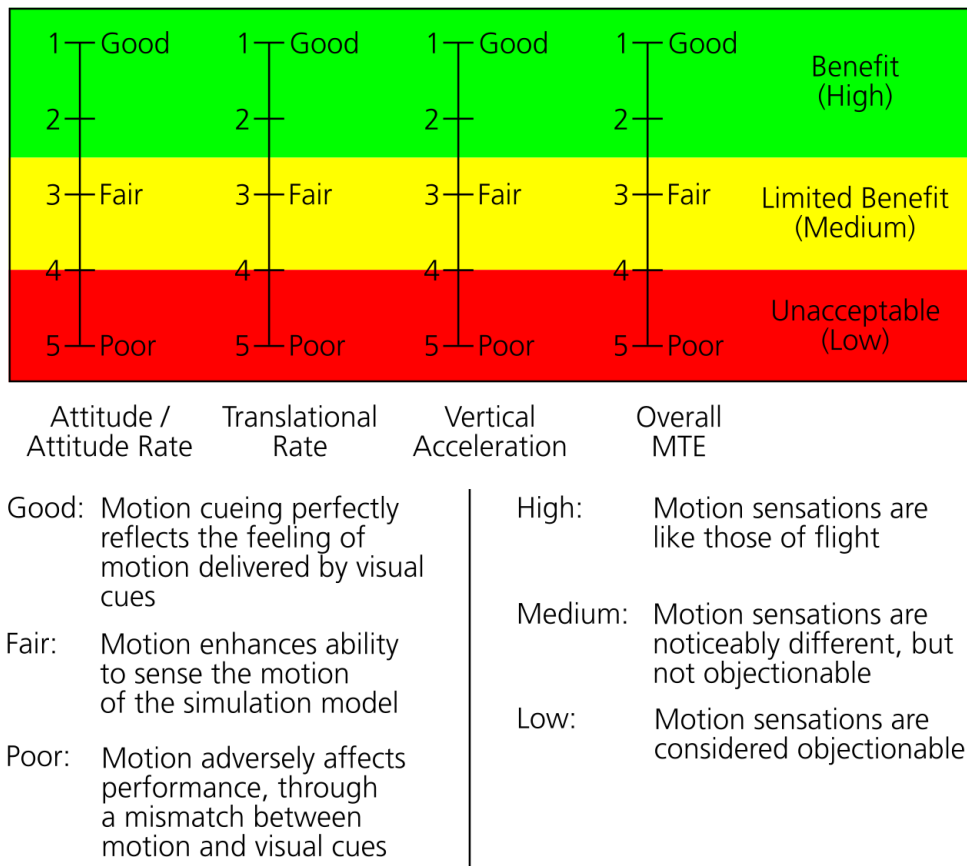
Table 2.4.: Frequencies and Amplitudes for each Test Point according to [9]

Frequency Signal Number	Frequency [rad/s]	Frequency [Hz]	Attitude Amplitude A [°]	Angular Rate Amplitude A_ω [°/s]	Angular Acceleration Amplitude A_{ω^2} [°/s ²]
1	0.100	0.0159	6.000	0.600	0.060
2	0.158	0.0251	6.000	0.948	0.150
3	0.251	0.0399	3.984	1.000	0.251
4	0.398	0.0633	2.513	1.000	0.398
5	0.631	0.1004	1.585	1.000	0.631
6	1.000	0.1591	1.000	1.000	1.000
7	1.585	0.2510	0.631	1.000	1.585
8	2.512	0.3990	0.398	1.000	2.512
9	3.981	0.6330	0.251	1.000	3.981
10	6.310	1.0040	0.158	1.000	6.310
11	10.000	1.5910	0.100	1.000	10.000
12	15.849	2.5150	0.040	0.631	10.000

2.4.2. Subjective Methods

In this section two motion rating scales are presented as possible methods for a subjective evaluation in combination with flight test trials.

The motion rating by Jones [2] is based upon the descriptions used by Schroeder in [27] and shown in Fig. 2.8. In total four appraisals are given by the pilot. Those are assigned to "Attitude/Attitude Rate", "Translational Rate", "Vertical Acceleration" and "Overall MTE". In general each rating complies with one of the categories "Benefit", "Limited Benefit" or "Unacceptable". The scales are reaching from 1 to 5, where 1 is "Good", 3 "Fair" and 5 "Poor". All those terms are defined in Fig. 2.8. To give a motion rating the pilot compares his impressions with the major categories and afterwards with the statements.

Figure 2.8.: **Motion Rating Scale by Jones [2]**

The motion rating scale by Hodge [4] is built as a decision tree as shown in Fig. 2.9. This scale is based on the same structure as the established Handling Quality Rating (HQR) by Cooper and Harper [32]. Starting in the bottom left corner the pilot gets led through answering of the questions into the specific branches. In the branches each numerical rating is combined with a statement. The pilot has to compare his impression with the statements to give a numerical rating. The rating scale offers 10 different ratings from 1 (best) to 10 (worst). In addition the pilot can add a character as a suffix to describe the motion fidelity in more detail.

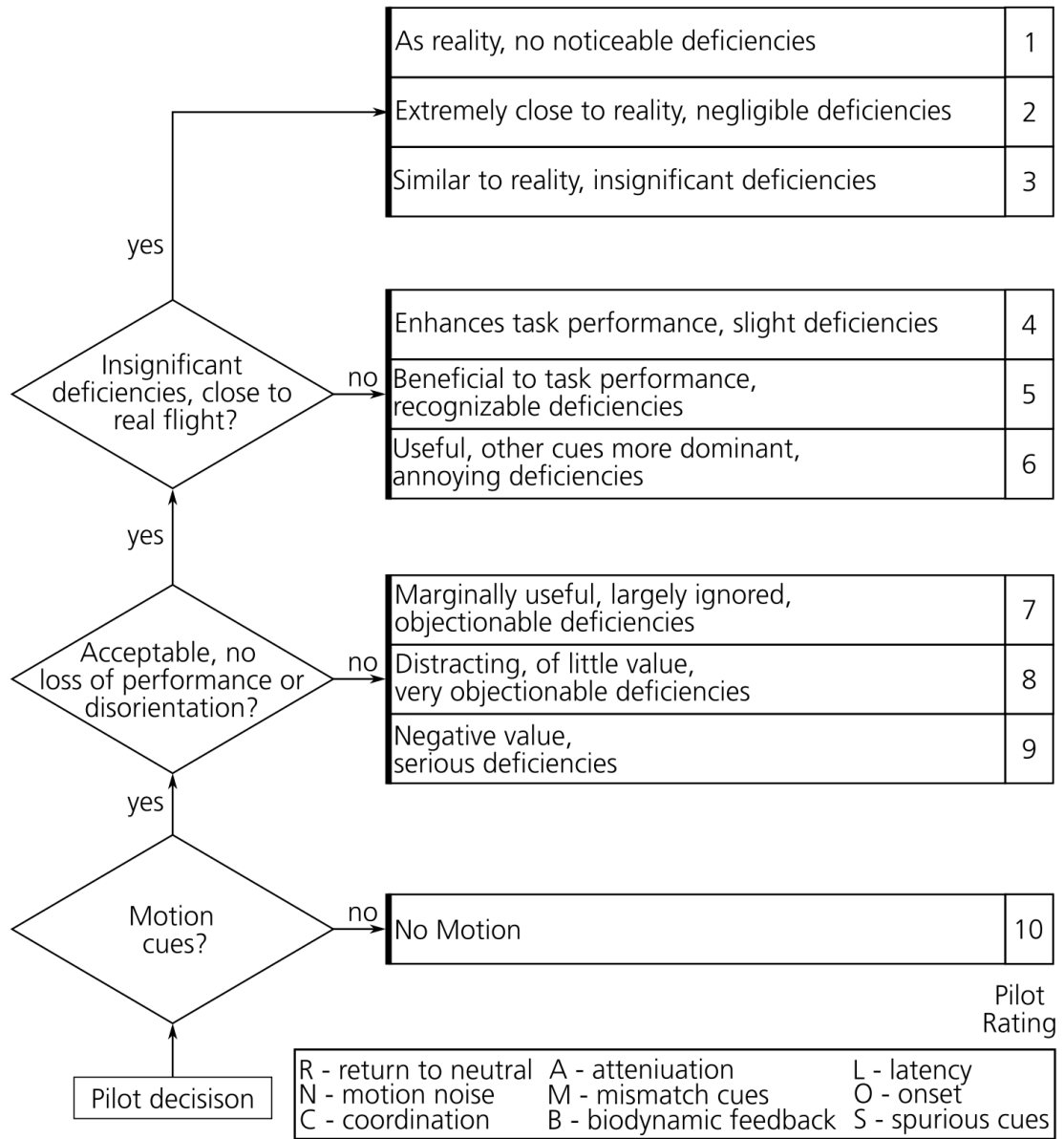


Figure 2.9.: Motion Rating Scale by Hodge [4]

2.5. AVES Research Facility

The AVES is DLR's research flight simulation facility in Braunschweig and described in detail in [33]. The simulator offers different cockpits that can be changed between a fixed based and a motion platform via a roll-on/roll-off (RORO) system. Those cockpits are replica of the A320 ATRA, the EC135 ACT/FHS and a single aisle passenger cabin. Both platforms are provided with a projection system with a very wide field of view (FoV). For the helicopter this means a vertical FoV of -53° to 40° and a horizontal FoV of 240° . Furthermore the resolution was measured to be 5 arc-min/OLP, the brightness was 13.5 cd/m^2 and the contrast ratio was 7:1. As stated out in [5] for the simulation a distributed software architecture was chosen. The applications can run on multiple computers in an ethernet network with UDP communication. The hole data traffic is coordinated by an interface computer (IC). Time critical applications run on real time operating systems (RTOS). As a simulation framework application programming interface (API) 2simulate was developed [34]. This is the base for all applications and provides deterministic scheduling functions for real time operation.

The helicopter cockpit at AVES is a replica of the active control technology demonstrator and flying helicopter simulator (ACT/FHS), a highly modified EC135 that is shown in Fig. 2.10. It features the fly-by-wire/fly-by-light flight control system and is decribed in detail in [35] and [36].



Figure 2.10.: DLR's ACT/FHS

2.5.1. Motion Platform



Figure 2.11.: AVES Motion Platform

As shown in Fig. 2.11 the motion platform is a hexapod platform, also called 6 DoF Stewart-Gough platform, that was introduced in [23]. The system is provided by the manufacturer MOOG. According to [2] it is capable of achieving the highest motion standards recommended by EASA. The motion platform limits are shown in Tab. 2.5. In addition each actuator leg has a maximum stroke of about 1.5 m. The standard MDA is provided by the manufacturer and is proprietary by MOOG. It features rotational HP 3rd order filters and translational HP 1st order filters with the use of the MOOG APK.

Table 2.5.: AVES motion platform limits [10]

	Max. excursion	Max. velocity	Max. acceleration
Surge	+1.44/-1.45 m	± 1.0 m/s	± 6.5 m/s ²
Sway	+1.26/-1.26 m	± 1.0 m/s	± 6.5 m/s ²
Heave	+0.95/-0.95 m	± 0.75 m/s	± 9.0 m/s ²
Roll	+27/-27°	± 21 °/s	$> \pm 140$ °/s ²
Pitch	+34/-31°	± 21 °/s	$> \pm 140$ °/s ²
Yaw	+32/-32°	± 24 °/s	$> \pm 240$ °/s ²

2.5.2. Helicopter Flight Model

At AVES the real time non-linear helicopter model HeliWorX is used to calculate the helicopter flight dynamics. It is based on the helicopter model SIMH [37] and was former used to model a Bo105. It has been adapted to represent the ACT/FHS, a strongly modified EC 135 [35] [36]. As described in [5] the helicopter is modelled as a rigid body with several components (main and tail rotor, fuselage, horizontal and vertical stabilizer, engine and actuator). To represent the fundamental flapping and lagging natural frequencies of the main rotor a model of a fully articulated rotor with an equivalent hinge offset and spring restraint is used. The aerodynamic forces and moments are determined with the blade element theory for rigid blades. Each blade is divided into ten blade sections and the dynamic rotor inflow model by Pitt&Peters [38] is used.

As an additional feature an interface for external wind fields was implemented in [39]. The total wind speed $V_{W,T}$ is divided into the global wind speed $V_{W,G}$ as a constant parameter with no variations in space and time and the local wind speed $V_{W,L}$ that describes local effects as a deviation from the global wind speed (see equation 2.27).

$$V_{W,T}(x, y, z, t) = V_{W,G} + V_{W,L}(x, y, z, t) \quad (2.27)$$

As a result of the local wind speed $V_{W,L}$, additional angle of attack and Mach number of the aerodynamic elements are calculated. Those are superimposed to 45 distributed Airload Computation Points (ACPs) as shown in Fig. 2.12. A spacial and temporal linear interpolation is used during the piloted simulation. The interaction of the wind field with the tail rotor has not been implemented yet. [40]

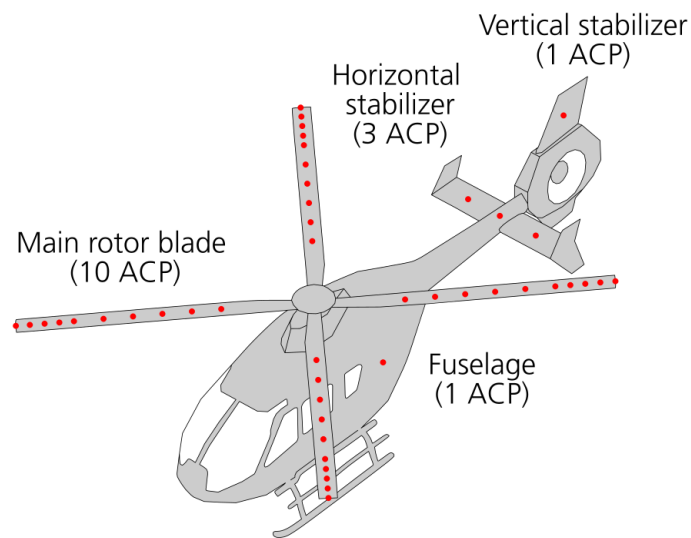


Figure 2.12.: ACP in HeliWorX [5]

2.5.3. Ship Dynamic Model

In the maritime environment it is possible to add ships [5]. For example a F124 “Sachsen class” frigate was integrated to perform ship deck landing research as shown in Fig. 2.13. The ship dynamics are controlled by VehicleControl, an enhanced traffic server developed with the 2simulate API. Two control modes offer a 3 DoF path following algorithm and an additional 6 DoF complex ship dynamic model.



Figure 2.13.: **Maritime Simulation Environment [5]**

The dynamics are generated with the Marine Systems Simulator (MSS) library by Perez et al. [41] that is nested into a MathWork's Simulink Model. This model uses a generalized equation of motion for maritime systems as shown in equation 2.28.

$$M\dot{v} + C(v, v_r) + D(v_r, \mu) + g(\eta) = \tau_{env} + \tau_{ctrl} \quad (2.28)$$

Equation 2.28 contains the mass matrix M , terms for the effects from fictitious forces (Coriolis and centrifugal) in C , from damping forces (e.g. viscous forces) in D and restoring forces from gravity and buoyancy in g . On the right hand side are the environmental forces τ_{env} and control forces τ_{ctrl} . As an example Fig. 2.14 shows the Euler angle and heave movement of the F124 for a significant wave height of 5.3 m and a mean wave direction of 0° to the ship. It can be seen, that the time plots contain the characteristic peaks and resting periods. According to [5] the pilots wait for the resting periods for the touch down of the helicopter.

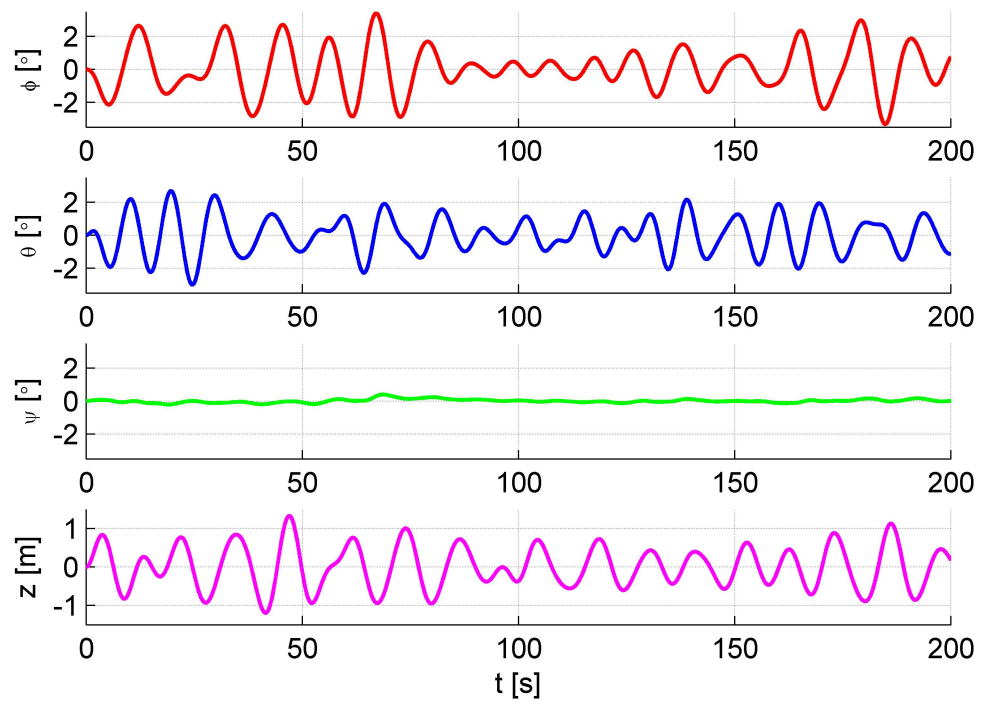


Figure 2.14.: Example of the Ship Dynamics

3. Development of a Simulator Campaign for a Helicopter Ship Deck Landing

In this chapter the simulator campaign is going to be developed. The flight task is defined before the simulation environment that has to be built is described. In the end of this section the test matrix is defined.

In [42] Carignan et al. propose the superslide task as a maritime MTE for a shipborn recovery task. For this the in section 1.2.2 presented MTEs were combined to form a new MTE. The superslide task is started at hover position 20 feet above ground and 40 feet to the left of the task area. After the lateral translation to the high hover position with a groundspeed of approximately 10 knots the hover position should be maintained for about 30 seconds. To imitate the ship movement the hover board is also movable. In a quiescent period the pilot should translate to the low hover position and maintain this position for about 5 seconds. The pole offers two targets, for the high and low hover positions. The task and the according limits are defined for a cargo/utility rotorcraft in a good visual environment (GVE). The conducted flight trials were flown with a Bell 205 with rate damped controller. The objectives of this maritime MTE are to check the ability to transition from translating flight to a stabilized hover and the ability to maintain precise relative position, altitude and heading. Another objective is to check for suitable vertical axis handling and for objectionable axes cross-coupling. Furthermore the handling qualities for aggressive manoeuvring at simulated sea states should be checked with this flight task. In Tab. 3.1 the desired and adequate boundaries are described according to [42].

Table 3.1.: **Desired/Adequate Boundaries of the Superslide Task**

Superslide Task	Desired	Adequate
Achieve a target airspeed of X knots	10	10
Maintain a stabilized hover for at least X seconds	30	30
Maintain the longitudinal and lateral position within +/- X ft	5	10
Maintain altitude within +/- X ft	5	10
Maintain low-hover position for at least X seconds	5	5

3.1. Definition of the Flight Task

According to the described MTEs, the flight task for the planned simulator campaign is determined within this section. The benefit of the superslide task proposed in [42] is the kind of abstraction of the helicopter ship deck landing procedure that is inspired by existing MTEs. In comparison to a helicopter ship deck landing the superslide task is easier and more precise to define. A well defined flight task is important to achieve a reproducible and reliable experimental setup that is needed to compare the results of different test points and pilots. Another advantage of the superslide task compared to the hover task is the movable hover board that changes the character of the flight task from an open-loop control input of the pilot to a closed-loop control input. Therefore it is chosen as a suitable flight task. As an extension of the original superslide task and due to the capability of the simulation environment, the turbulent airwake of a frigate is implemented. Furthermore, the helicopter is going to be flown with a 3-axes stability augmentation system (SAS) control input. The longitudinal, lateral and pedal control inputs are stabilized, whereas the collective control input is not stabilized. This should lead to a workload reduction to improve the pilot's capability to better focus on the motion system. The flight task will be adapted within this section.

During the planned simulator campaign only the sidestep manoeuvre and the hover task of the superslide task will be carried out. The available flight test data that is used for the offline tuning of the motion system was recorded during an earlier simulator campaign with a hover task in a turbulent environment. To receive motion sets that are as reliable as possible, the helicopter's accelerations of the recorded flight test data and the planned simulator campaign have to be comparable. Otherwise the generated motion sets might be not applicable. This excludes commanded heave movements with higher accelerations. For the same reason the sidestep manoeuvre has to be attenuated due to its original characterization in [19] as an aggressive manoeuvre. This also gives the opportunity to test

the capability of the motion system in a wider range without violating the limits.

According to [42] the desired and adequate boundaries were defined for a utility/cargo helicopter in a GVE as documented in Tab. 3.1. For the above mentioned reasons adoptions have to be made that are shown in Tab. 3.2. To minimize the aggressiveness during the sidestep manoeuvre no specific airspeed should be achieved. Instead a timespan to attain a stabilized hover is defined to define the sidestep manoeuvre adequately. Because the vertical manoeuvre is not carried out the timespan to maintain low-hover position is no longer needed.

Table 3.2.: **Desired/Adequate Boundaries of the adapted Superslide Task**

Adapted Superslide Task	Desired	Adequate
Attain a stabilized hover within X seconds	15	25
Maintain a stabilized hover for at least X seconds	30	30
Maintain the longitudinal and lateral position within +/- X ft	5	10
Maintain altitude within +/- X ft	5	10

3.2. Set up of the Test Environment

The basic design of the task is shown in Fig. 3.1 and 3.4. When viewed side on during hovering the helicopter stands in line with the target and the moving hover board. The distances x_1 and x_2 are taken from an already existing superslide task at the simulator and are documented in Tab. 3.3. The use of the targets is demonstrated in Fig. 3.2 where the relations target to hover board are shown for the cases "desired", "adequate", and "not adequate". To calculate the dimensions of the target and the hover board the geometric correlations are used as shown in detail in Fig. 3.3. The eyepoint EP_1 lies on the border between desired and adequate whereas the eyepoint EP_2 is located on the border between adequate and not adequate. h_{31} and h_{32} correspond to the altitude desired and adequate boundaries of the superslide task in Tab. 3.2. With the intercept theorem the height of the target and the hover board h_2 and h_1 is calculated in equations 3.1 and 3.2.

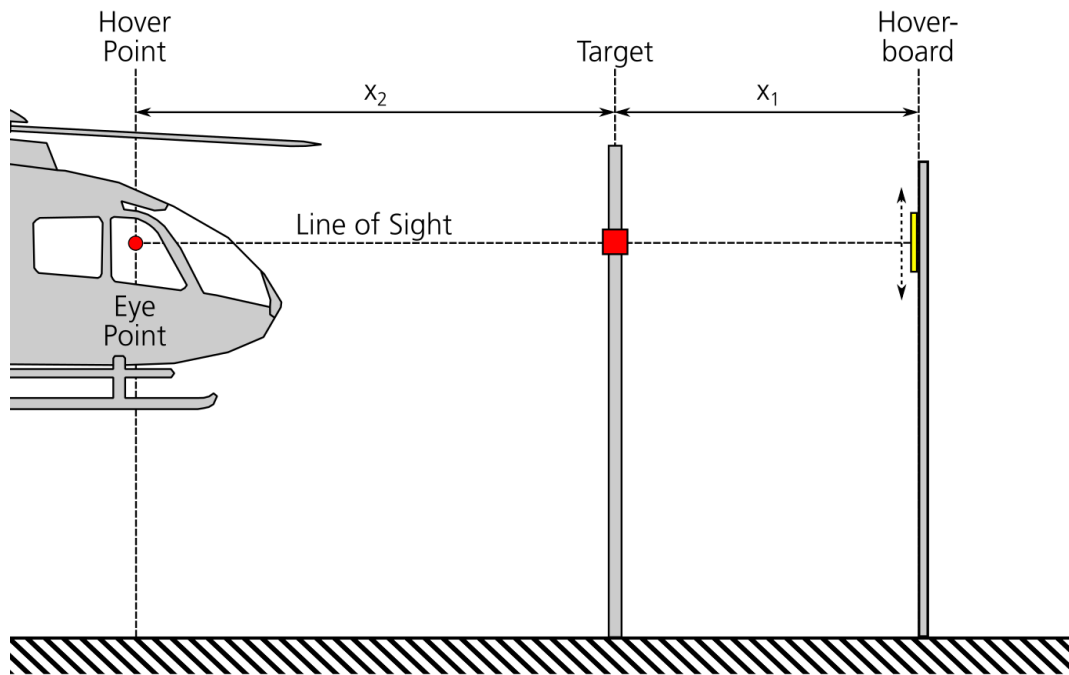


Figure 3.1.: Superslide Task - Side View

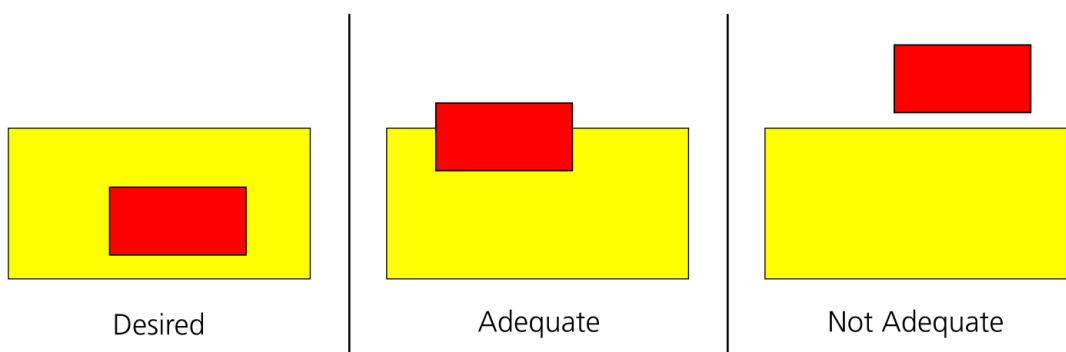


Figure 3.2.: Desired/Adequate Target Boundaries

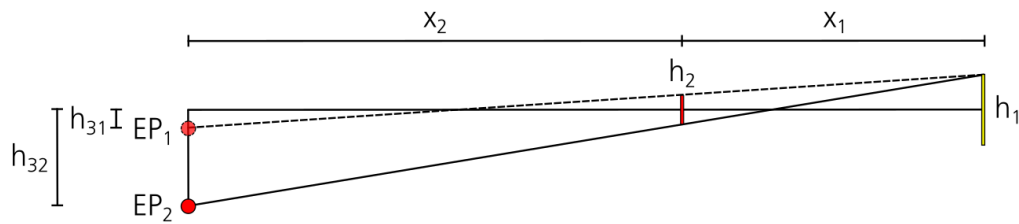


Figure 3.3.: Superslide Task - geometric Correlations

$$\frac{h_1 - h_2}{x_1} = \frac{h_2 - h_{31}}{x_2} \quad (3.1)$$

$$\frac{h_1 + h_2}{x_1} = \frac{h_{32} - h_2}{x_2} \quad (3.2)$$

Table 3.3.: Distances of the adapted Superslide Task

Parameter	Distance [m]
x_1	12.2
x_2	33.5
y_a	8.3
y_b	18.5
dx	1.5
dy	1.5
h_1	1.22
h_2	0.55
h_{31}	1.5
h_{32}	3.0

Fig. 3.4 shows the top view of the superslide task. Additionally the green, yellow and red shaded areas indicate the desired, adequate and not adequate boundaries in longitudinal direction. The distance between the pylons dx correspond to the desired/adequate boundaries in Tab. 3.2. The pilot can use the pylons as a visual reference for the longitudinal positioning of the helicopter. Due to the use of the turbulent airwake of a F124 "Sachsen class" frigate, the design must offer the opportunity for the pilot to predict the type of air turbulence adequately. The distances y_a and y_b are adjusted according to the geometric dimensions of the frigate. y_a corresponds to the half of the width of the landing

deck. y_b is an estimation of the hover point at the port side of the ship before the lateral translation of the helicopter. Due to missing references in the literature, y_b was defined as the lateral position two rotor radii away from the edge of the ship landing deck. The wind field was placed in lateral and longitudinal direction, so that the geometry of the task environment and of the frigate fit each other. In addition, the height of the airwake was chosen in such a way, that it corresponds to the altitude difference during the vertical manoeuvre. In the beginning of the manoeuvre the distance between landing skid and ship deck is about 2.28 m.

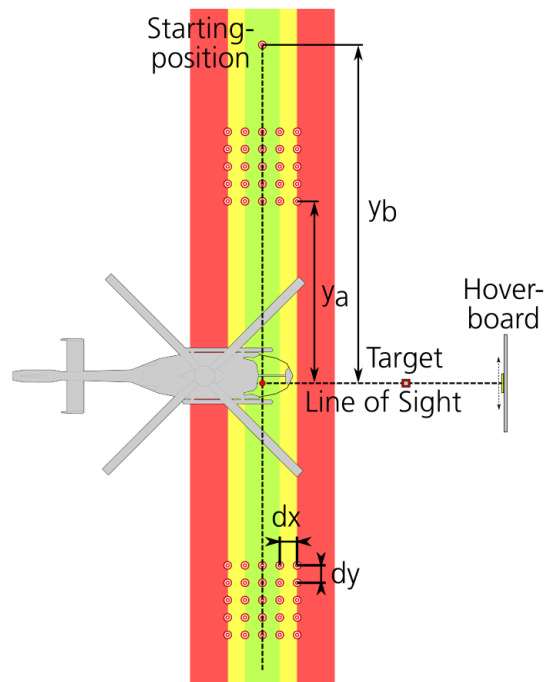


Figure 3.4.: **Superslide Task - Top View**

Although in [42] a general frequency bandwidth and magnitude is given for the ship movement, during the simulator campaign VehicleControl is used to control the movement of the hover board. In order to generate the correct ship movements corresponding to different sea states (SS), the corresponding wave heights in Tab. 3.4 are used.

During the campaign the unsteady airwake of the F124 "Sachsen class" frigate is used. The airwake based on computational fluid dynamics (CFD) solutions. The wind conditions used are a global wind speed $V_{W,G}$ of 49 kts and a relative side slip angle β of 0° to the ship. As shown in Fig. 3.5 the strongest turbulences are located behind the ship superstructures

at the landing deck. According to the flight task the pilot starts in a calm environment. After the lateral translation to the hover point the helicopter should be influenced by the high-frequency turbulence of the ship superstructures.

Table 3.4.: **Sea State Code from the World Meteorological Organization (WMO) [11]**

Sea State Code	Description of the Sea	Significant Wave Height [m]	Wind Speed [kts]
0	Calm (Glassy)	0	0 - 3
1	Calm (Rippled)	0 to 0.1	4 - 6
2	Smooth (Wavelets)	0.1 to 0.5	7 - 10
3	Slight	0.5 to 1.25	11 - 16
4	Moderate	1.25 to 2.5	17 - 21
5	Rough	2.5 to 4	22 - 27
6	Very Rough	4 to 6	28 - 47
7	High	6 to 9	48 - 55
8	Very High	9 to 14	56 - 63
9	Phenomenal	Over 14	64 - 118

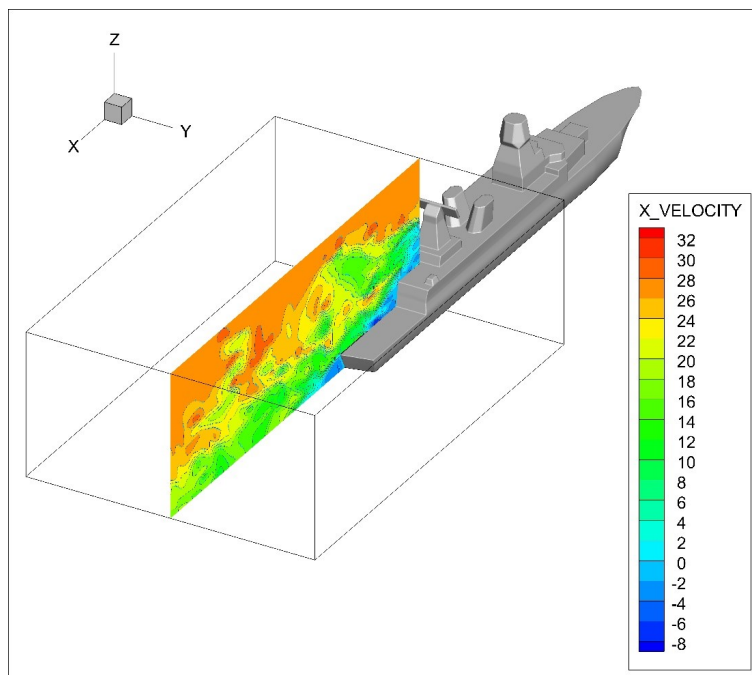


Figure 3.5.: **Unsteady Airwake of a F124 "Sachsen class" Frigate**

To also use the airwake that was computed for a wind speed $V_{W,G}$ of 49 kts for smaller wind speeds, the scaling method by Hodge et al. [13] is used. It is based on a constant Strouhal number S_t as shown in equation 3.3. It is assumed that the frequency content of an airwake f_W scales with the wind speed $V_{W,G}$ and the ship size, represented by the characteristic body dimension d . For example, if the desired wind speed $V_{W,G}$ is half that as high as the one used in the original airwake, then the velocity would be halved and the airwake would also be replayed at half the speed.

$$f_W = \frac{V_{W,G} S_t}{d} \quad (3.3)$$

3.3. Design of the Test Matrix

The test matrix is shown in Tab. 3.5. As a baseline reference two scenarios were chosen. Due to different SS one baseline is the case SS 0 without any turbulences and ship movements. Another baseline is drawn by the case without motion NO. Both should give a sufficient frame to other test points. These vary according to the SS and the motion set. For this three different SS and five different motion sets are used. The maximum SS is defined according to offshore operational limits of the helicopter and offshore mean wind speed. For offshore operations, helicopters have to be equipped with an Emergency Floatation System (EFS) [43]. Most helicopters are certified with an EFS up to SS 4. In [44] the mean wind speed at 10 m above the sea surface in german offshore territory is 20 kts. For this the maximum SS is defined as SS 4. The third SS in the test matrix is defined as SS 2 to show the course between the minimum and maximum SS. In addition to the motion set NO without any motion feedback to the pilot, another four motion sets have to be defined. As shown in Tab. 3.5 the test matrix contains a standard motion set ST that is based on the results of Hodge et al. [4]. As a starting point for an offline motion tuning, enough spare capacity for a tuning procedure must be present. For this the motion set ST was adapted as shown in Tab. 4.7. After the offline tuning three additional motion sets should be derived. Motion set TRA is a motion set based on motion set ST where only the translational gains $K_{x,y,z}$ and second order frequencies $\omega_{x,y,z}$ are tuned. Motion set ROT is a motion set where only the rotational gains $K_{\phi,\theta,\psi}$ and second order frequencies $\omega_{\phi,\theta,\psi}$ are tuned. Motion set OP is an optimized motion set where every gain K and second order break frequency ω is tuned.

Finally, the subjective rating scales for the pilot questioning have to be chosen. Because different turbulences are used the pilot's impression of the turbulence is important. The

pilot has to give a rating based on the turbulent air scale [45] shown in Tab. 3.6. With this scale the turbulence is divided into five major groups and ten finer ratings. Those are accompanied by a short statement that the pilot can compare to his impression.

Table 3.5.: Test Matrix including Number of the Test Points

	Sea State Global Wind	SS 0 0 kts	SS 2 10 kts	SS 4 20 kts
Motion Set	NO	1	6	11
	ST	2	7	12
	TRA	3	8	13
	ROT	4	9	14
	OP	5	10	15

Another indicator that might be important and must be rated is the workload of the pilot. For this purpose the Bedford Workload Rating (BWR) [6] is used. As shown in Fig. 3.6 BWR is based on a decision tree in four levels based on the HQR [32]. The pilot starts in the bottom left corner and is guided through the major workload levels with questions. Afterwards each rating is accompanied with a short statement. The pilot is able to compare those statements to his impression. A secondary task is helpful, because it is easier to rate the spare workload capacity instead of the workload itself [6]. As a secondary task the pilot is asked to give a regular feedback every 3 seconds on the radar altitude and groundspeed of the helicopter.

Table 3.6.: Turbulent Air Scale

Scale	Definition	Air Conditions
1	-	Flat calm
2	Light	Fairly smooth, occasional gentle displacement
3		Small movements requiring correction if in manual control
4	Moderate	Continuous small bumps
5		Continuous medium bumps
6		Medium bumps with occasional heavy ones
7	Severe	Continuous heavy bumps
8		Occasional negativ "g"
9	Extreme	Rotorcraft difficult to control
10		Rotorcraft lifted bodily several hundreds of feet

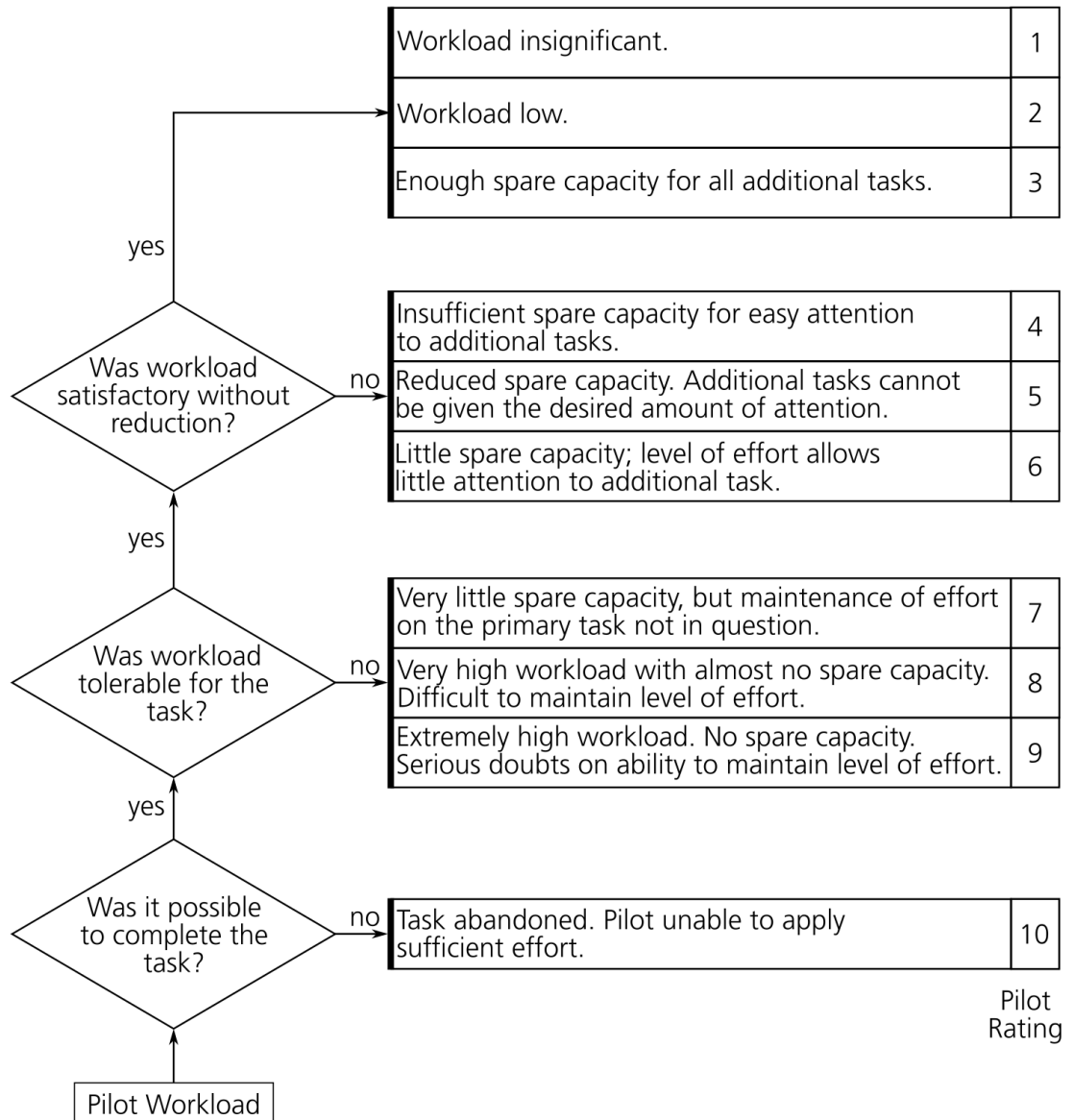


Figure 3.6.: **Bedford Workload Rating according to [6]**

As a third rating scale the motion rating by Jones [2] is used to get a feedback of the pilot's impression of the motion feedback (see Fig. 2.8). In comparison to the motion rating by Hodge [24] (see Fig. 2.9) the main advantage of the used one is the differentiation between the rotational and the translational axes. This can lead to a better understanding of the

motion set. All in all these ratings lead to a better comparison between the different test points and the different pilots.

At the end of this chapter the flight test cards are given that are used to document the test trials properly. These are found in the appendix at section A in the Fig. A.1-A.3.

4. Methodology of an MDA Implementation and Optimization

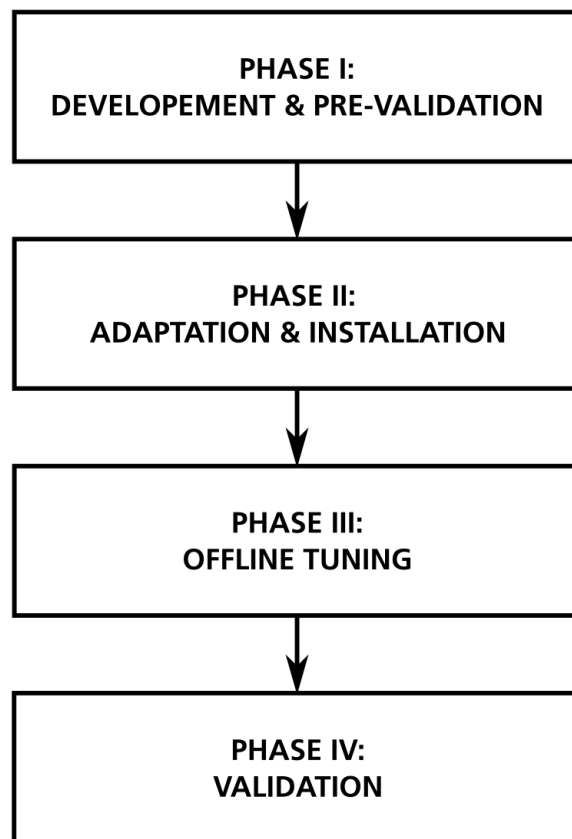


Figure 4.1.: Developed Methodology of an MDA Implementation and Optimization

The applied methodology can be separated into four phases, where one phase builds on another as shown in Fig. 4.1. During the first phase the basic MDA is built and pre-validated. During the second phase the MDA gets adapted according to the interface and installed into the simulator environment. Another part of validation proves that the MDA correctly works together with the simulator. The third phase is called "offline tuning". Within this phase tuning sets for the MDA are generated with a GA and the fitness function. To ensure the results are as reliable as possible the motion envelope gets determined and checked whether it is within the motion limits. In the fourth phase the final validation is carried out. The MDA in combination with the determined tuning sets is tested in piloted and unpiloted test trials.

4.1. Construction and Pre-Validation of an MDA

According to the flowchart in Fig. 4.2 the basic MDA was built first. In this case the CWA (see Fig. 2.3) by Reid and Nahon [1] was chosen. The HP-Filter was designed as a third order transfer function where the LP-Filter was a second order transfer function.

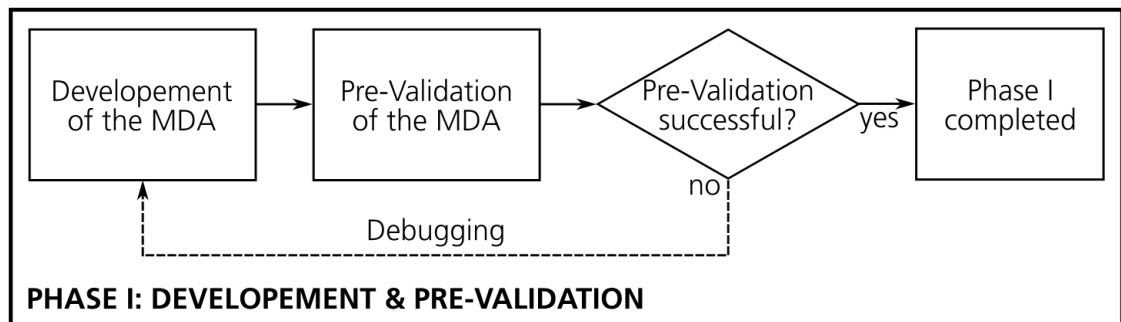


Figure 4.2.: Phase I - Development & Pre-Validation

In a second step the CWA was pre-validated. Easy test signals were used instead of complex flight test data. The first test scenario is based on a well documented example in [1], section 5.6. Reid and Nahon used an acceleration pulse in x direction in combination with motion set A in Tab. 4.1 and a rate limiter of $5.8^\circ/s$. This test case represents the longitudinal acceleration of a starting aircraft. The generated input and the corresponding output are documented in [1] in the figures 5.5, 5.10 and 5.11. This was repeated with the new constructed CWA. Fig. 4.3 shows the input signals. In the longitudinal direction the acceleration pulse starts at 1 s with a magnitude of 1 m/s^2 and is held for 10 s before

turning back to zero. The simulator response is shown in Fig. 4.4. The characteristic spikes at a_x are caused by the input pulse in combination with the HP filter. All displacements turn back to zero as time increases. Therefore the washout process was successful. In comparison to [1] the results shown in Fig. 4.4 are in a good agreement according to quality and quantity. Afterwards this test case was expanded to the other axes. The outputs are documented in the appendix in section B (see Fig. B.1-B.5). The input is similar to Fig. 4.3 and differs according to the respective input axis. In all cases the washout process was successful as all displacements return to zero as time increases.

Table 4.1.: Motion Set A according to [1]

Set	K	ω	ζ	ω_2
A	1.0	1.25	0.707	0.125

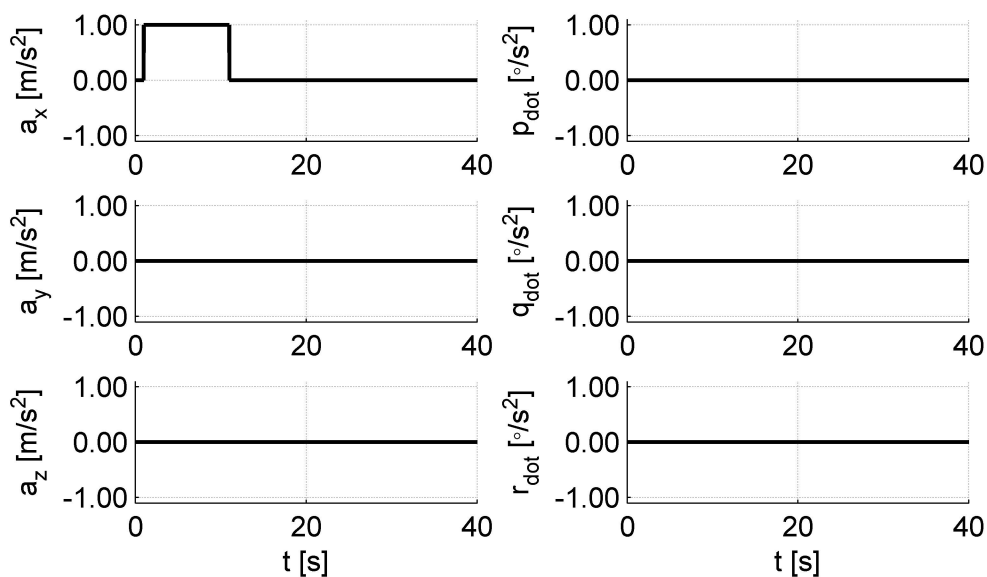


Figure 4.3.: Pulse Input of a longitudinal Acceleration

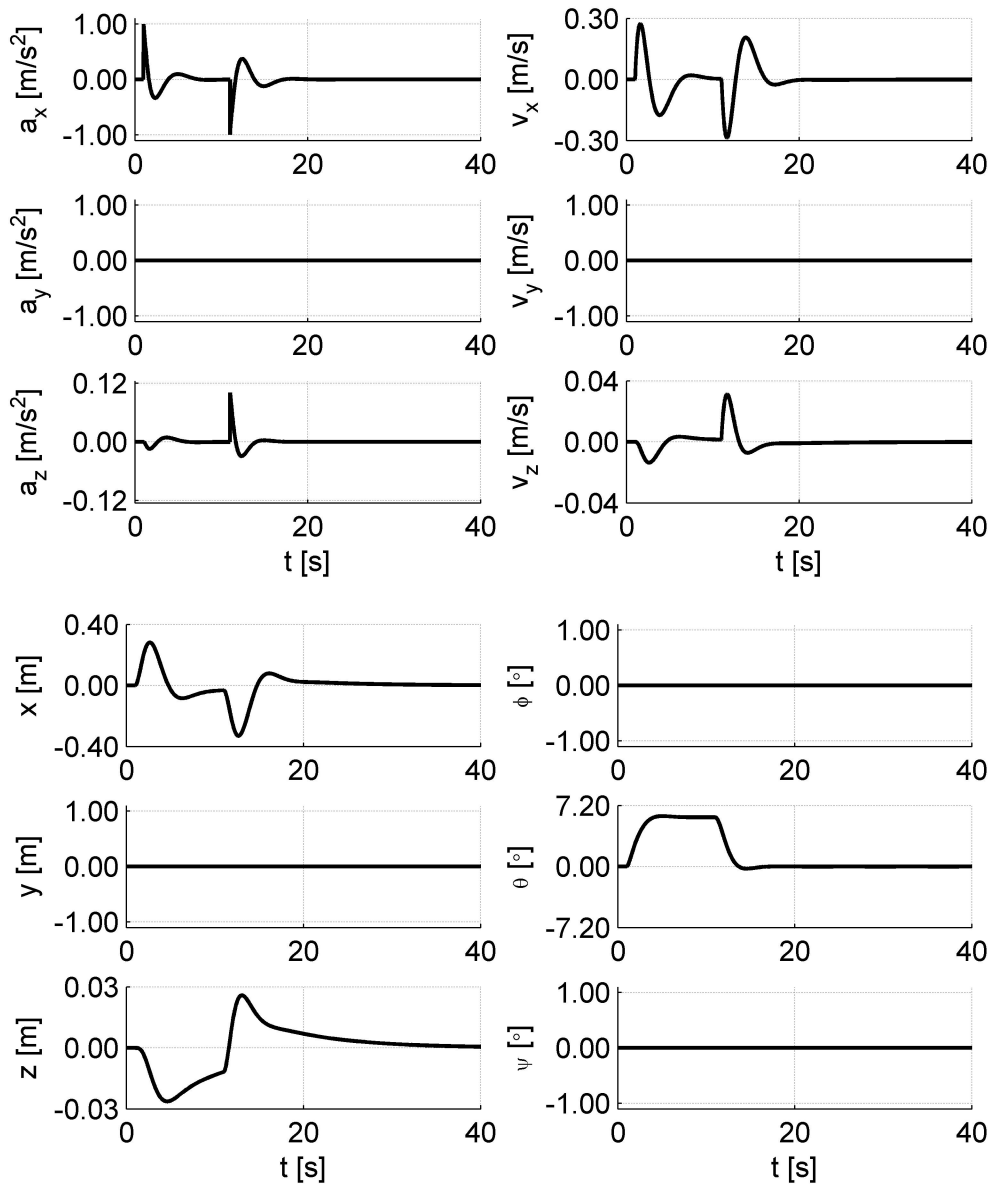


Figure 4.4.: **CWA Output according to a Pulse Input of a longitudinal Acceleration**

As a second test case an acceleration input at one axes in the shape of a ramp was generated as shown in Fig. 4.5. The output of the CWA is shown in Fig. 4.6. In the beginning the steady increasing acceleration is filtered out by HP filters. Instead the LP filters let the input through so that the translation of the input acceleration is mainly done by the tilt

coordination. As shown in Fig. 4.6 at the time plot of the pitch angle θ the sustaining acceleration in longitudinal direction leads to a positive output pitch angle θ . The result is a tilted gravitation vector with a negative longitudinal acceleration in the body frame "S" of the motion dome. This suggests the positive longitudinal acceleration of an aircraft and is the intended functionality of the tilt coordination with the LP filter. In addition to the ramp input of a longitudinal acceleration the output for a ramp input of a lateral acceleration is documented in the appendix in section B in Fig. B.6. The results for a ramp input of a lateral acceleration are plausible as well as for a longitudinal ramp input.

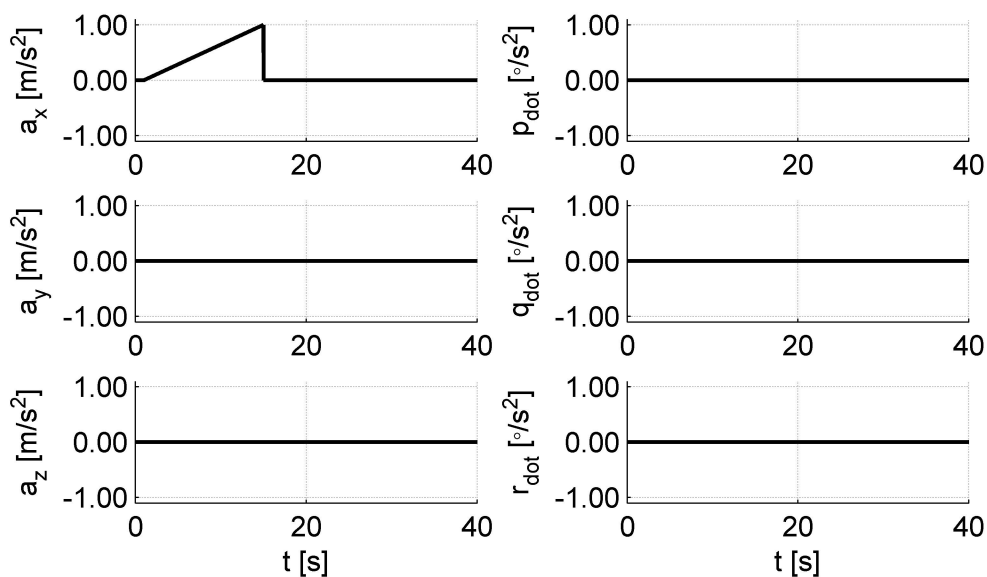


Figure 4.5.: Ramp Input of a longitudinal Acceleration

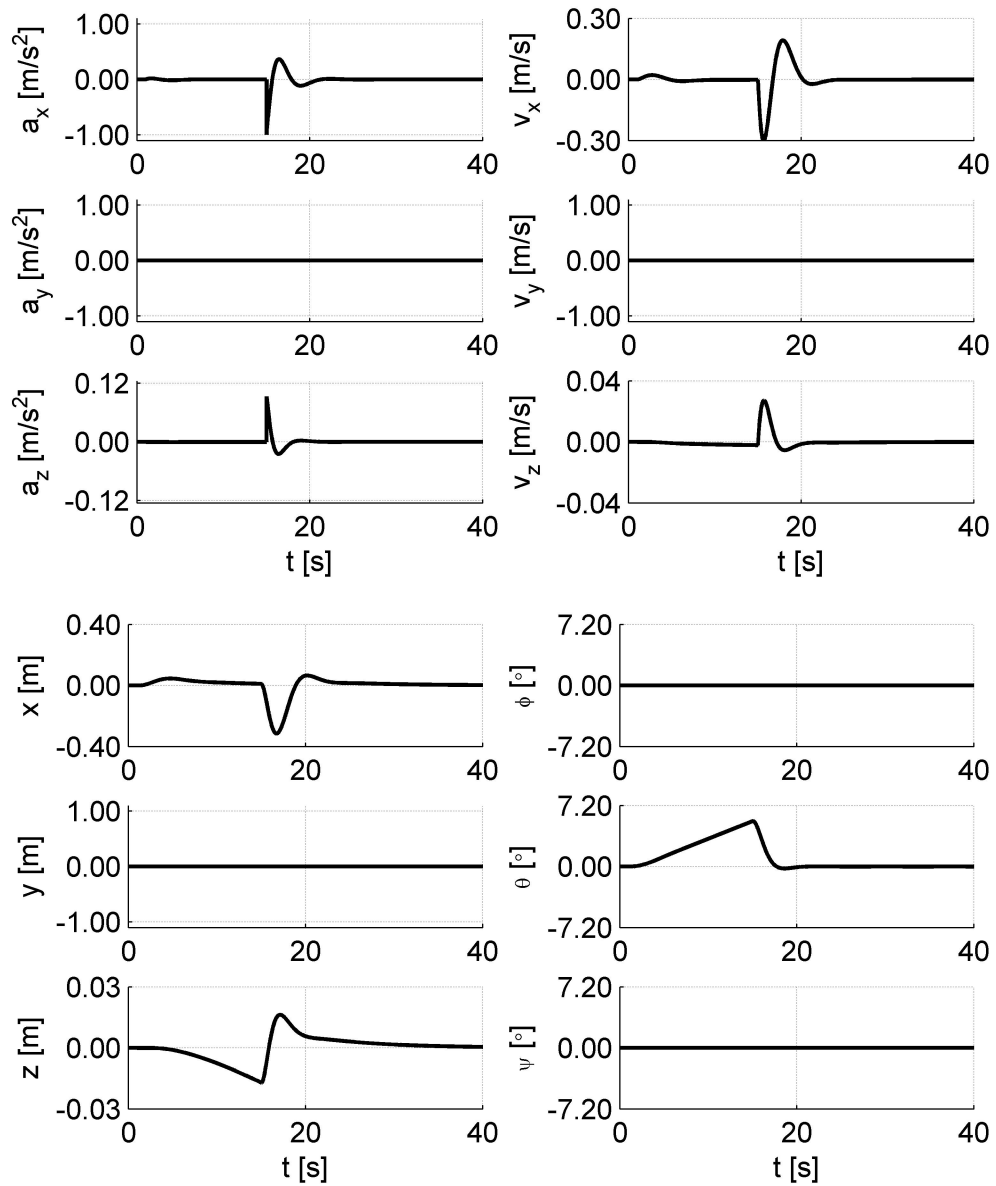


Figure 4.6.: **CWA Output according to a Ramp Input of a longitudinal Acceleration**

In the end of this pre-validation the overall structure of the CWA was tested according to the literature. Moreover with the first test the basic characteristic of the HP filter could be verified. With the second test the LP filter characteristic could be shown. The output of the tilt coordination is also plausible. After testing the main parts of the CWA everything

works as expected and phase I is completed.

4.2. Adaptation and Installation into the Simulator Environment

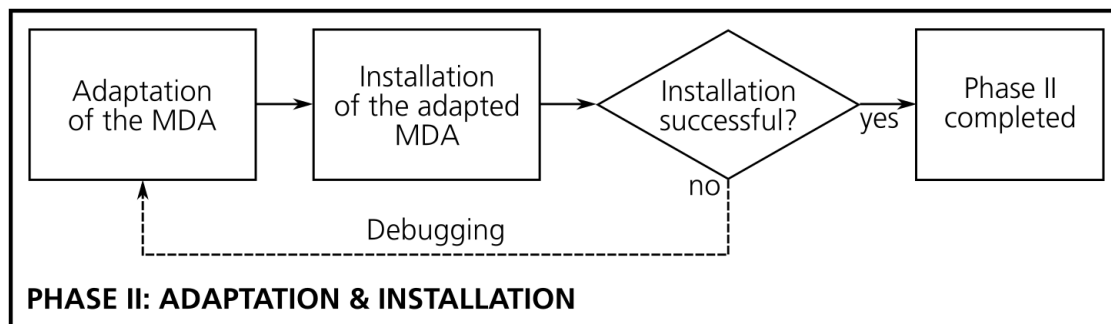


Figure 4.7.: Phase II - Adaptation & Installation

In the second phase the MDA was installed in the simulator. For preparation the CWA was embedded into the safety environment. This safety environment consists of a safety shell and a front- and back-end protection. This is to ensure that no steady accelerations with high magnitude go directly into the CWA. Furthermore it clears the input and output signals of the CWA from high frequency background noises.

In the next step of adaptation the correct interface was set up. The arrangement and the terms of the input and output signals has to be in agreement with the ones in the simulator environment. The signals relevant for the CWA are described in Tab. 4.2.

Finally, the source code of the CWA Simulink model has to be built and afterwards compiled with a 32-bit linux compiler. The built file is loaded into the motion system of the simulator. If the loading process is successful the acceptance of the new MDA by the system is proven and the first step of validation is done. The next step of validation is the verification of static stability. The helicopter in the simulation was trimmed in stable un-accelerated flight condition and the filter parameter of the MDA were set according to motion set B in Tab. 4.3 with a rate limiter of $2.0^\circ/s$. During simulation the motion system was activated via remote. The motion dome is not allowed to do any harsh movements as the helicopter in the simulation maintain its stable un-accelerated flight condition. If these do not occur, the test was successful and static stability of the implemented MDA

Table 4.2.: Interface of the MOOG Motion System

No.	Input Term	Description
1	f_aa_x_PA	longitudinal acc., body frame
2	f_aa_y_PA	lateral acc., body frame
3	f_aa_z_PA	vertical acc., body frame
4	w_aay_PA	<i>terminated, no input</i>
5	w_aax_PA	<i>terminated, no input</i>
6	w_aaz_PA	<i>terminated, no input</i>
7	w_aay_p_PA	attitude acc., roll axes, body frame
8	w_aax_p_PA	attitude acc., pitch axes, body frame
9	w_aaz_p_PA	attitude acc., yaw axes, body frame

is proven. Afterwards first flight test trials with the focus of a correct steering sense can be carried out. For example a positive roll input should lead to a positive roll movement of the motion system as well. This test should prove that the reference frames of the implemented CWA and the motion system are in agreement. In a stepwise process the gains K can be increased up to 0.3 except of the heave gain K_z . It is helpful to check one axis after another with isolated control inputs on the corresponding axis.

Table 4.3.: Motion Set B

Set	K	$\omega_{HP\phi,HP\theta,HP\psi}$	$\omega_{HPx,HPy,HPz}$	ζ	ω_2
B	0.1	0.4	2.0	0.707	0.01

The test trials have been carried out with the newly built CWA. As shown in Fig. 4.8 the accelerations commanded by the model and the measured accelerations by the dome are in a good agreement. Therefore the new CWA was successfully imported into the simulator and phase II is completed.

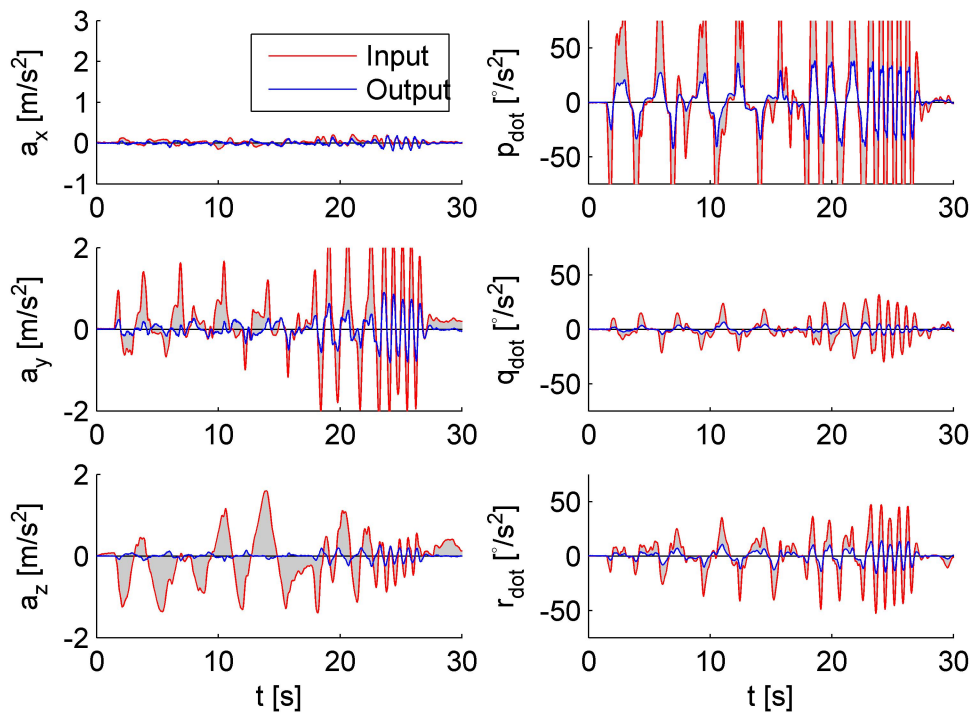


Figure 4.8.: Example: Flight Test Trial - Roll Axis

4.3. Offline Tuning with a Genetic Algorithm

In the next phase motion sets have to be defined according to the test matrix in Tab. 3.5. For this a GA was used in combination with the fitness function by Jones [46] for the optimization function. As shown in Fig. 4.9 the offline tuning that was carried out consists of the tuning process with the GA itself and an estimation of the potential motion envelope. Only if this motion envelope stays within the limits the process is successful.

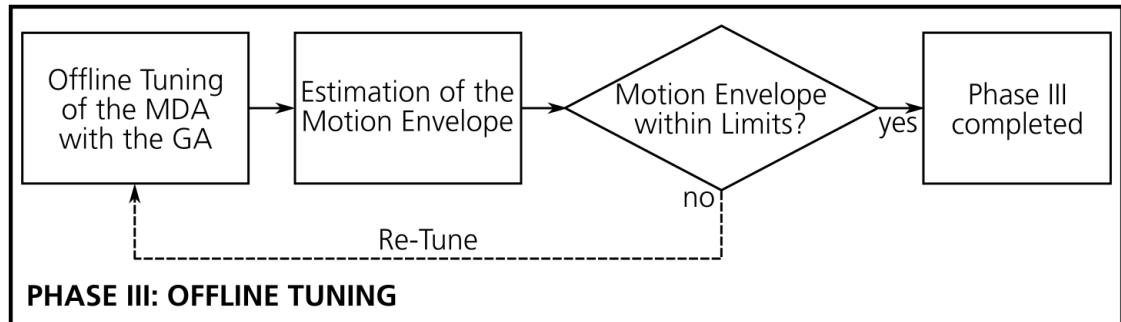


Figure 4.9.: Phase III - Offline Tuning

4.3.1. Construction of the Genetic Algorithm

A GA is a possible algorithm that is being used to solve problems with many unknowns. In the case of the offline tuning of the CWA there are up to 30 variables that have to be optimized independently of each other. The genetic algorithm is an adaptation of the natural process of evolution. Terms and mechanisms lean on the natural evolution process. One of these is the term chromosome. As shown in Fig. 4.10 a chromosome consists of several genes. Every gene stands for one optimization variable. In this example six variables are going to be optimized and therefore one chromosome consists of six genes. The value of one variable is translated from decimal to binary format. In the end a chromosome only contains a string of binary values. A population consists of a predefined number of chromosomes and builds the base of the optimization process. This process aims at making the population fitter from one generation to the next with the help of the optimization function. In this way the population evolves from one generation to the next.

This process of evolution is shown in Fig. 4.11. In this example the population consists of seven chromosomes with unknown fitness. The first step is to calculate the fitness of each chromosome with the optimization function. Before creating the new population the chromosomes are sorted according to decreasing fitness. Afterwards the population evolves by creating a new population. Only healthy chromosomes are able to reproduce. For this three mechanisms are used: survival of the fittest, crossover and mutation.

CHROMOSOME

1	2	3	4	5	6
$K_{HP,p}$	$\omega_{HP,p}$	$K_{HP,q}$	$\omega_{HP,q}$	$K_{HP,r}$	$\omega_{HP,r}$
0.4	0.7	0.5	0.6	0.2	1.7
0000100	0000111	0000101	0000110	0000010	0010001

Gene number

Variable

Value (decimal)

Value (binary)

Figure 4.10.: Structure and Information within a Chromosome

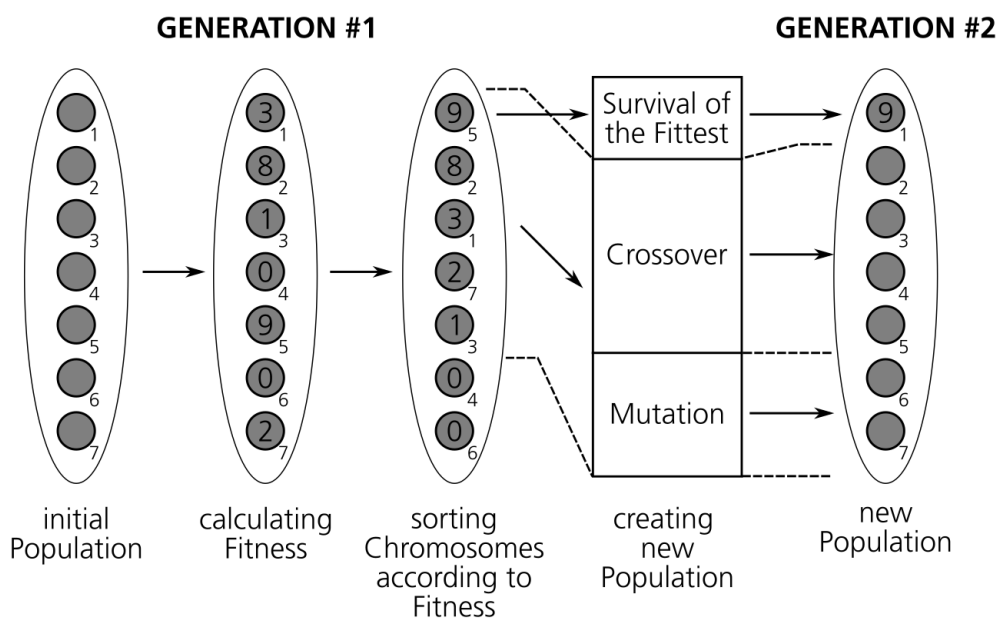
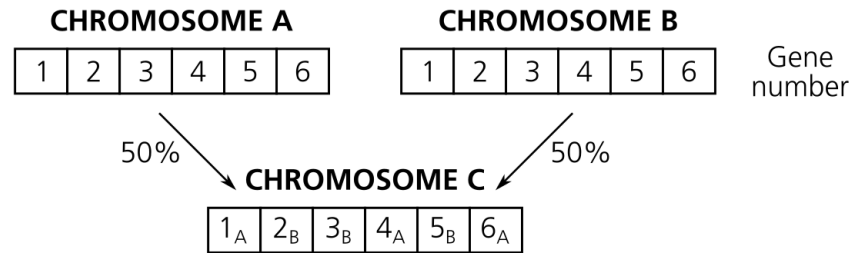
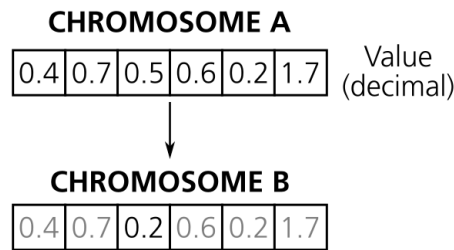


Figure 4.11.: Evolution Process of a Genetic Algorithm

The first mechanism ensures that the best solution does not get lost during the evolution process. It is called survival of the fittest. The fittest chromosome of a generation always gets directly transferred to the next generation. The crossover mechanism imitates the common reproduction process and is shown in Fig. 4.12. Two chromosomes A and B that are able to reproduce are chosen randomly. Both donate fifty percent of their genes to a recipient chromosome C. The last mechanism is called mutation and is shown in Fig. 4.13. A chromosome A that is able to reproduce is chosen. Afterwards only one gene is changed randomly. This leads to a new chromosome B, that is part of the population of the new

generation. The proportion of the crossover and mutation rate as well as the number of chromosomes have to be defined in the beginning of the optimization process. During the evolution process only the chromosomes that did not violate any limits of the motion envelope are able to reproduce. The optimization process is completed when the fitness of the fittest chromosome converges over the generations.

Figure 4.12.: **Crossover**Figure 4.13.: **Mutation**

During the development process of the GA some refinements have to be made on the GA and the fitness function. Firstly a safety margin at the motion envelope was introduced. On the one hand the GA is still able to use the full limits of the motion envelope, but if a motion set lays above a given safety margin S the fitness value F is sanctioned according to equation 4.1. The created spare capacity should help to make a motion set more applicable if the flight regime of the planned flight task differs from the flight test data more than expected.

$$F_{weighted} = \frac{F}{(\max(Limits) / S)^2} \quad (4.1)$$

Secondly, to get a more balanced solution between the axes, the fitness value $F_{weighted}$ is sanctioned depending on the variance VAR_F of the fitness values of each axis. It is multiplied according to the variance VAR_F with the values in Tab. 4.4.

Table 4.4.: Variance Factors

VAR_F	Factor
$VAR_F < 3$	$F_{weighted} \cdot 1.0$
$3 \leq VAR_F < 4$	$F_{weighted} \cdot 0.8$
$4 \leq VAR_F < 5$	$F_{weighted} \cdot 0.5$
$5 \leq VAR_F$	$F_{weighted} \cdot 0.2$

4.3.2. Execution of the GA

The optimization runs started with the starting parameters in Tab. 4.5. The evolution mechanisms crossover and mutation generate in this example 99% of the new population. Chromosomes with randomly chosen values for the genes are created to complete the population. The constants K_1 , K_2 and K_3 are selected as defined in equation 4.2.

Table 4.5.: Evolution Parameter

Parameter	Value
number of chromosomes	500
crossover rate	39%
mutation rate	60%
safety margin	60%

$$K_1 = 1, \quad K_2 = 10, \quad K_3 = 10 \quad (4.2)$$

For each motion set it was checked during the optimization runs whether the specific motion envelope stayed within the limits. Recorded flight test data was used as input for the CWA that was installed in the simulator. Due to time limitation it was not possible to produce flight test data in the final test environment. Instead, comparable flight test data was used. The data was recorded during an earlier simulator campaign with a hoisting task

at an offshore wind turbine (WT). To characterize the flight condition, Fig. 4.14 shows the power spectral density (PSD) of the accelerations. Note the higher amplitudes in low and high frequency ranges for accelerations in lateral and vertical direction. A higher amplitude was also recorded in a high frequency range for accelerations of the roll axis.

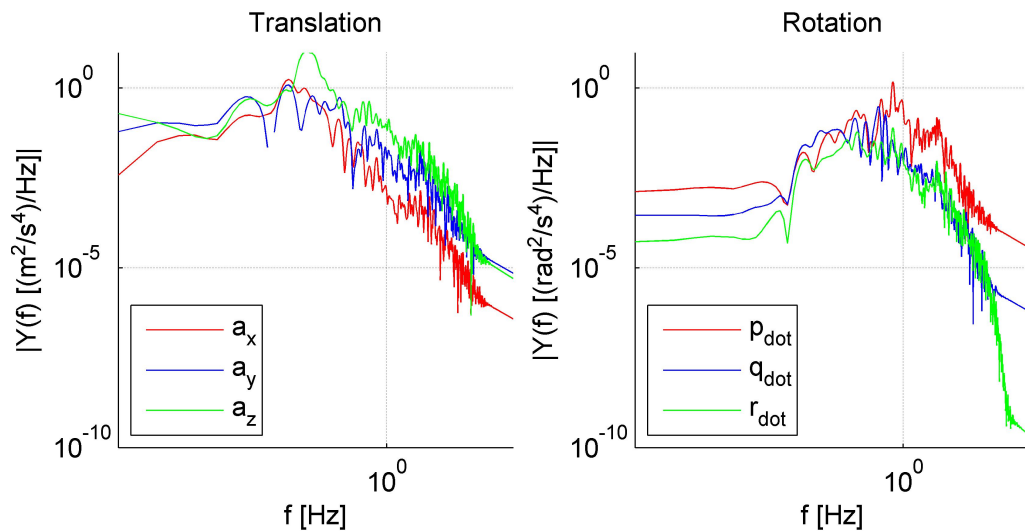


Figure 4.14.: **Characterization of used Flight Test Data**

During the simulator campaign of the used flight test data different kinds of turbulent airwakes were used. Those were varying in strength and frequency. In general they built up on CFD solutions of the unsteady airwake caused by a non rotating offshore WT with different global wind speed $V_{W,G}$. Fig. 4.15 shows the PSD of the wind velocity of the airwake at the rotor hub $V_{E,HUB}$ of the flight test data used in the GA. In comparison to the PSD of an airwake of a generic naval frigate in Fig. 8 at [47] a mismatch at the amplitude with higher frequencies was observed. This has to be taken into account during evaluation of the simulator campaign.

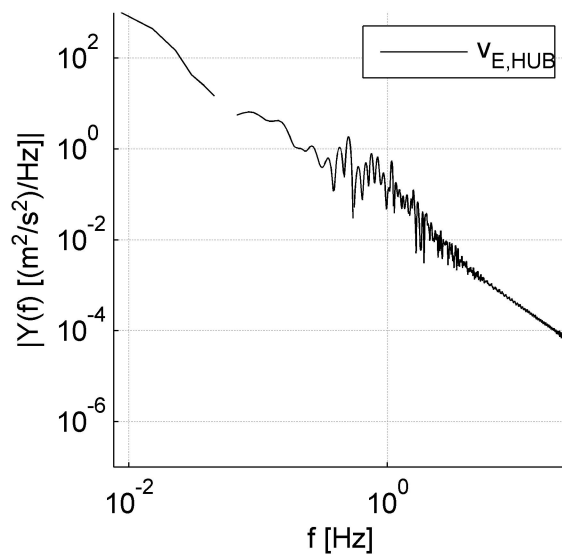


Figure 4.15.: PSD of an unsteady airwake at a WT

To reduce the computation time, the number of unknowns optimized with the GA was minimized in accordance to a literature review. This leads to predefined fixed values for the damping ratio ζ and the second angular frequency ω_2 . Moreover, the maximum gain K was limited. Those predefined parameters were summarized in Tab. 4.6 as motion set C. According to the test matrix in Tab. 3.5 four different runs with the GA were carried out.

Table 4.6.: Fixed Motion Parameter

Set	K	ζ	ω_2	rate limiter
C	< 0.8	0.8	0.01	$2.0^\circ/s$

4.3.3. Processing and Evaluation of the Results

During processing of the results the solutions of the optimization process were tested in a larger database. The database includes six files of flight test data at different test points of the same simulator campaign with a hoisting task at an offshore WT and is characterized

based on its PSD in Fig. 4.16. Those test points were varying due to different global wind speeds $V_{W,G}$ between 22 kts and 49 kts and due to an attitude command or bare airframe control input type. The spread between the PSDs of each file of flight test data within the database is marked by the grey shaded area in Fig. 4.16. As an additional reference the flight test data used in the GA is presented with a black dashed line.

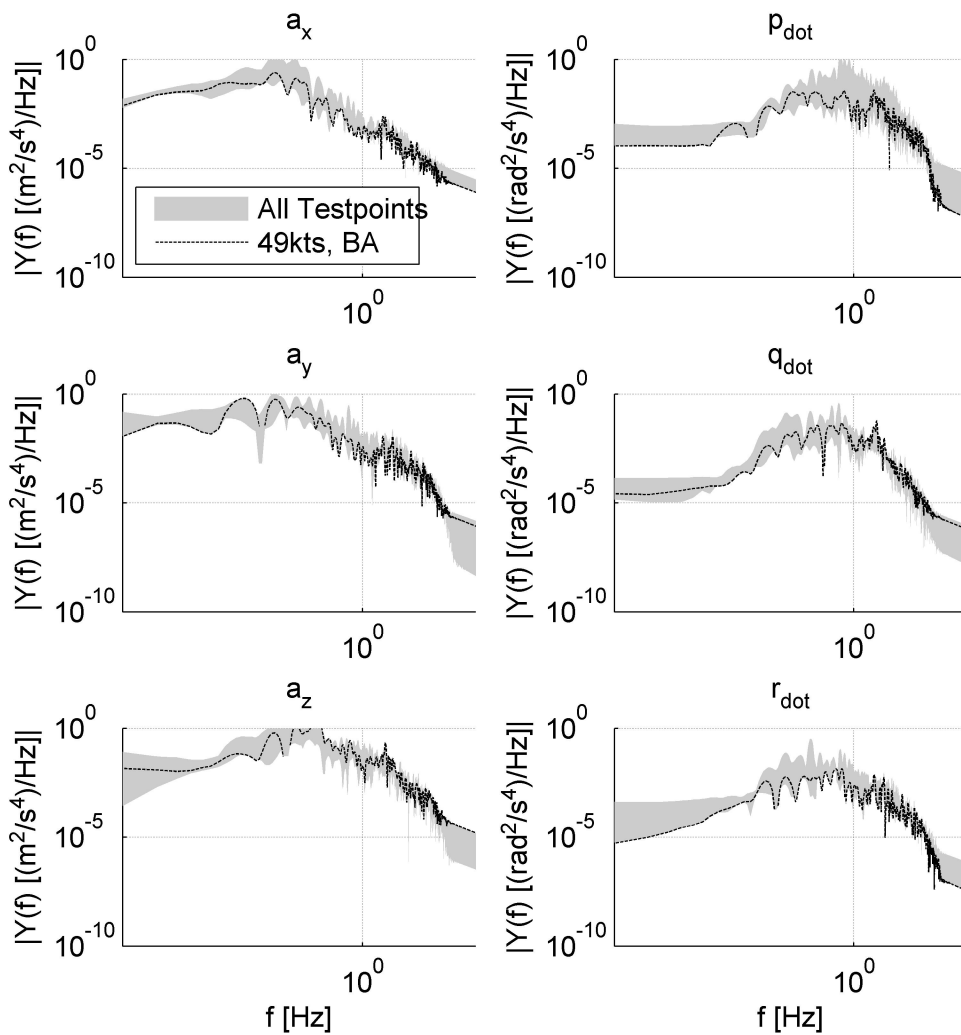


Figure 4.16.: Characterization of used Database of Flight Test Data

Afterwards a manual retuning of the parameter set was carried out while focusing on several aspects. Firstly, for all cases the motion system must stay within the physical limits of the simulator. Secondly, as little action of the rate limiter as possible should be acquired. Thirdly, due to differences between the used flight test data and the planned flight task it might not be useful to prefer one specific axis. Therefore the tuning parameter of all translational axes except for the heave axis and all rotational axes were unified. All considered, the retuning leads to an extended motion envelope and a new fitness value.

In Tab. 4.7 the final motion sets are listed. The values with grey text colour at the motion sets TRA, ROT and OP were not optimized with the GA and are directly taken from the motion set ST. The frequency response for each setting is shown in Fig. 4.17. In comparison to the motion set ST, the GA preferred slightly lower break frequencies of the LP and HP filter of the surge and sway channels $\omega_{LPx,LPy}$ and $\omega_{HPx,HPy}$ at the motion sets TRA and OP. But foremost the GA tends to significant lower break frequencies and higher gains of the rotational DoF $\omega_{HP\phi,HP\theta,HP\psi}$ and $K_{HP\phi,HP\theta,HP\psi}$ at the motion sets ROT and OP. According to the break frequency of the heave channel ω_{HPz} at the motion sets TRA and OP the heave axis was tuned down during the optimization process.

Table 4.7.: Final Motion Sets

Parameter/Set		ST	TRA	ROT	OP
Surge	K_{HPx}	0.35	0.30	0.35	0.30
	ω_{HPx}	1.40	1.00	1.40	1.00
Sway	K_{HPy}	0.35	0.30	0.35	0.30
	ω_{HPy}	1.40	1.00	1.40	1.00
Heave	K_{HPz}	0.15	0.12	0.15	0.20
	ω_{HPz}	2.00	2.50	2.00	7.17
Roll	$K_{HP\phi}$	0.35	0.35	0.60	0.60
	$\omega_{HP\phi}$	0.90	0.90	0.20	0.25
Pitch	$K_{HP\theta}$	0.35	0.35	0.60	0.60
	$\omega_{HP\theta}$	0.90	0.90	0.20	0.25
Yaw	$K_{HP\psi}$	0.35	0.35	0.60	0.60
	$\omega_{HP\psi}$	0.90	0.90	0.20	0.25
Surge LP	K_{LPx}	0.20	0.20	0.20	0.18
	ω_{LPx}	3.80	3.20	3.80	3.50
Sway LP	K_{LPy}	0.20	0.20	0.20	0.18
	ω_{LPy}	3.80	3.20	3.80	3.50

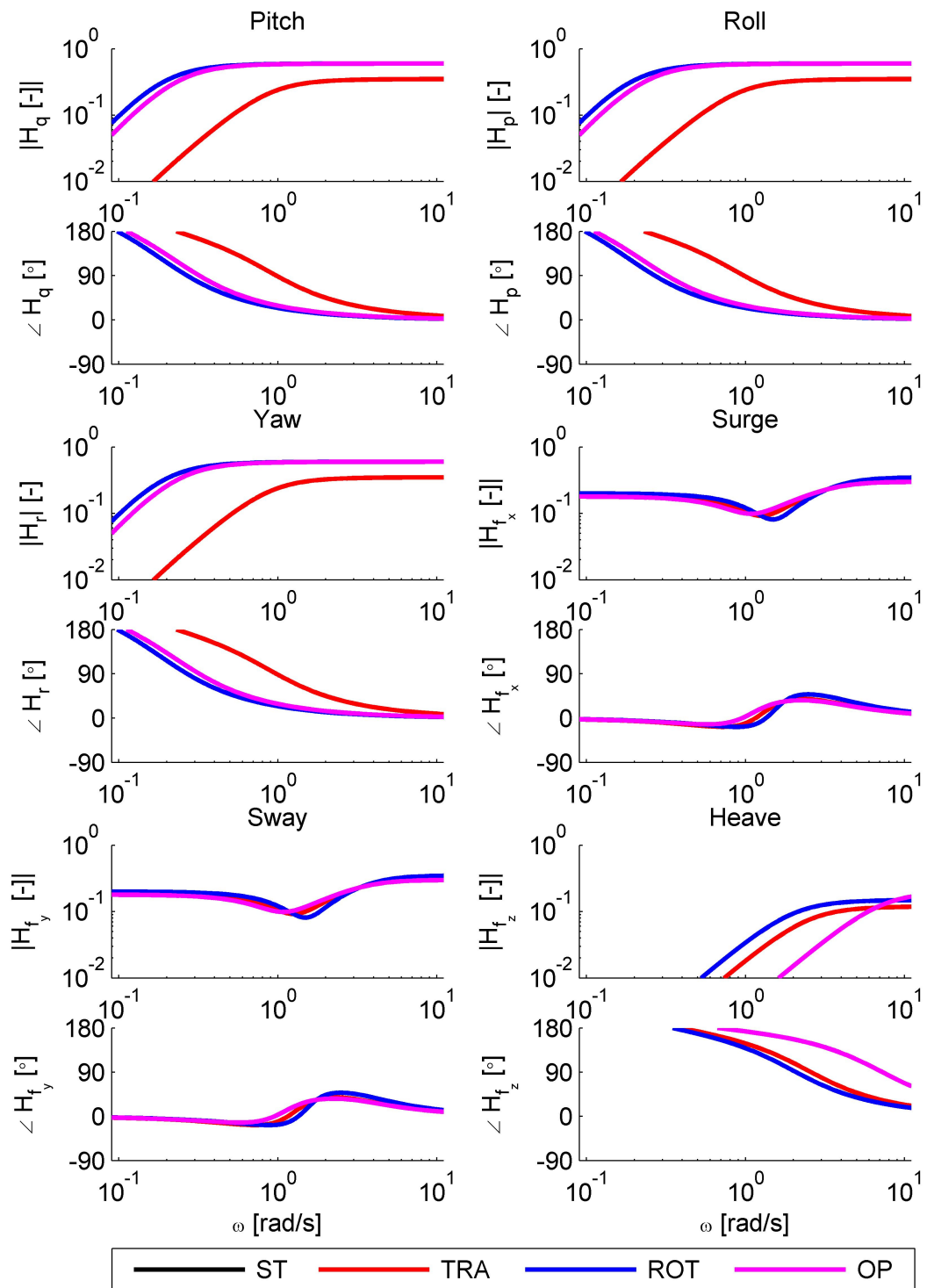


Figure 4.17.: Frequency Response of the Motion Sets

As the Sinacori/Schroeder plot in Fig. 4.18 shows, only the filter parameters of the rotational DoF of the tuning sets ROT and OP do not lay within the low fidelity area. The optimization process with the GA leads to motion sets with higher gains and lower motion phase at 1 rad/s in the rotational DoF. This also corresponds to the plot of motion break frequency ω over motion gain K in Fig. 4.19. Both plots show the same tendency at the surge/sway and heave axis, too. The deviations between the tuning sets in the surge/sway axis are small. With higher fitness they tend to smaller gains K and break frequencies ω . The heave axis is the only DoF that decreases with higher fitness.

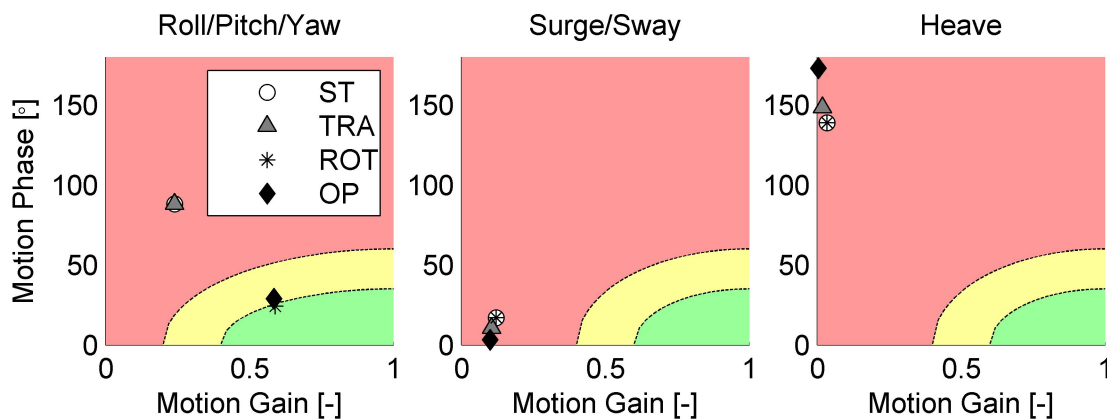


Figure 4.18.: Final Motion Settings against Schroeder Boundaries at 1 rad/s

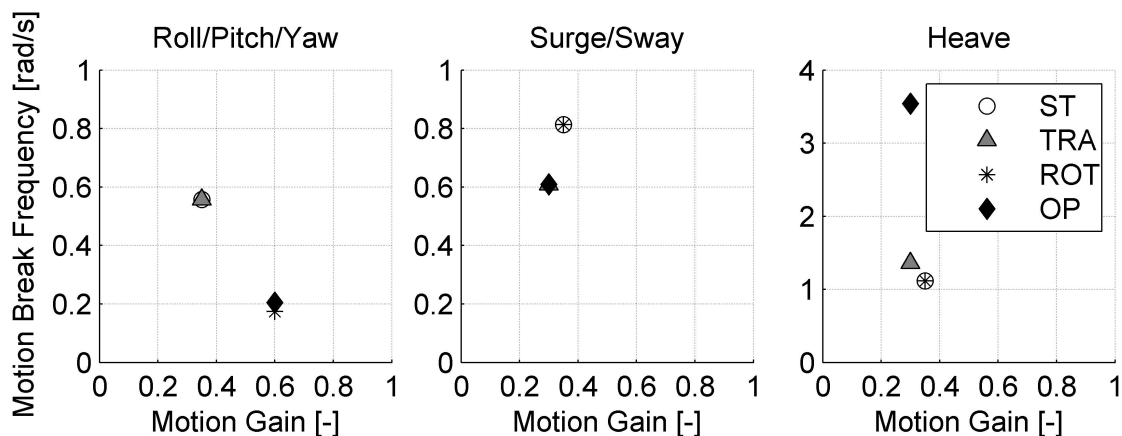


Figure 4.19.: Final Motion Settings - Break Frequencies

The motion sets and the larger database lead to the predicted motion envelopes shown in Fig. 4.20. The motion envelope is a prediction of how many percent of each limit from Tab. 2.5 is used. The maximum value of each listed parameter for each set of flight test data is determined and divided with the specific limit of Tab. 2.5. The figures list the translational and rotational values as well as the leg extensions. Due to six different runs of flight test data, the percentage span of motion used can be derived. Each mean value is highlighted by a marker. In the end the motion envelopes should offer the opportunity of predicting whether the motion system in combination with the motion sets and the flight regime of the flight test data will stay within the specified limits. During the optimization with the GA all motion sets which showed a motion limit greater than 60% were penalized. The roll movement seems to be the most critical axes. As the roll rate approaches 60% of the motion limit in the motion sets ST and TRA, it goes up to 90% in the motion sets ROT and OP. This is mainly caused by the LP filter that must be tuned down in the post-processing of the optimization results. All other limits are less critical and stay within the safety margin of 60%. Note that these motion envelopes depend on the used flight test data. If the flight regime in a planned simulator campaign differs from those characterized in Fig. 4.14, no statement can be derived from the predicted motion envelopes.

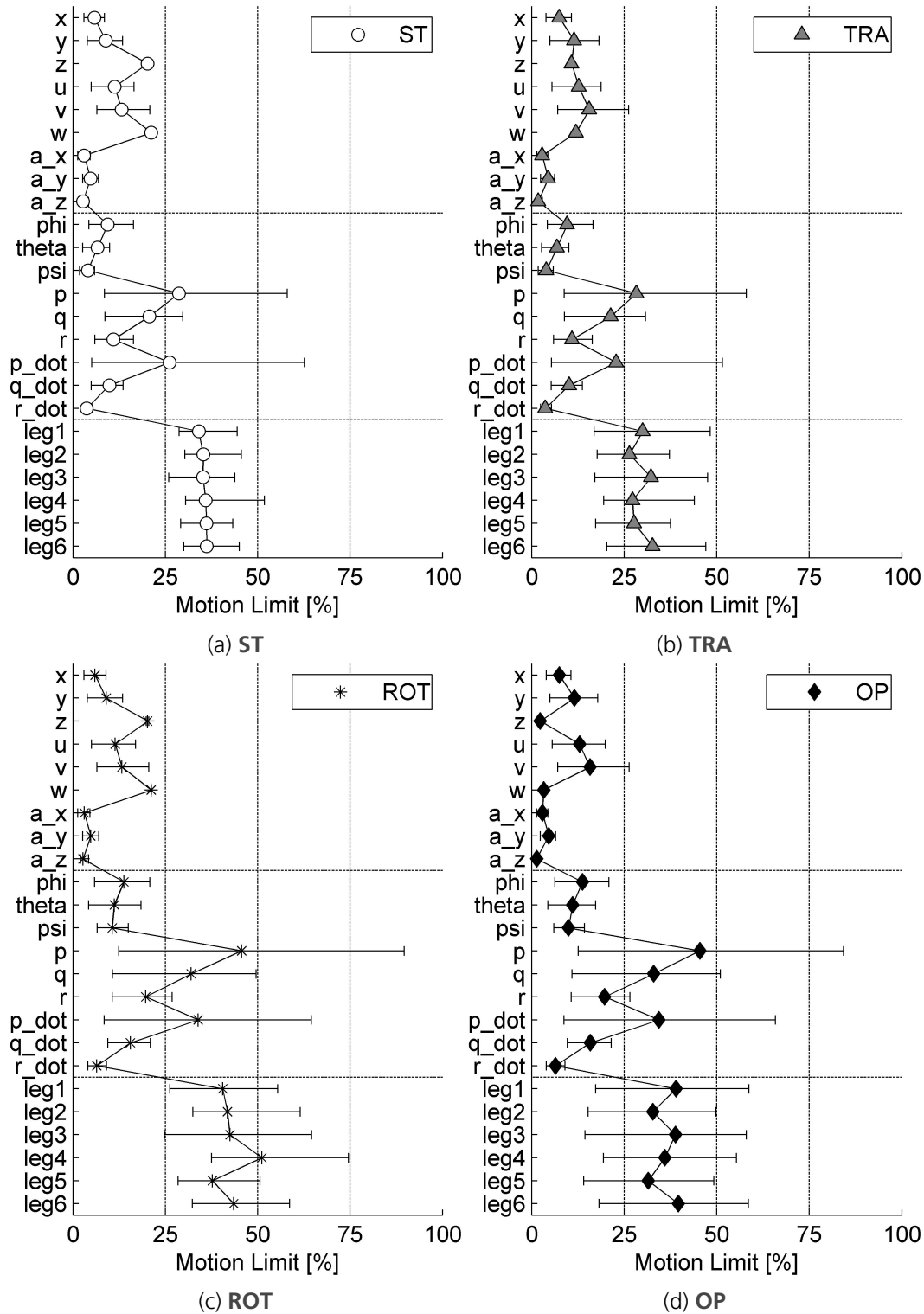


Figure 4.20.: Predicted Motion Envelope of each Motion Set

Finally, the motion sets can also be characterized due to their fitness and VMPE value. To compare the VMPE on different flight test data this value has to be normalized. For this a new method is introduced. The VMPE is based on the sum of the root-mean-square values of the difference between the accelerations of the simulated aircraft and the motion system. A baseline is marked by the case without motion. This can also be characterized with its VMPE value $VMPE_{NO}$, which is the root-mean-square value of the whole curve of the time plots for the simulated aircraft. Equations 4.3 - 4.7 sum up the normalized RMSE and VMPE values. If these values are smaller than 1, the area under the curve of the simulated aircraft is larger than the area in between the curves of the simulated aircraft and motion system. The use of motion may be an advantage.

$$RMSE_{norm,fi} = \frac{RMSE_{VMPE,fi}}{RMSE_{NO,fi}} \quad (4.3)$$

$$RMSE_{norm,wi} = \frac{RMSE_{VMPE,wi}}{RMSE_{NO,wi}} \quad (4.4)$$

$$VMPE_{norm,f} = \frac{VMPE_{RMSE-MTS-f}}{VMPE_{NO,f}} \quad (4.5)$$

$$VMPE_{norm,w} = \frac{VMPE_{RMSE-MTS-w}}{VMPE_{NO,w}} \quad (4.6)$$

$$VMPE_{norm} = \frac{VMPE_{norm,f} + VMPE_{norm,w}}{2} \quad (4.7)$$

In Fig. 4.21 - 4.24 the fitness values and the normalized VMPE for each tuning set are shown. For a better comparison, the fitness values are inverted. A smaller normalized VMPE indicates a better motion fitness as well as a smaller inverted fitness value. Furthermore, the VMPE and fitness values for each DoF are listed. Due to the large database, the VMPE can differ from one run to another. This causes a span which is also shown in the figures. In general the tendencies between the normalized VMPE and the inverted fitness value are in a good agreement to each other. Only the total VMPE and the fitness value differ due to influence of the use of the variance at the fitness function (see equation 2.17). A more balanced solution between the axes is thus expected. In addition to figures 4.21 - 4.24 the fitness values and the mean value of the VMPE are also listed in Tab. 4.8.

Table 4.8.: Fitness and mean VMPE of the Motion Sets

Set/Value	Fitness	normalized VMPE
ST	6.38	0.9124
TRA	6.67	0.8971
ROT	14.82	0.7421
OP	13.98	0.7374

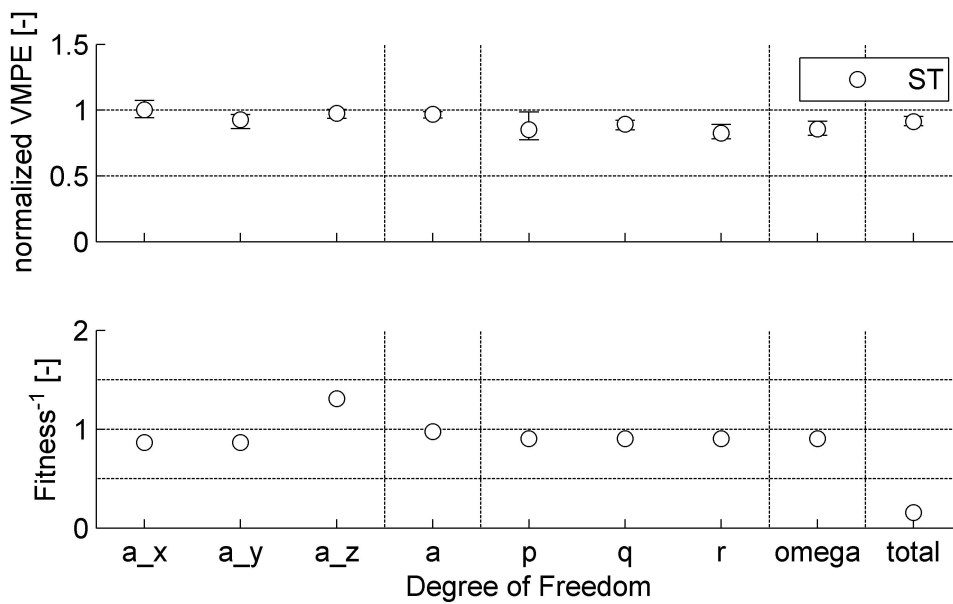


Figure 4.21.: Comparison of VMPE against Fitness Function - ST

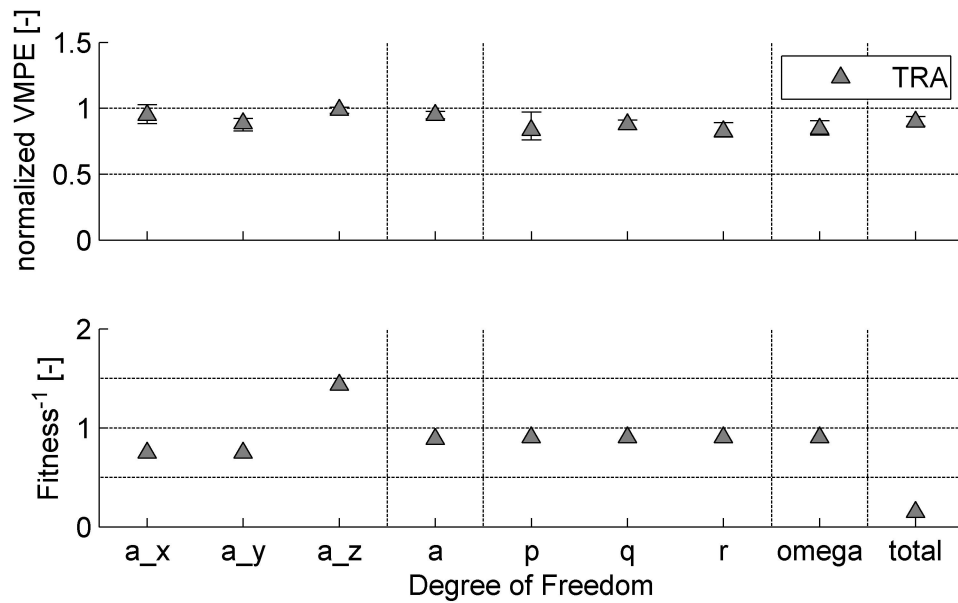


Figure 4.22.: Comparison of VMPE against Fitness Function - TRA

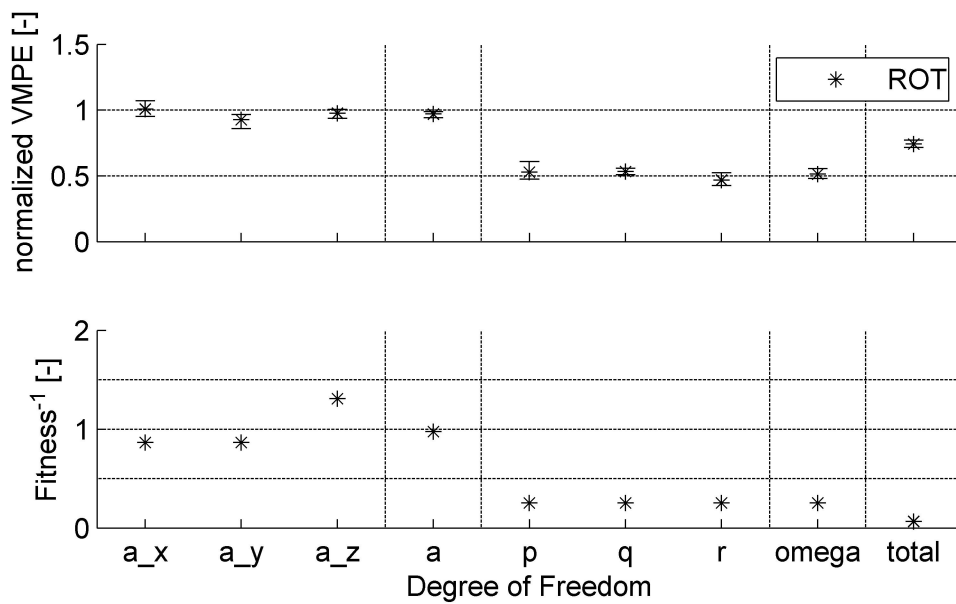


Figure 4.23.: Comparison of VMPE against Fitness Function - ROT

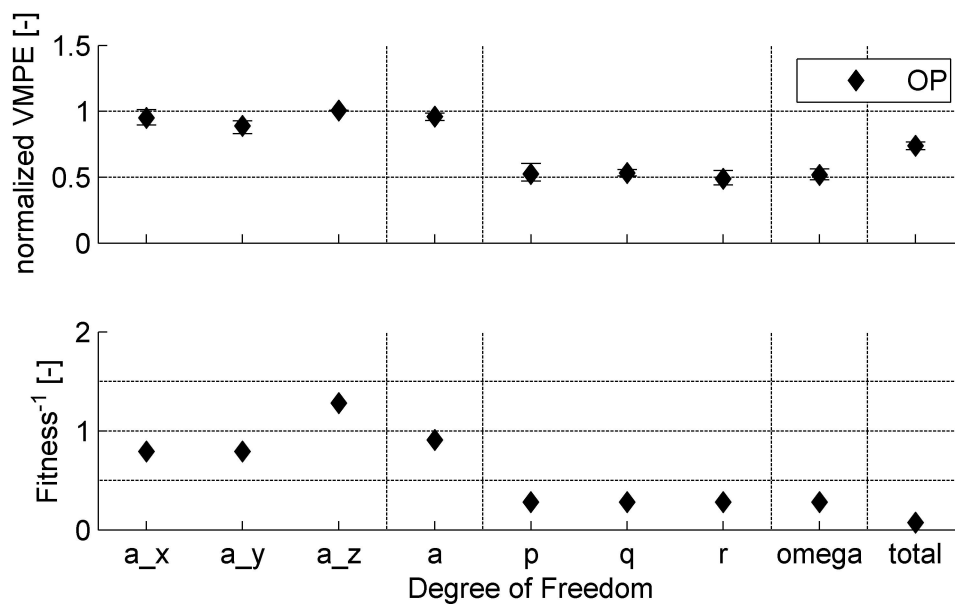


Figure 4.24.: Comparison of VMPE against Fitness Function - OP

In the end four motion sets have been derived based on an optimization process with a GA and the fitness function. All motion sets were tested in detail and characterized based on different criteria. During the prediction of the motion envelope no motion set violated any of the motion limits. According to the flowchart in Fig. 4.9 phase III is completed.

4.4. Validation of the Optimized Motion Settings

During phase IV the final validation is carried out. As shown in Fig. 4.25 this includes an unpiloted and a piloted part with subjective and objective methods. Those methods are OMCTs, ratings given by the pilots and the recorded flight test data. This section describes the execution of the OMCTs and the simulator campaign. The analysis and discussion of the results is part of the following chapter as well as the comparison.

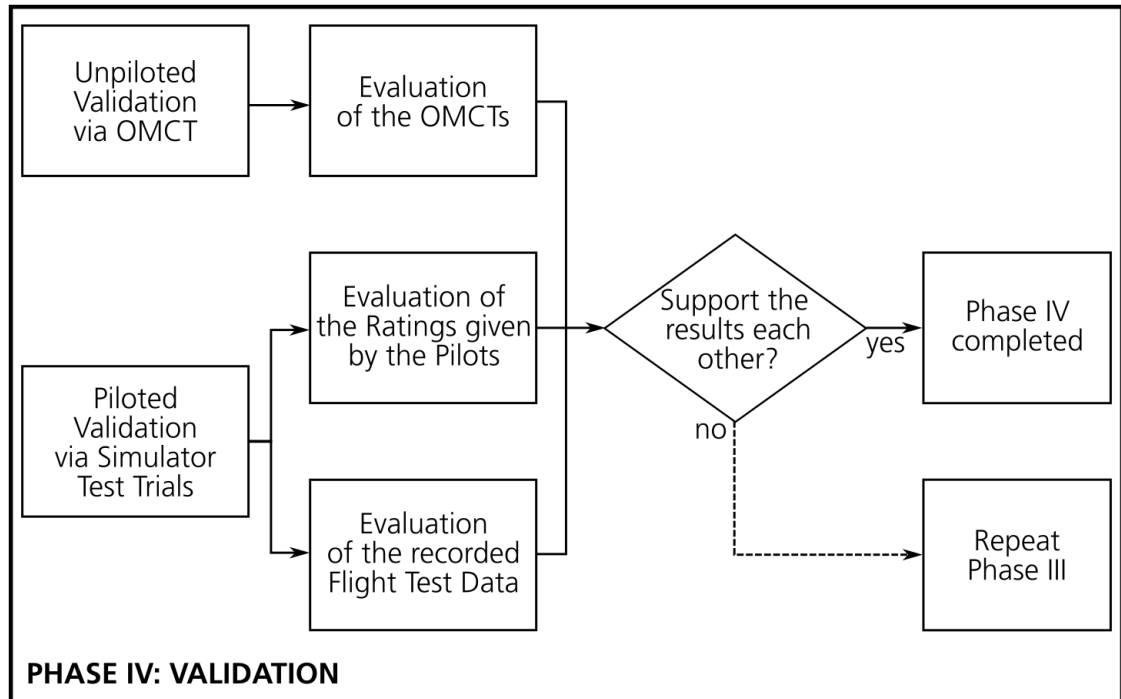


Figure 4.25.: Phase IV - Validation

4.4.1. Objective Motion Cueing Test

For all motion sets OMCTs were carried out according to the ICAO Manual 9625 [9]. For this an already existing test environment at AVES was used. During the OMCTs no problems on the execution were noticed. For the evaluation of the results an analysis based on a Fourier transformation was carried out as mentioned in [30].

4.4.2. Piloted Simulator Campaign

Two pilots joined the simulator campaign. An overview of the pilots' experience is given in Tab. 4.9. Due to time constraints the test matrix was shortened. Pilot A completed test points 1 to 5 whereas Pilot B accomplished test points 1 to 10 according to the test matrix (see Tab. 3.5).

Pilot A stated out that he was unsatisfied with the used SAS. The control input that was

Table 4.9.: Overview of Pilot Experience

	Pilot A	Pilot B
Pilot license	42 years	14 years
Experimental Test Pilot	yes	no
Aircraft experience	EC135, Bo105, Bell UH 1-D, Bell 412, Alouette II	EC135, Bo105, Bell UH 1-D, CH-53
Flight hours	6700	1050
Offshore flights per year	0	0
Manoeuvre: Ship deck landing	0	0

needed was much too low and therefore did not give him a comfortable feeling in flight. He mentioned that he suspected problems with the SAS. Another aspect he criticized was the flight task. He often differentiated between the lateral reposition and the hover task. To get into hover position was challenging for him. To hold the hover position was much easier. Also he stated that the longitudinal visual reference was difficult to observe due to the hover position of the helicopter, which was too high. All in all pilot A experienced a high mental workload and a low physical workload. According to Pilot A all tested motion sets were excessively sensible. Additionally, he stated out deficiencies in lateral movement with motion set ST and in longitudinal movement with motion set ROT. Only the feeling in the vertical movement was always satisfying. Due to too small accelerations he was not able to rate the motion set OP.

After Pilot A was unsatisfied with the SAS, Pilot B was asked to do a free flight without motion. He mentioned that the SAS is a common one and that he did not determine any abnormalities. During test points 1 to 5 he stated out that the accelerations of the helicopter and also of the motion were quite small. During test points 6 to 10 he issued that he could not differentiate between the accelerations caused by the airwake of the frigate and those ones caused by the control input. Both circumstances made it more difficult for him to rate the motion quality. During the rating of the motion he often assessed attitude and attitude rate separately. The attitude rate was always rated worse due to an overreaction. Once he caused a pilot-induced-oscillation (PIO), that was initially caused by the motion. At test points 4, 5 and 10 he stated out that he felt a time delay between the visual sensation and the motion. During the test points 6 to 10, which were flown with the airwake of the frigate, he complained about the static visual environment. This made it difficult to predict the magnitude of the turbulence.

With the airwake of the frigate VehicleControl with ship dynamics according to SS 2 was used to control the movements of the hover board. It was found that the movements of the hover board were too small to force the pilot to correct the position of the helicopter.

5. Analysis and Discussion of the Results

In this chapter the results of the validation are presented and discussed. First the results of the OMCT and of the simulator flight test trials are independently discussed. Afterwards they are compared to each other.

5.1. Objective Motion Cueing Test

The Fig. 5.1 and 5.2 show the result of the OMCTs for each motion set. The grey shaded area marks the fidelity region by Hosman/Advani whereas the dotted lines indicate the refined boundaries by Zaal et al.. In most of the test cases the results are within the grey shaded area over a wide frequency range and should offer a good motion fidelity. For low frequencies the amplitude ratio of the translational test cases "Surge to Surge" and "Sway to Sway" are not within the fidelity boundaries. This is caused by the tuning of the LP filter. To prevent reaching the rate limiter the LP filter was tuned down. The small filter gains K_{LP} led to the shown results for all motion sets. In the test case "Pitch to Pitch", where the effect of gravitation \vec{g} is taken into account in contrast to the other rotational test cases, the motion sets ST and TRA are out of the fidelity boundaries for most of the observed frequencies. Especially at low frequencies this is the case. For the motion sets ROT and OP this behaviour can also be observed, but with less shaping. As stated out by Dalmeijer et al. [17] this is caused by a cross-coupling from surge to pitch and depends on the tuning of the surge channel. At "Heave to Heave" only the motion set OP is outside of the fidelity boundary. The results of the other motion sets lie mostly on the edge of the fidelity boundary.

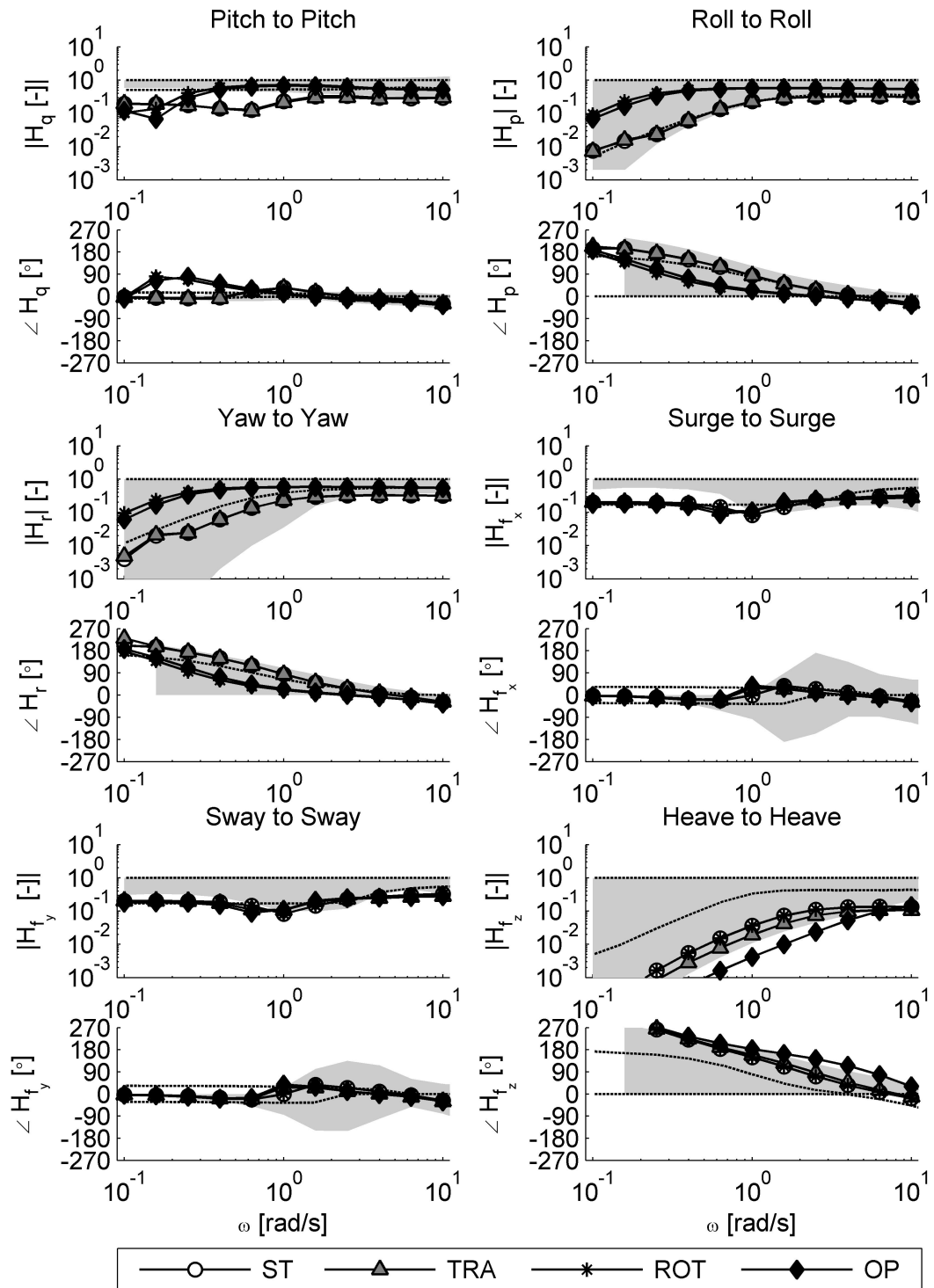


Figure 5.1.: OMCT Results of the Motion Sets: On-Axis

Out of the test cases with cross-coupling of axes only "Sway to Roll" shows noticeable results because only a few frequencies of the motion set ROT and OP are within the boundaries of the phase plot. As mentioned by Dalmeijer et al. [17] the test case "Surge to Pitch" can indicate false cueing due to the tilt coordination as well as the test case "Sway to Roll". In all cases the amplitude ratio was within the fidelity boundaries. This especially applies for the results of the motion sets ROT and OP where pilot B reported a time delay.

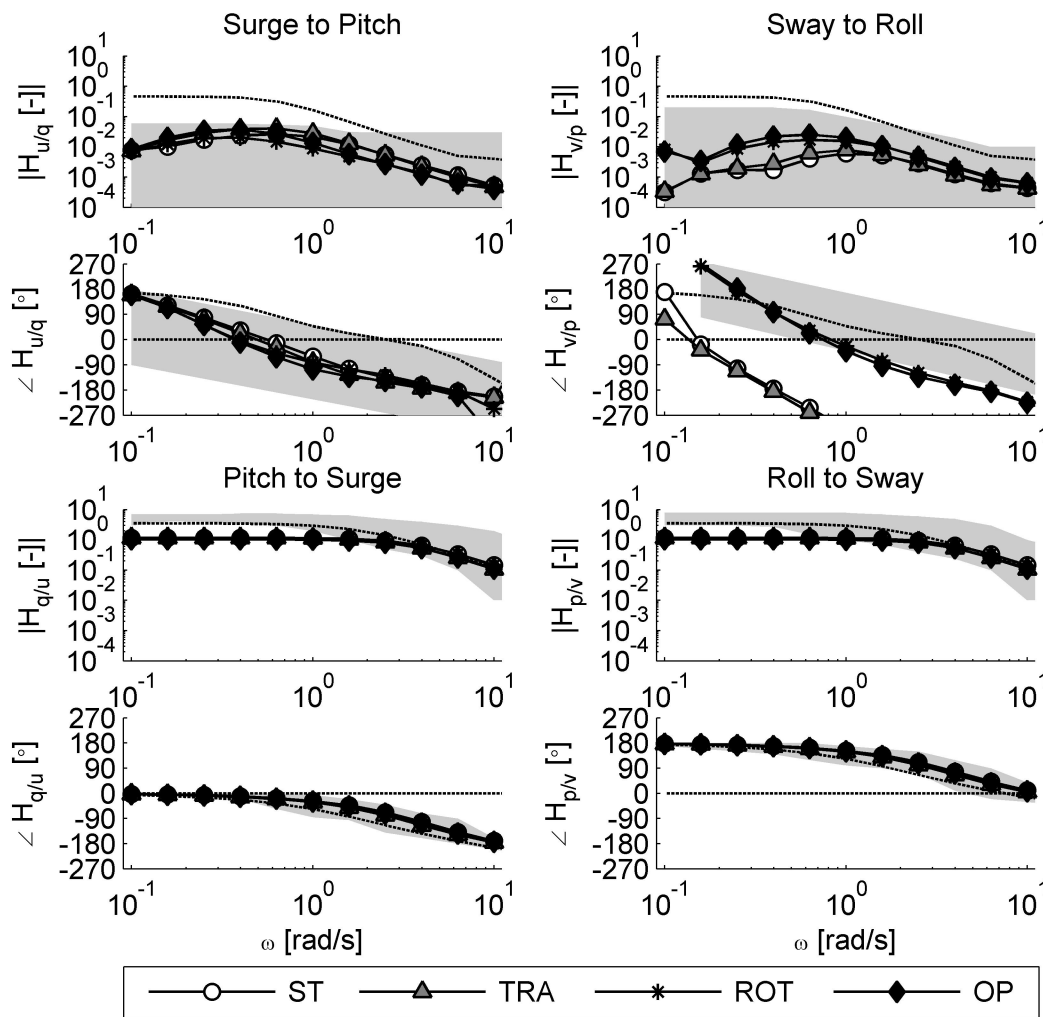


Figure 5.2.: OMCT Results of the Motion Sets: Off-Axis

Fig. 5.3 shows the bode plot of the motion set OP as a prediction of the OMCT and the

results of the OMCT itself. It can be seen that the prediction and the results are in a good agreement. The used test environment at AVES that was already existing can be used in combination with the new implemented CWA. There is no prediction for "Pitch to Pitch" because this test case takes the gravitation into account. At "Heave to Heave" the prediction has a lower phase shift for small frequencies than the results of the OMCT. The other translational test cases "Surge to Surge" and "Sway to Sway" have slightly shifted extrema. The prediction shows the magnitude or phase shift extrema at a little higher frequency than the results of the OMCT. The mentioned findings in the comparison of the prediction and the results of the OMCT for the motion set OP are exemplary for all other motion sets as can be seen in the appendix in section C in the Fig. C.1-C.3.

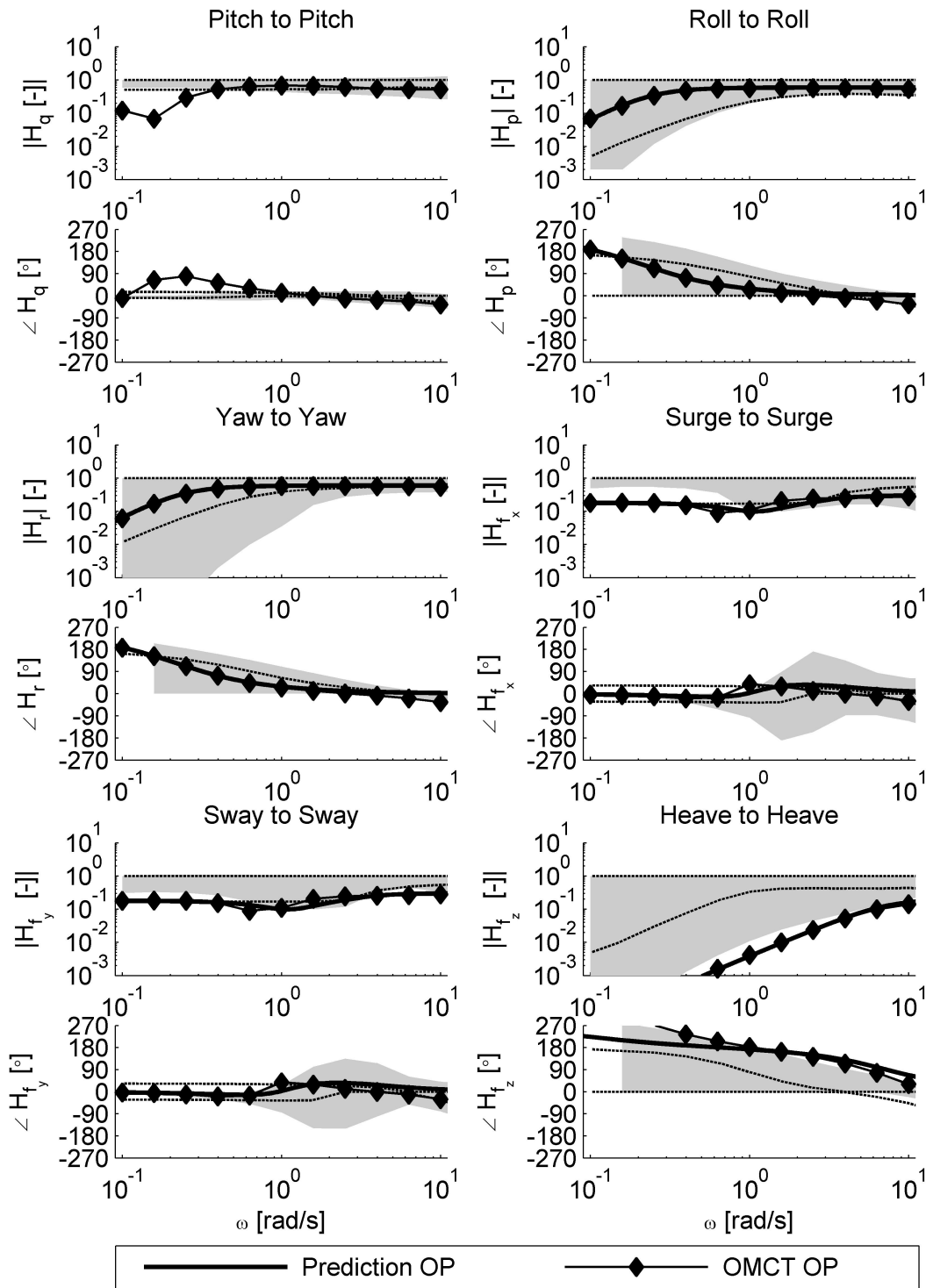


Figure 5.3.: Prediction and Results of the OMCT for motion set OP

5.2. Piloted Simulator Campaign

In this section the piloted simulator campaign is analysed and discussed. As shown in Fig. 5.4 the workload rating of the pilots across all test points is within level 2. According to pilot B, the turbulent airwake of the frigate corresponding to SS 2 leads to a small increase of the workload. He rated the kind of turbulence with value 3 according to the turbulent air scale (see Tab. 3.6) across all test points that were flown with the airwake of the frigate.

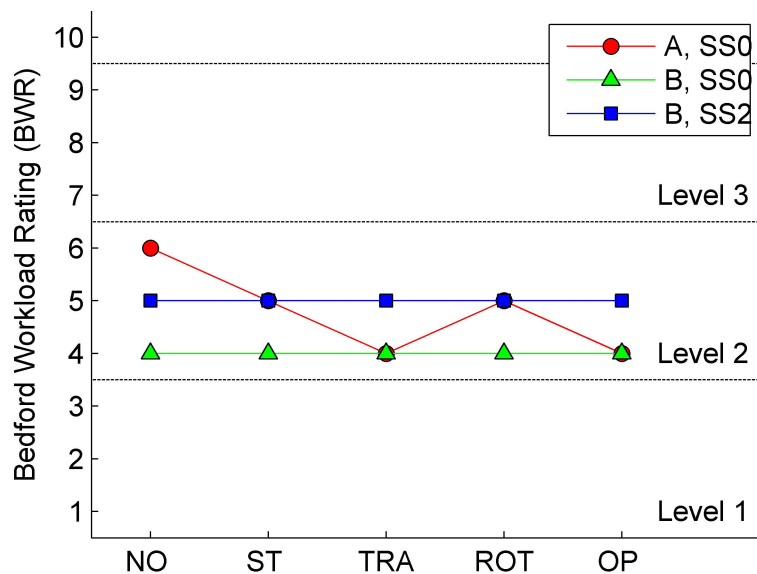


Figure 5.4.: Bedford Workload Rating given by the Pilots

The motion rating is shown in Fig. 5.5. All motion sets were rated with a medium or high rating. Every motion set offered at least a limited benefit for this specific flight task according to the pilots' opinions. In general, the vertical acceleration were slightly higher rated than those of the translational rate. The translational rate were slightly higher rated than these of the attitude/attitude rate. Both pilots preferred the motion sets TRA and ROT, whereas motion set OP got the lowest rating. The ratings given by pilot B did not change significantly when including turbulence.

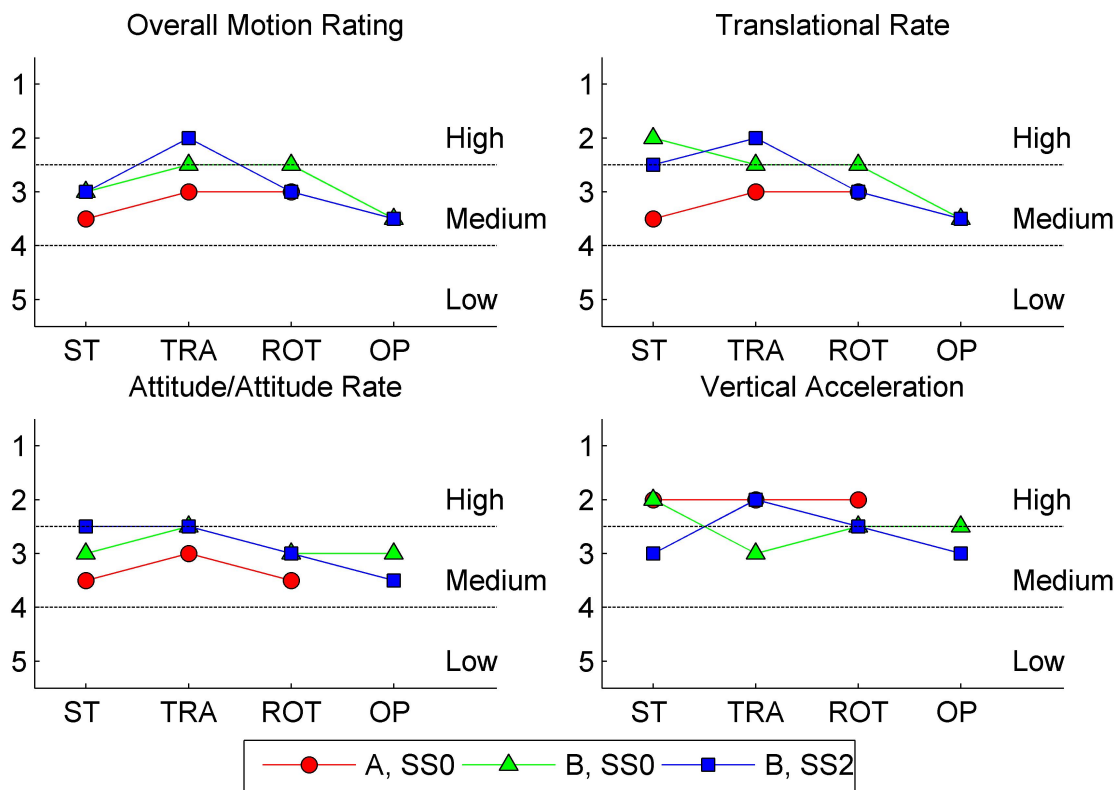


Figure 5.5.: Motion Rating given by the Pilots

In Fig. 5.6 and 5.7 two flight paths are compared. The test points 1 and 5 were chosen as an example. Fig. 5.6 shows the flight path of pilot A whereas Fig. 5.7 shows that of pilot B. The rear view and the top view of the flight path are depicted. A green and a red box mark the desired and the adequate boundary of the hover task. The bold blue and magenta lines indicate the flight path of the hover task whereas the thin lines show the flight path the pilots took to the hover point. In comparison to each other the flight path of pilot A to the test point with motion set OP is more centred and smaller than the one without motion (see Fig. 5.6). The flight paths of pilot B are similar to each other. Independently of pilot and test point the flight paths show a greater span in north direction Δx_N than in any other direction.

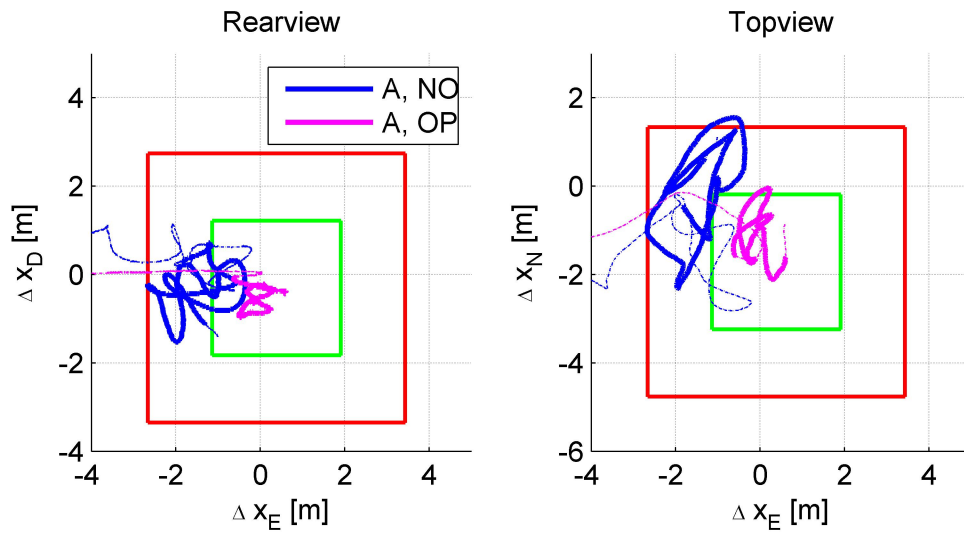


Figure 5.6.: Flightpath - Pilot A, SS0

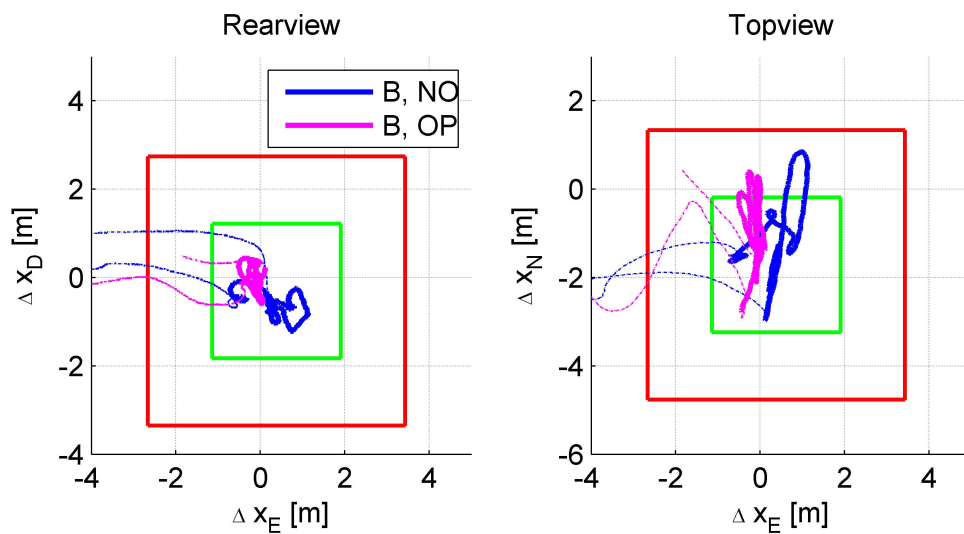


Figure 5.7.: Flightpath - Pilot B, SS0

In addition to the presented flight paths in Fig. 5.6 and 5.7, Fig. 5.8 shows the cyclic input of the pilots for the same test points. The control input of pilot A is smaller for the test point with motion set OP than for the test point without motion. Again, the cyclic input of pilot B is similar between the test points.

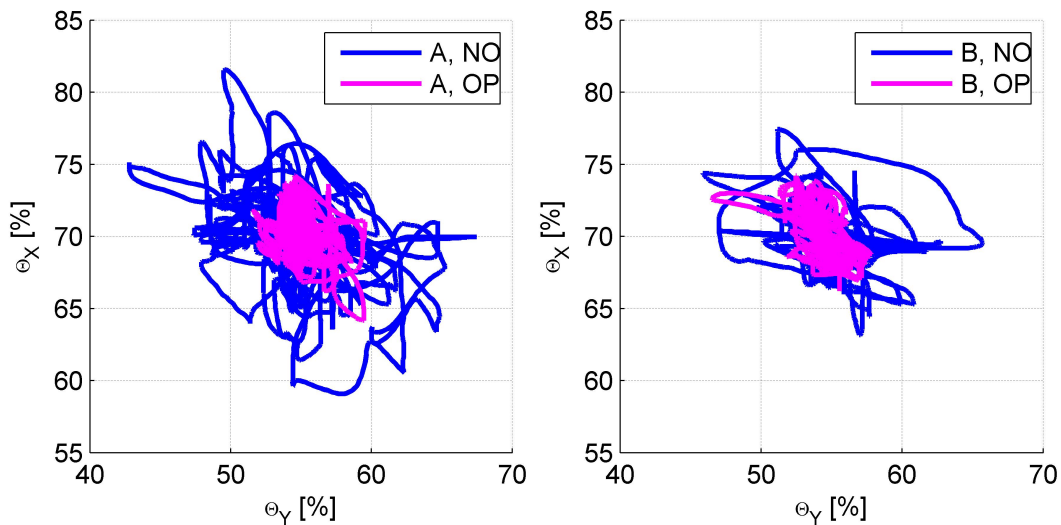


Figure 5.8.: Control Input- SS0

Next, the desired performance was determined. For this the time was determined when the flight path of the helicopter was within the desired boundaries. The received value was divided by the desired duration of the hover task of 30 s according to Tab. 3.5. The results are shown in Fig. 5.9. The desired performance for the test points without any turbulence continuously increases from the motion set ST to the motion set OP. This tendency is independent of the pilot. This however does not apply to the test points with turbulence according to SS 2. Within those test points no tendency was found.

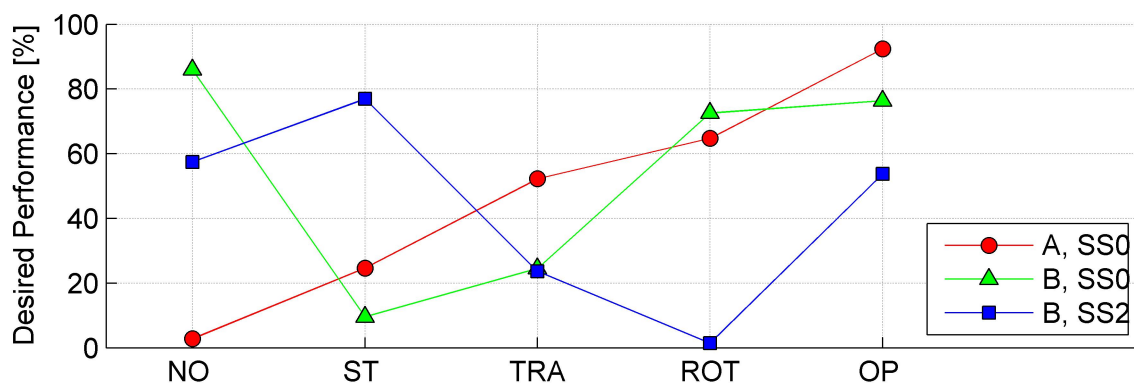


Figure 5.9.: Desired Performance for the Hover Task

The accelerations of the helicopter model HeliWorX and the measured accelerations of the motion dome are shown in the Fig. 5.10 and 5.11. Test point 5 with pilot B was chosen as an example. During this flight the pilot also experienced time delays. In general the accelerations of the motion and of the CWA are in good agreement to the accelerations of the model. A small time delay, which accumulated with increasing time, can be seen in longitudinal direction. As an additional reference the human motion perception thresholds of [7] (see Tab. 2.1) are plotted with a dashed line. The area between the perception thresholds, to which the pilot is not expected to feel a vestibular feedback is marked in light grey. It can be seen that most of the time the translational accelerations of the motion dome are below the perception thresholds. This applies especially for the heave acceleration. It is questionable whether the observed delay in longitudinal direction is the experienced time delay by the pilot.

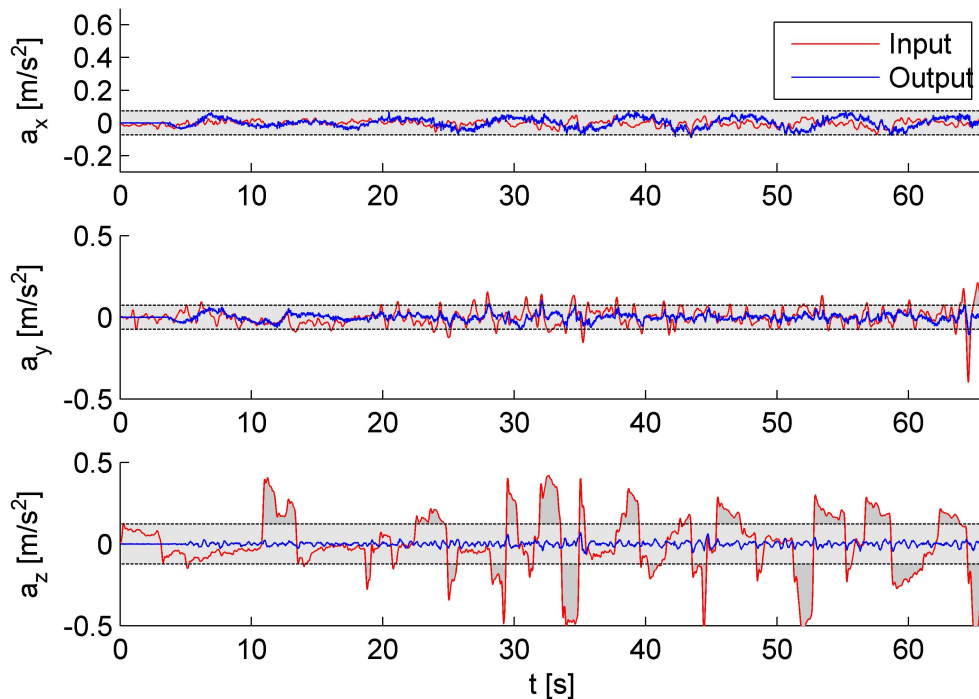


Figure 5.10.: Time Plot of the translational Accelerations

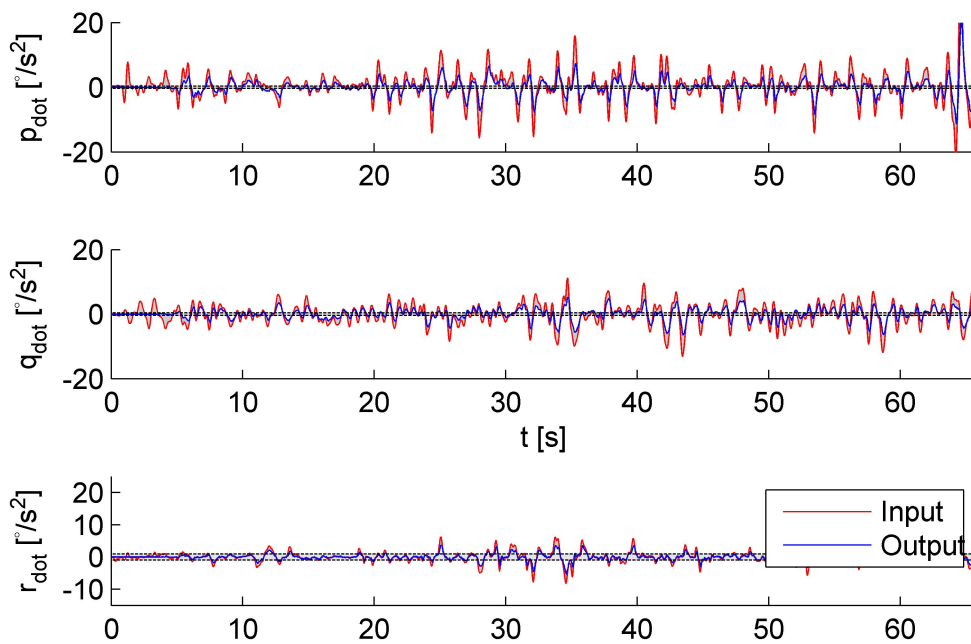


Figure 5.11.: **Time Plot of the rotational Accelerations**

Due to current problems with the control loading system (CLS) and the flight control system (FCS) this is going to be further investigated. An issue with the CLS or the FCS could explain the comments of pilot A about the SAS as well as the time delay of pilot B. The control input of pilot B and the output of the FCS of test point 5 are shown in Fig. 5.12. Due to proprietary issues the CLS cannot be further investigated. A 3-axes SAS was used where the cyclic and pedal inputs of the pilot were regulated. The input of the collective is unprocessed. Furthermore the filtering technique of the SAS can be observed. High amplitude inputs of the pilot are limited as is the input rate. All in all the SAS behaved as expected. An issue with a time delay could not be verified. After the FCS all data are led to the IC of the simulation environment. All other data, for example of the visual system or the helicopter model, flow to the IC. With the IC a real time processing of the whole simulation is guaranteed. As a bottom line assumption real time processing was undisturbed at any time of the simulator campaign. Therefore a time delay between separated parts of the simulation can be excluded.

It is noticeable that both pilots rated the vertical accelerations by the motion continuously

higher than the other accelerations (see Fig. 5.5, although they might not have felt any vertical acceleration according to the motion perception thresholds in the time plots in Fig. 5.10). When taking typical flight profiles of pilots into consideration, another explanation for the pilot comments might be plausible. Typically the participating pilots fly the helicopter bare airframe and are not used to a SAS. The collective input is also unregulated during SAS and corresponds to the bare airframe. It is the only axis that the pilots are familiar with according to their usual flight perception. After the exclusion of many potential sources for time delays it is possible that the pilots rated the unknown flight behaviour of the SAS instead of the motion set.

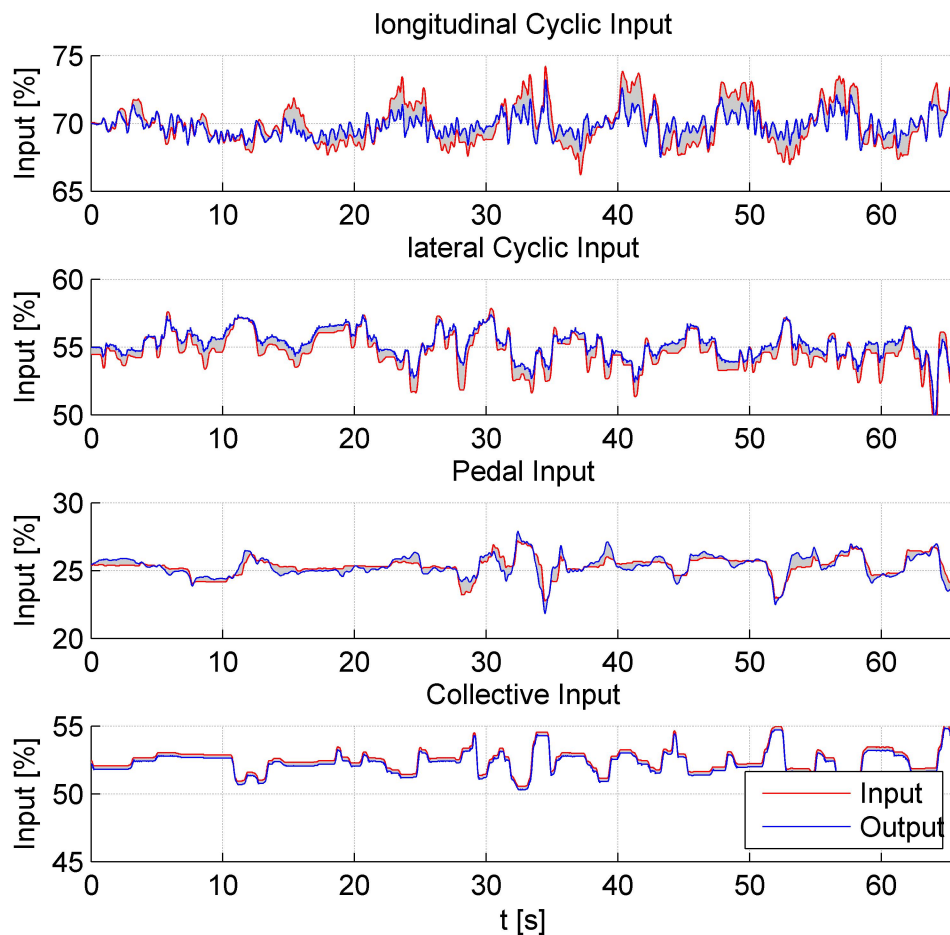


Figure 5.12.: Input/Output of the FCS

According to the pilots' motion ratings (see Fig. 5.5) the offline tuning was successful. During the offline tuning flight test data with a different but similar flight task were used. Fig. 5.13 shows the PSD of the used flight test data and the recorded flight data of all test points. In all axes the flight test data that were used for the offline tuning have more power over most of the observed frequency range than the recorded flight data of the simulator flight test trials. In comparison the PSDs in longitudinal and lateral direction are slightly differing. In all other axes the differences are more significant with frequencies above 0.25 Hz. As shown in Fig. 5.14 the local wind speed $V_{W,L}$ of the WT wake field is at least 10^2 times higher than of the frigate's airwake above a frequency of 0.5 Hz. The disturbances caused by the airwake of the frigate during the simulator campaign were much lower than by the airwake of the WT at the flight test data used for the offline tuning. In comparison of the airwakes (see Fig. 5.14) and the PSD of the helicopter accelerations (see Fig. 5.13) the differences in the PSD of the helicopter accelerations can mainly traced back to the influence of the different airwakes. The different airwakes might have a strong influence on the offline tuning that has to be further investigated.

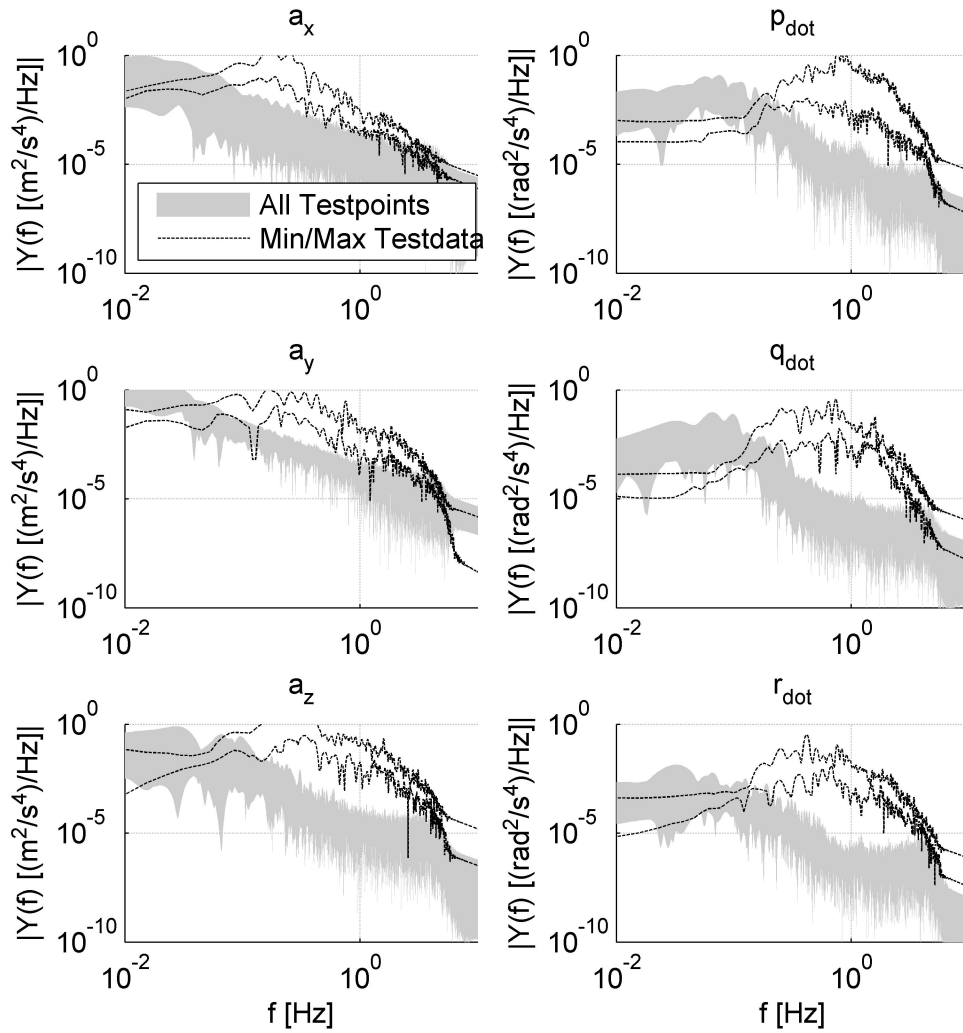


Figure 5.13.: Comparison of used Flight Test Data and recorded Flight Data

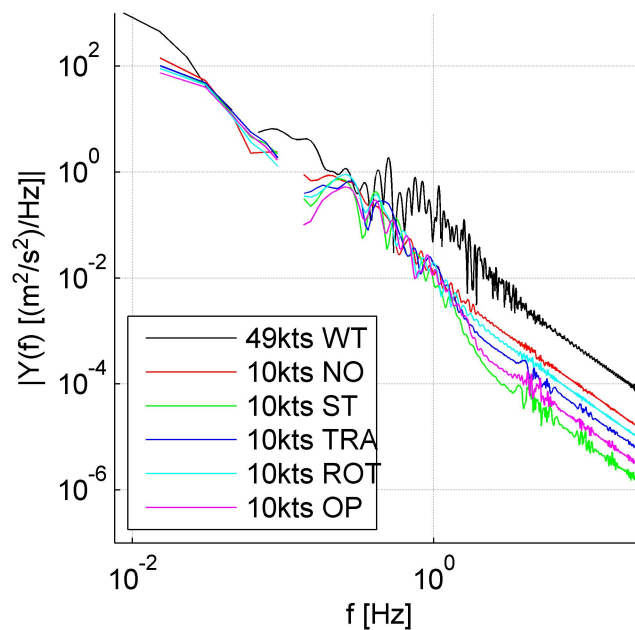


Figure 5.14.: **Comparison of the different Airwakes used during the offline Tuning and recorded during the Simulator Flight Test Trials**

The adaptation of the superslide task has to be discussed considering three aspects. First, due to the higher altitude during hover and the smaller lateral distance to the pylons compared to the original superslide task by Carignan et al., the visual reference for the longitudinal position took a strong influence on the flight performance. According to the pilots' comments and as shown in Fig. 5.6 and 5.7 the longitudinal limits were the most difficult to achieve. Second, due to only small or no movements of the hover board, the characteristic of the flight task changed from a closed loop to an open loop task. This is accompanied with the issue of low accelerations during the runs that made it difficult for the pilots to rate the motion adequately. The turbulences amplified the open loop characteristic of the flight task. Another aspect that is connected to this problem is the input strategy of the pilots. The pilots always tried to keep them as low as possible to reduce the self induced disturbances. The final aspect is the combination of the superslide task with a turbulent wake field of a frigate. No pilot commented on problems concerning turbulences. The sidestep manoeuvre as a means for a smooth entrance into the strong wake field worked as well as the adapted position of the pylons for a better predictability of the turbulence's character. All in all the adapted superslide task was successfully utilized to investigate different motion sets, yet with some improvements still to be made.

5.3. Comparison of the Results

In comparison to each other the findings by Jones [16] are in agreement with the results of the simulator flight test trials and the OMCTs because some of the results show a contradiction. For the motion sets ST and TRA the results of the OMCTs are partially outside of the fidelity boundaries. However, the motion ratings by the pilots are better than expected. The motion sets ROT and OP are almost entirely within the fidelity boundaries of the OMCT. However, they did not get the highest motion ratings by the pilots as expected. The expectations were not only caused by the results of the OMCT, moreover by the results of the fitness function and the VMPE as well. According to Tab. 4.8 the best motion rating would have been expected for motion set OP whereas the worst rating for motion set ST. The offline tuning with the GA was carried out with the goal to improve the motion fidelity by improving physical fidelity with the fitness function. Neither the recorded flight test data nor the OMCTs indicate false cueing that can explain the reported time delay by pilot B or the general dissatisfaction of pilot A. These results indicate the difference between a physical and a functional fidelity. To reach a good functional fidelity the link to the physical fidelity is still missing. Nevertheless the validation of the CWA in combination with the offline tuned motion sets was successful. According to the pilots every motion set offers at least a limited benefit.

With the discussion of the results and as shown in Fig. 4.25 Phase IV is successfully completed. This concludes the implementation and the optimization of the CWA. The CWA is at this stage validated and ready for use.

6. Conclusions and Future Work

In this chapter the thesis is summarized and considerations for future work are drawn. A general overview was given of the major topics of this work based on a literature review. A simulator campaign was developed to systematically examine different motion tunings of a CWA for a helicopter ship deck landing. For the simulator campaign the superslide task was chosen because it is a well defined and a reproducible flight task. Adaptations of the simulation environment were made to use the turbulent airwake of a frigate in combination with the task and to control the hover board with realistic ship dynamics. The second part of the thesis presented a method to develop and validate a CWA. An offline tuning method was also used to determine motion sets for the simulator campaign. A GA was used to solve the problem of multiple unknowns with the fitness function as the optimization function. An unpiloted evaluation was carried with the OMCT as well as a piloted evaluation while the simulator campaign was conducted. The results of both evaluation methods are in a good agreement to each other. The tested motion settings offer at least a limited benefit to the pilot. Therefore the offline tuning with the GA and the fitness function proved successful, although room for improvements is left.

The following conclusions can be drawn:

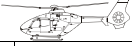
1. With the presented methodology it was possible to successfully implement and validate a CWA in the simulator. The process was comprehensible and reproducible at all times. The implemented CWA is validated and ready for use by the time of writing.
2. The offline tuning with the GA in combination with the fitness function delivered motion sets that offer at least a limited benefit, rendering the tuning successful. Because the post processing was quite expensive and the fitness function was adapted for more balanced motion settings there is room left for improvements. Although the results of the fitness function were confirmed due to the VMPE, a completely independent method, it was found that there is a lack between a physical and a functional fidelity. It is not sufficient enough to increase the physical fidelity and take care of a balanced motion set and of a tilt coordination that operates far below the

rate limiter. Further research has to focus on the missing link between the physical and the functional fidelity to improve the offline tuning.

3. The use of a turbulent airwake of a frigate in combination with the superslide task is a useful addition to the flight task. This makes it possible to examine the influence of the airwake during a helicopter ship deck landing under laboratory conditions. For this adaptations of the task according to the dimensions of the ship offer a good visual reference for the pilot. The test pilots were able to accurately predict the location and strength of the turbulence.
4. During testing of the motion sets a main advantage of the superslide task against the hover MTE was the closed loop character due to the moving hover board. For this the movement of the hover board has to be dominant compared to self induced disturbances or disturbances caused by the unsteady airwake. Otherwise it could lead to an uncertainty of the pilots or to accelerations that were too small to sense the motion adequately.
5. The conducted OMCTs were mostly within the fidelity boundaries but helicopter specific deviations were found. If the results of an OMCT for a specific motion set are within the fidelity boundaries it does not indicate a good motion fidelity. Thus improving the fidelity boundaries should be strived for. The current fidelity boundaries based on fixed-wing simulators are at this stage not adequately applicable for helicopter-specific tuned motion systems.

Keeping the conclusions in mind, possible subjects of future work can be an extension and improvement of the simulator campaign. Pilots who are familiar with SAS might help to extend the database and render the current results more valid. Also the design of the simulator campaign can be improved through a more dominant hover board movement. This can possibly lead to a better pilot's impression of the motion cueing. Further research has to be done to investigate motion sets according to their physical and functional fidelity. A better understanding might be helpful to improve the offline tuning. More studies should be conducted to develop helicopter-specific fidelity boundaries for the OMCT. The results according to the current fixed-wing fidelity boundaries are not satisfactory.

A. Test Cards of the Simulator Flight Test Trials

DLR				Maritime Motion Tuning 2021		
Date	1 st Run	n th Run	Status AVES	A/C HeliWorX		Participant ID
Preparation						
<input type="checkbox"/> Print everything once and last 2 pages according to expected number of test points and spare <input type="checkbox"/> Print/Provide Superslide description <input type="checkbox"/> Print/Provide Rating Scales for Bedford Workload Rating Scale, OMFR and Turbulence Air Scale <input type="checkbox"/> Print/Provide Motion Settings <input type="checkbox"/> Print/Provide prepared charts <input type="checkbox"/> Start Helicopter Model via batch file <input type="checkbox"/> Select trimpoint and do trim calculation <input type="checkbox"/> Open DataAnalyzer and load configuration file <input type="checkbox"/> Start VehicleControl via batch file <input type="checkbox"/> IOS still working? yes -> start ExpSys Do following CHECKS: <input type="checkbox"/> Helicopter at starting position <input type="checkbox"/> Trimspeed at 0.019 kts <input type="checkbox"/> Local windfield active (position -60;0;5, dim: 4) <input type="checkbox"/> Blending gap (m_dWindblend: 0.02) <input type="checkbox"/> AC is set (ExpSys Scenario 2) <input type="checkbox"/> Hoverboard Control via SDSP is set (IOS param FUNC2) <input type="checkbox"/> Application loaded at MOOG Explorer is CWAModel <input type="checkbox"/> Check MapIn and Filter settings						
Explanation						
Modify motion settings and perform the Superslide task at several sea states and wind conditions as described in the test matrix below. As a secondary task the pilot should feedback every 3-5 seconds the groundspeed during lateral translation and radar altitude during hover.						

TEST MATRIX INCLUDING TESTNO.				
SEA STATE	SS 0	SS 2	SS 4	
GLOBAL WIND	0 KTS	10 KTS	20 KTS	
MOTION SET	WITHOUT MOTION	1	6	11
	STANDARD ST	2	7	12
	TRANSLATION TRA	3	8	13
	ROTATION ROT	4	9	14
	OPTIMIZED OP	5	10	15

Figure A.1.: Test Card Page 1: Preparation


DLR				Maritime Motion Tuning 2021		
Date	1 st Run	n th Run	Status AVES	A/C HeliWorX	Participant ID	
Settings				Time [UTC]	Fuel [kg]	
TestNo.: _____		Motion Setting: _____		Global Wind: vwn = _____	Scaling Windtable: _____	
<ul style="list-style-type: none"> Familiarization → 2x or according to pilot's decision Evaluation run → pilot's evaluation, questionnaire and ratings 						
RUN	Pilot remarks					
	FAM <input type="checkbox"/> or Hot Run <input type="checkbox"/>					Adequate <input type="checkbox"/> Desired <input type="checkbox"/>
	FAM <input type="checkbox"/> or Hot Run <input type="checkbox"/>					Adequate <input type="checkbox"/> Desired <input type="checkbox"/>
	FAM <input type="checkbox"/> or Hot Run <input type="checkbox"/>					Adequate <input type="checkbox"/> Desired <input type="checkbox"/>
	FAM <input type="checkbox"/> or Hot Run <input type="checkbox"/>					Adequate <input type="checkbox"/> Desired <input type="checkbox"/>
	FAM <input type="checkbox"/> or Hot Run <input type="checkbox"/>					Adequate <input type="checkbox"/> Desired <input type="checkbox"/>
	FAM <input type="checkbox"/> or Hot Run <input type="checkbox"/>					Adequate <input type="checkbox"/> Desired <input type="checkbox"/>
	FAM <input type="checkbox"/> or Hot Run <input type="checkbox"/>					Adequate <input type="checkbox"/> Desired <input type="checkbox"/>

Figure A.2.: Test Card Page 2: Documentation of the Runs carried out for one Test Point


DLR				Maritime Motion Tuning 2021																															
Date	1 st Run	n th Run	Status AVES	A/C HeliWorX		Participant ID																													
Questionnaire				Time [UTC]	Fuel [kg]																														
No	QUESTION						Rating																												
01	Describe ability to meet the desired/adequate performance standards.						Adequate <input type="checkbox"/> Desired <input type="checkbox"/>																												
02	Does the turbulence meet your expectations in accordance to free stream windspeed and -direction? Please explain why!						Yes <input type="checkbox"/> No <input type="checkbox"/>																												
03	Assign motion RATING using OMFR rating scale. Please highlight your decision-making process and adjectives that are best suited in the context of the task!																																		
	<table style="width: 100%; border-collapse: collapse;"> <tr> <td style="text-align: center;">1— Good</td> <td style="text-align: center;">1— Good</td> <td style="text-align: center;">1— Good</td> <td style="text-align: center;">1— Good</td> <td style="text-align: center;">Benefit (High)</td> </tr> <tr> <td style="text-align: center;">2—</td> <td style="text-align: center;">2—</td> <td style="text-align: center;">2—</td> <td style="text-align: center;">2—</td> <td></td> </tr> <tr> <td style="text-align: center;">3— Fair</td> <td style="text-align: center;">3— Fair</td> <td style="text-align: center;">3— Fair</td> <td style="text-align: center;">3— Fair</td> <td style="text-align: center;">Limited Benefit (Medium)</td> </tr> <tr> <td style="text-align: center;">4—</td> <td style="text-align: center;">4—</td> <td style="text-align: center;">4—</td> <td style="text-align: center;">4—</td> <td></td> </tr> <tr> <td style="text-align: center;">5— Poor</td> <td style="text-align: center;">5— Poor</td> <td style="text-align: center;">5— Poor</td> <td style="text-align: center;">5— Poor</td> <td style="text-align: center;">Unacceptable (Low)</td> </tr> <tr> <td style="text-align: center;">Attitude / Attitude Rate</td> <td style="text-align: center;">Translational Rate</td> <td style="text-align: center;">Vertical Acceleration</td> <td style="text-align: center;">Overall MTE</td> <td></td> </tr> </table>							1— Good	1— Good	1— Good	1— Good	Benefit (High)	2—	2—	2—	2—		3— Fair	3— Fair	3— Fair	3— Fair	Limited Benefit (Medium)	4—	4—	4—	4—		5— Poor	5— Poor	5— Poor	5— Poor	Unacceptable (Low)	Attitude / Attitude Rate	Translational Rate	Vertical Acceleration
1— Good	1— Good	1— Good	1— Good	Benefit (High)																															
2—	2—	2—	2—																																
3— Fair	3— Fair	3— Fair	3— Fair	Limited Benefit (Medium)																															
4—	4—	4—	4—																																
5— Poor	5— Poor	5— Poor	5— Poor	Unacceptable (Low)																															
Attitude / Attitude Rate	Translational Rate	Vertical Acceleration	Overall MTE																																
04	Assign workload RATING using BWR rating scale. Please highlight your decision-making process and adjectives that are best suited in the context of the task!						BWR																												
05	Assign RATING using Turbulence air scale. Please highlight your decision-making process and adjectives that are best suited in the context of the task!						TS																												

Figure A.3.: Test Card Page 3: Pilot Questionnaire

B. Outputs of easy Test Signals of the Pre-Validation

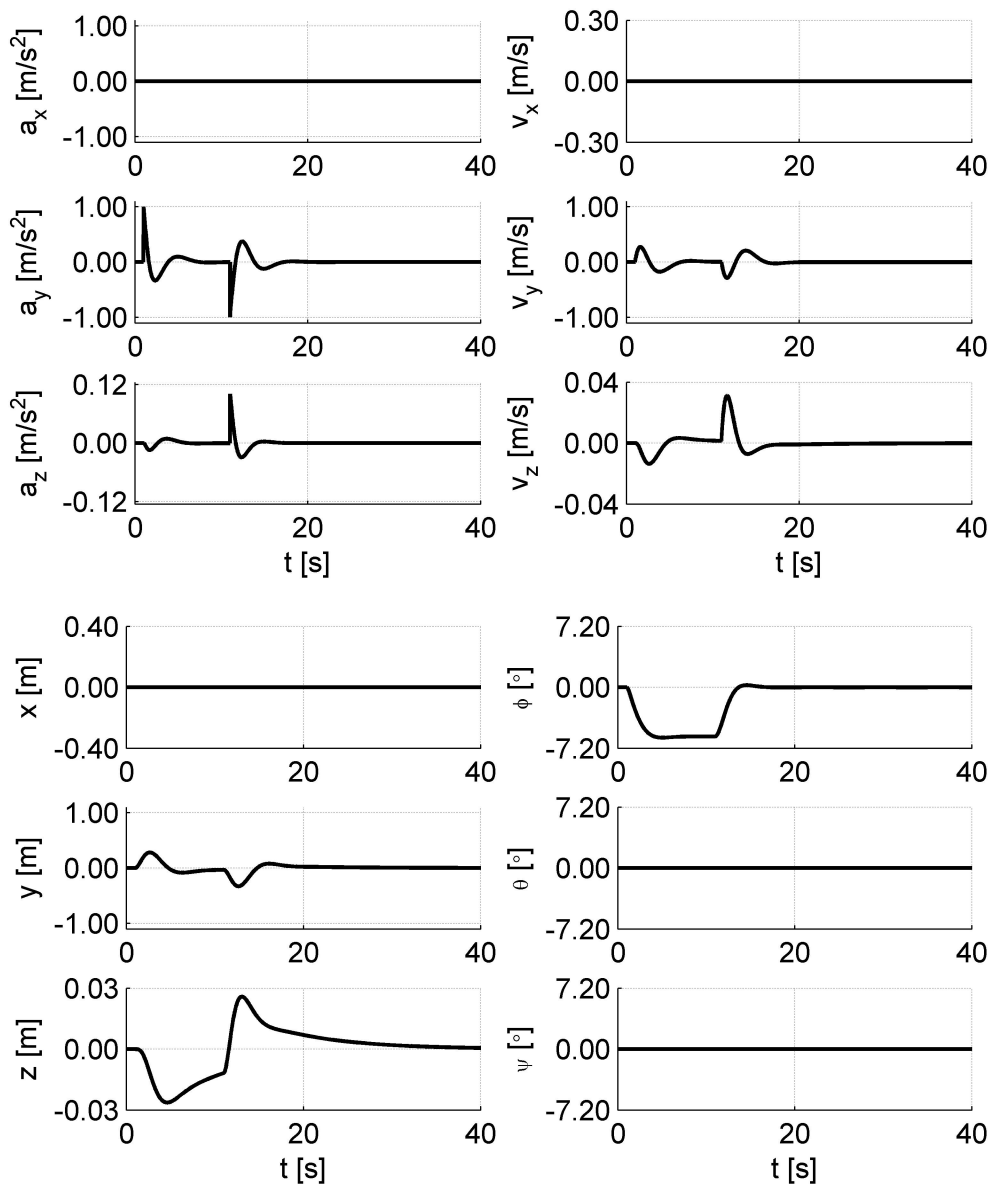


Figure B.1.: Output according to Pulse Input at sway axis

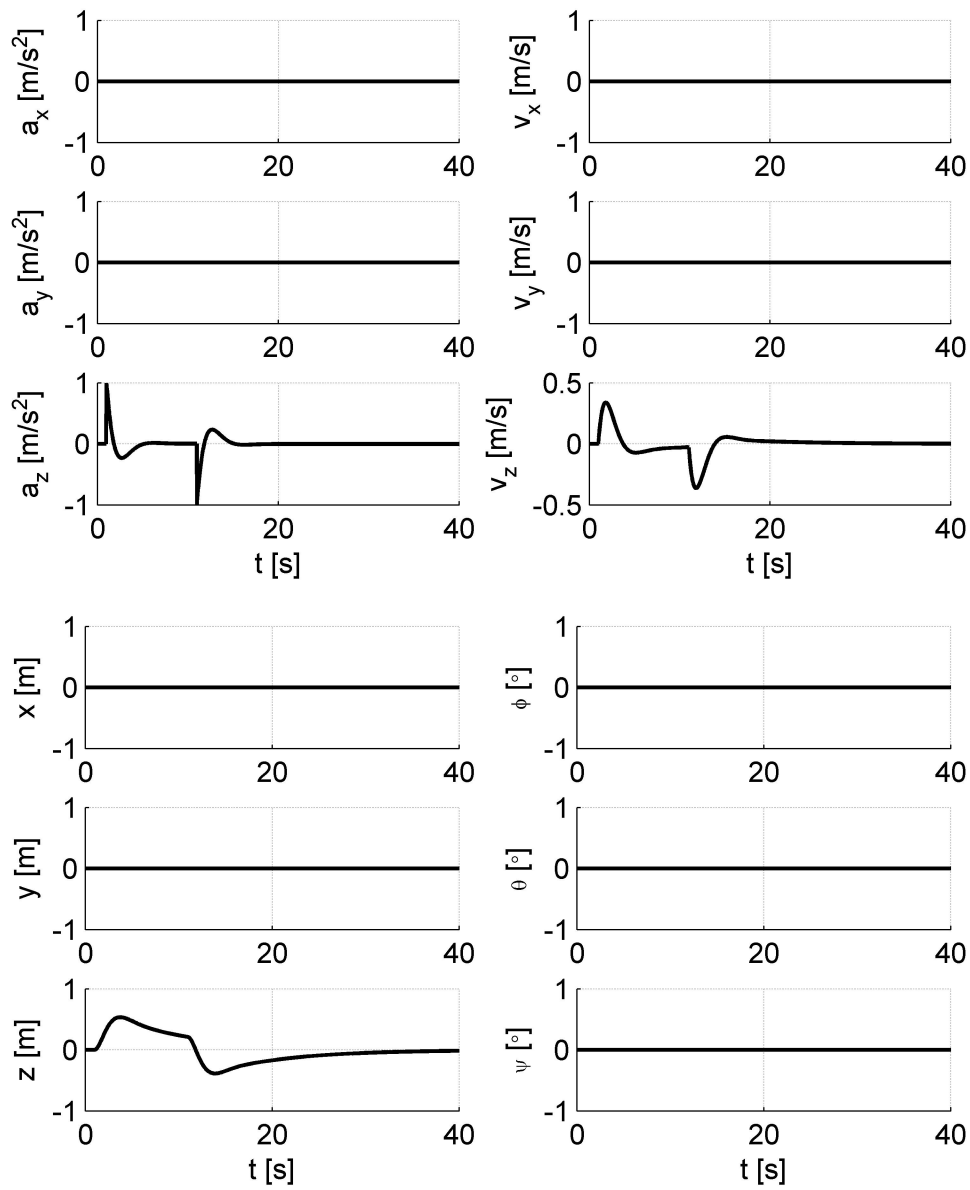


Figure B.2.: Output according to Pulse Input at heave axis

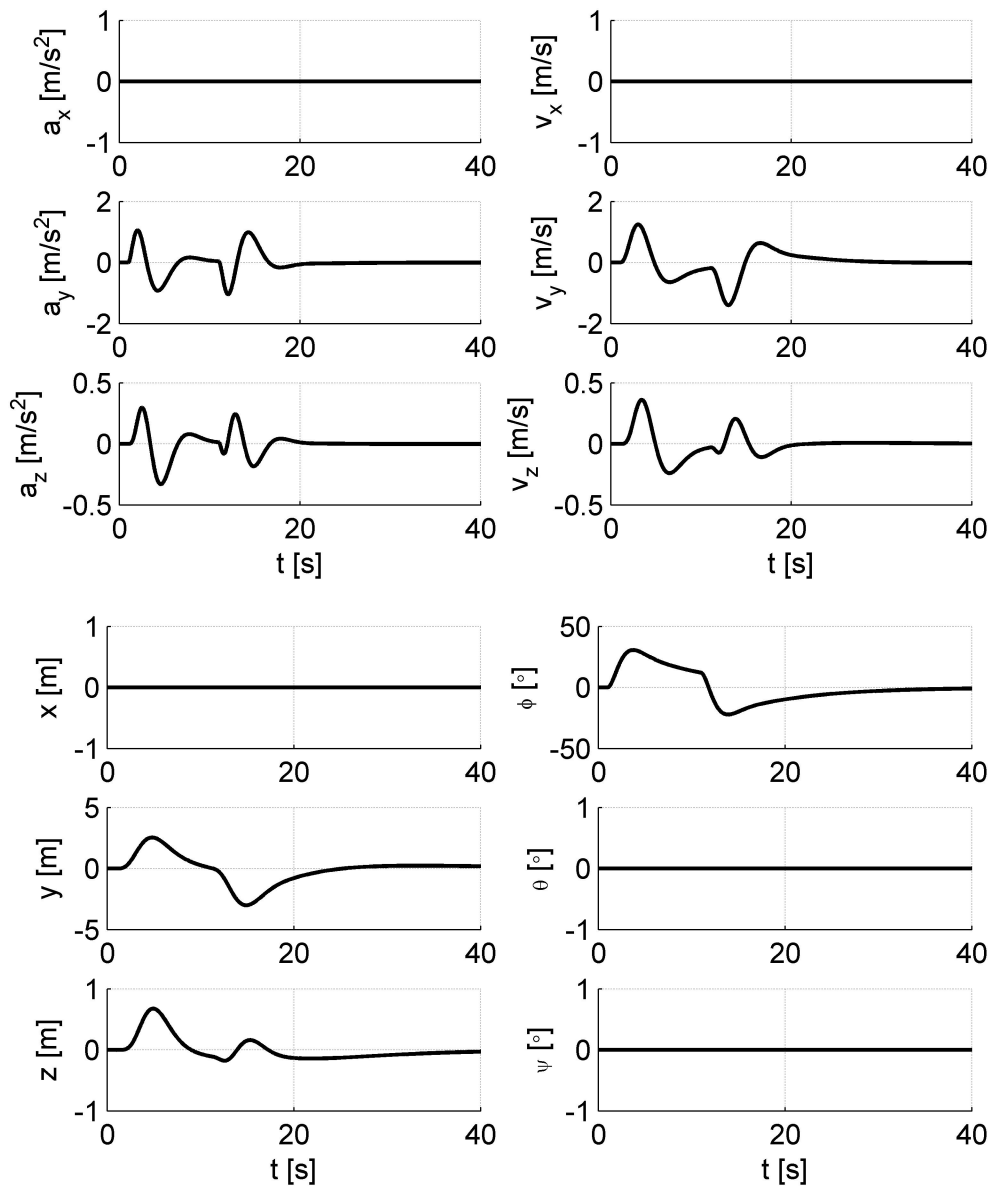


Figure B.3.: Output according to Pulse Input at roll axis

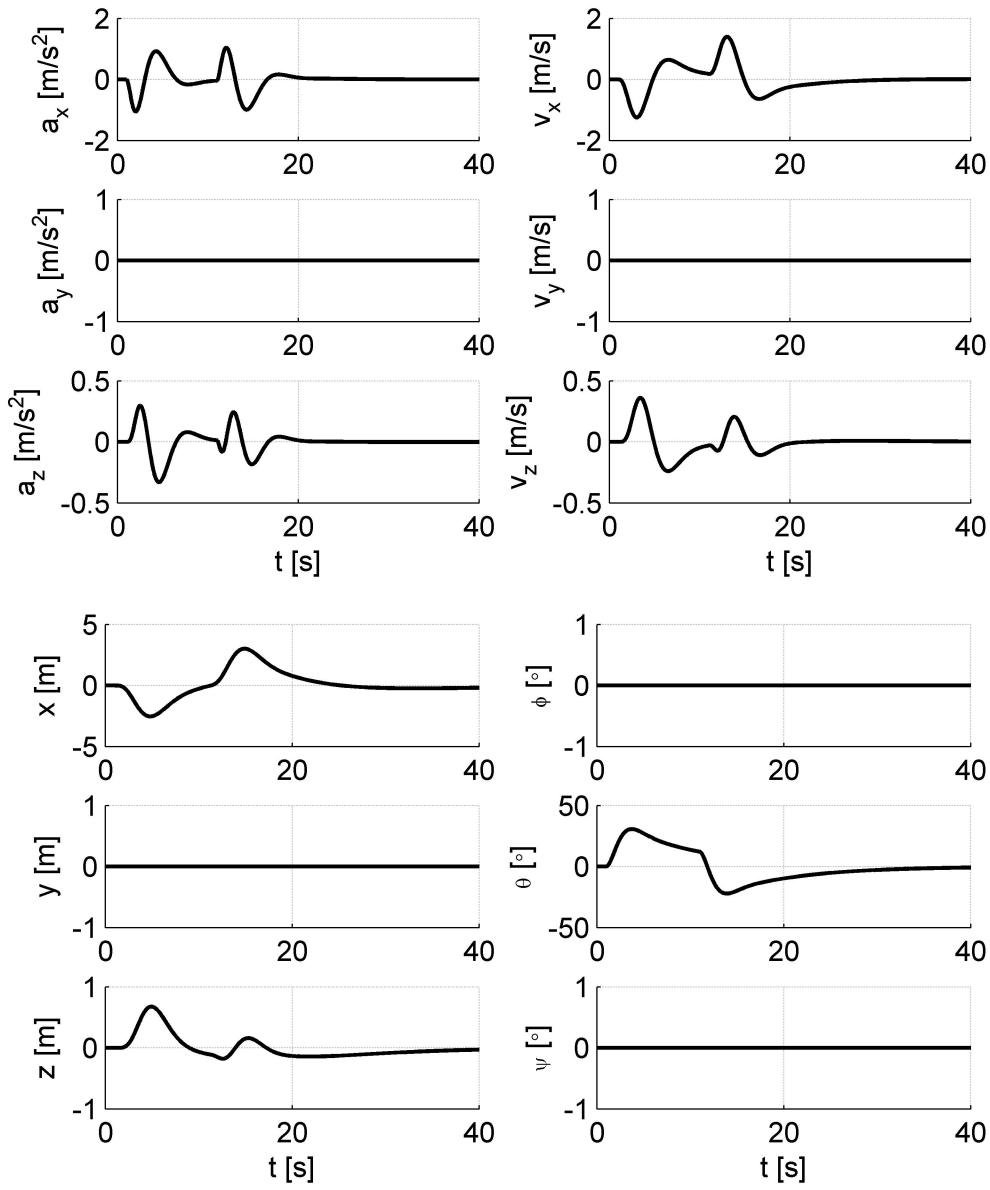


Figure B.4.: **Output according to Pulse Input at pitch axis**

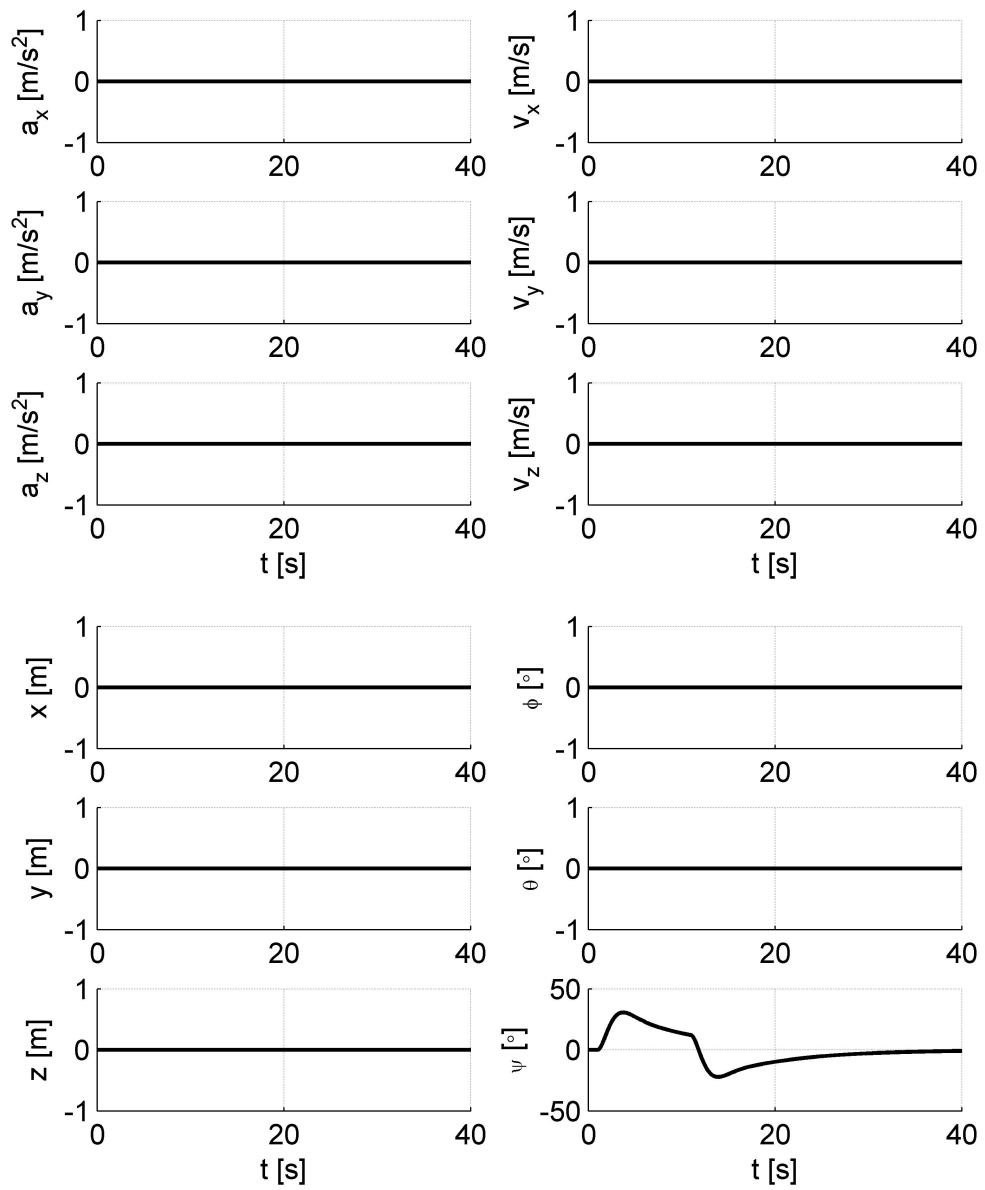


Figure B.5.: Output according to Pulse Input at yaw axis

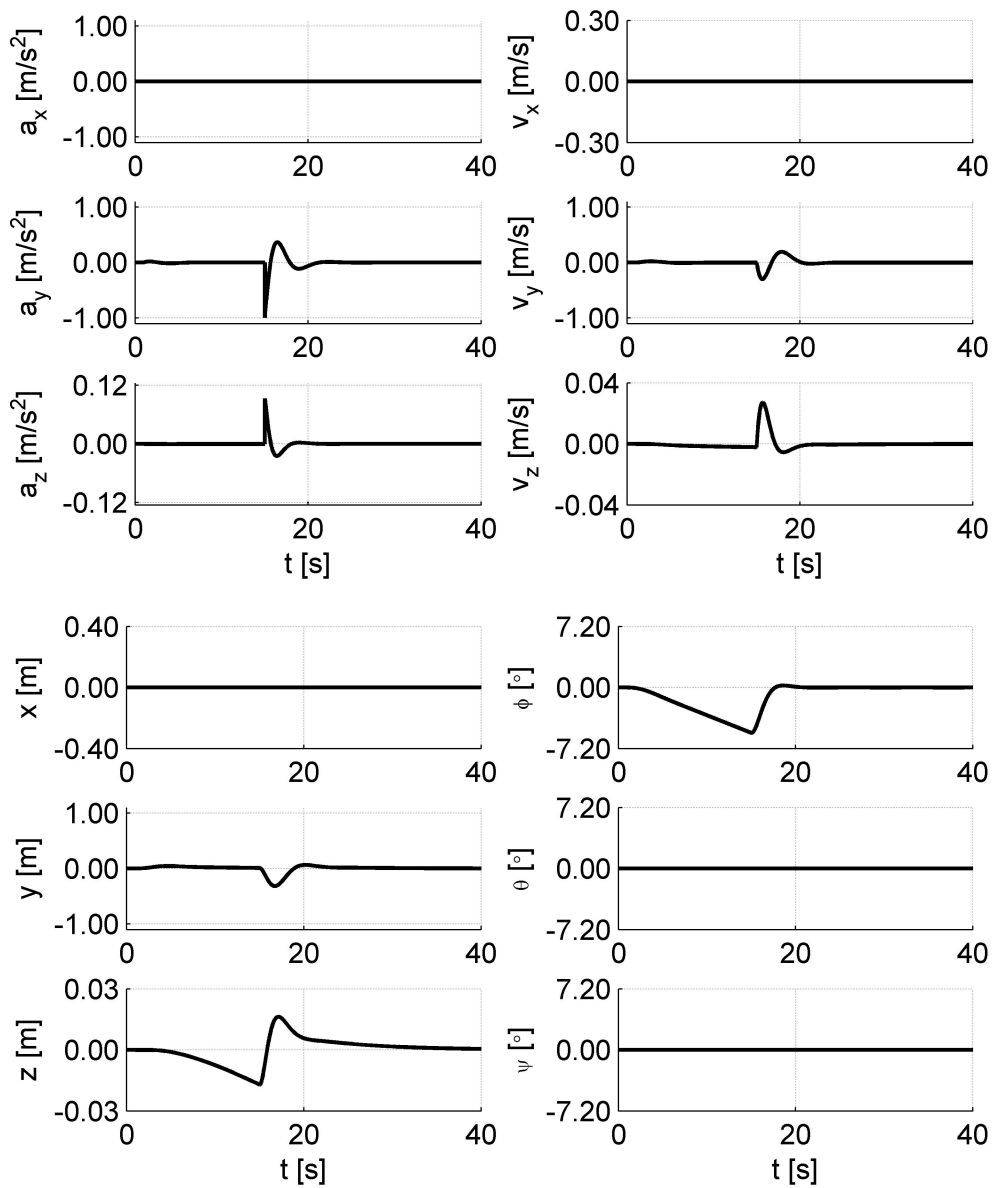


Figure B.6.: Output according to Ramp Input at sway axis

C. Comparison of the Prediction and the Results of the OMCT

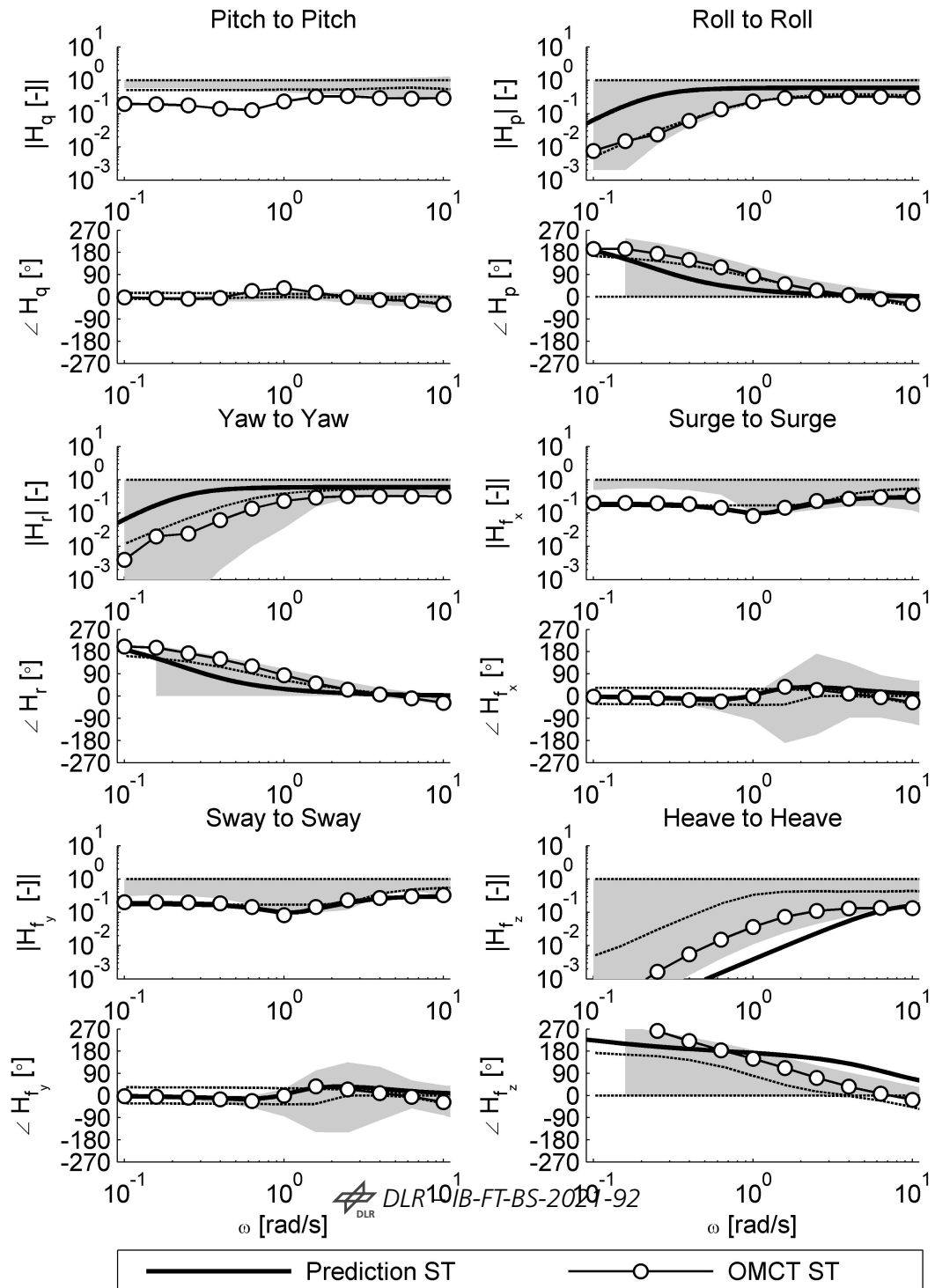


Figure C.1.: Prediction and Results of the OMCT for motion set ST

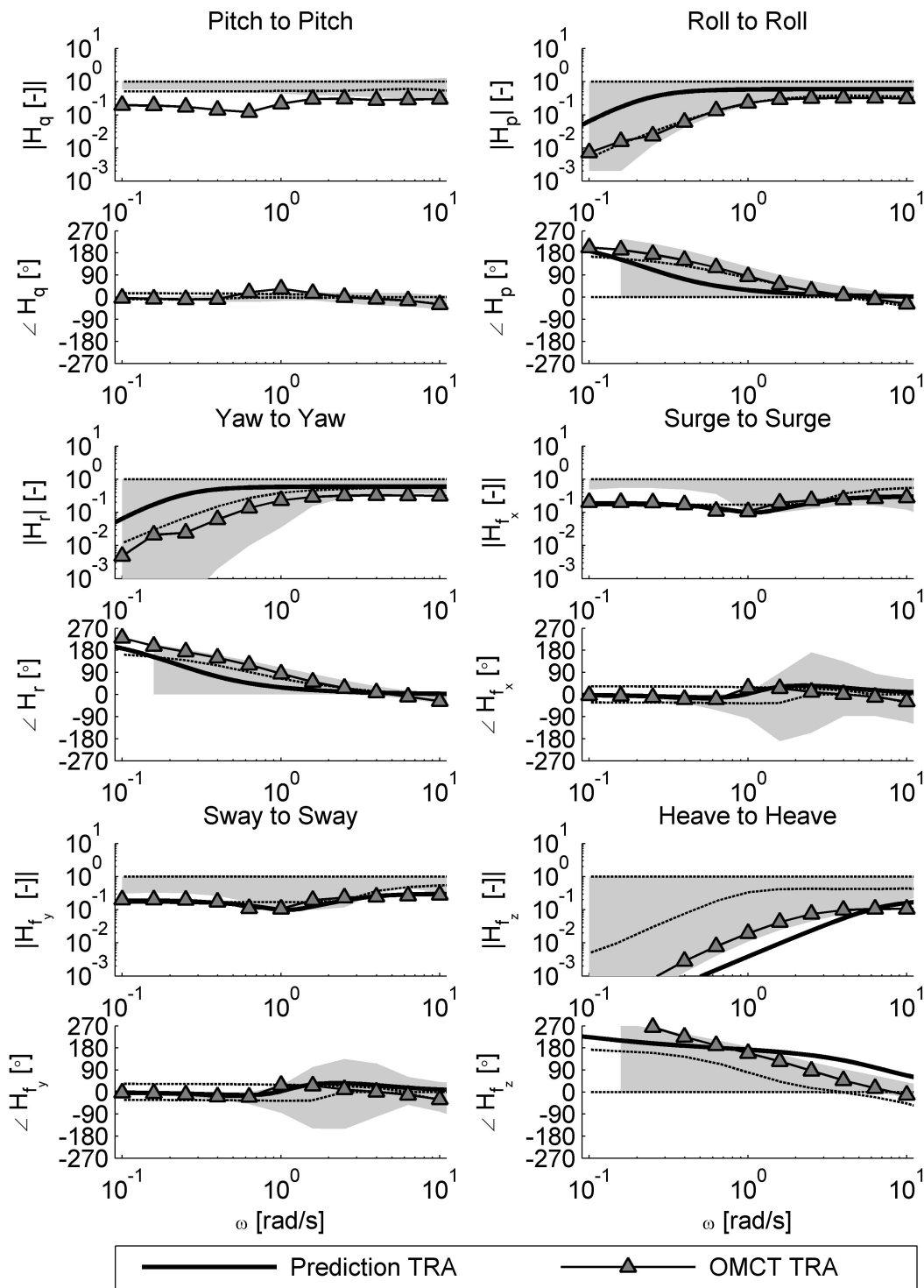


Figure C.2.: Prediction and Results of the OMCT for motion set TRA

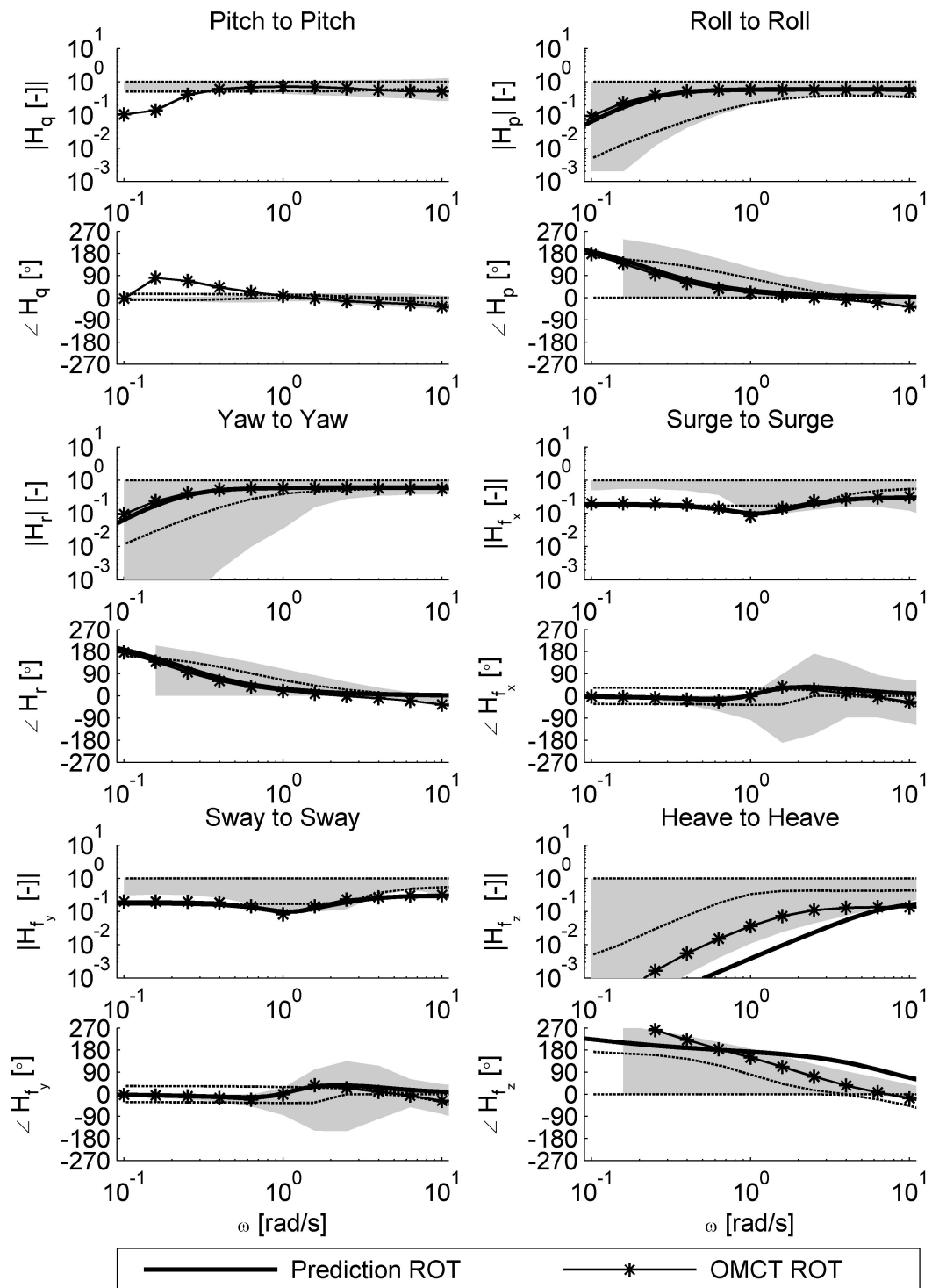


Figure C.3.: Prediction and Results of the OMCT for motion set ROT

Bibliography

- [1] L. D. Reid and M. A. Nahon, "Flight simulation motion-base drive algorithms: Part 1: Developing and testing the equations," December 1985.
- [2] M. Jones, "An objective method to determine the fidelity of rotorcraft motion platforms," in *AIAA Modeling and Simulation Technologies Conference*, (Reston, Virginia), American Institute of Aeronautics and Astronautics, September 2017.
- [3] W. A. Memon, M. D. White, and I. Owen, "Visual-vestibular motion cueing assessment in maritime rotorcraft flight simulators," in *45th European Rotorcraft Forum*, 2019.
- [4] S. J. Hodge, P. Perfect, G. D. Padfield, and M. D. White, "Optimising the yaw motion cues available from a short stroke hexapod motion platform," *The Aeronautical Journal*, vol. 119, no. 1211, pp. 1–21, 2015.
- [5] M.-J. Maibach, M. Jones, and A. Strbac, "Development of a simulator environment for maritime rotorcraft research applications," in *Deutscher Luft- und Raumfahrtkongress (DLRK) 2020*, September 2020.
- [6] A. H. Roscoe and G. A. Ellis, "A subjective rating scale for assessing pilot workload in flight: A decade of practical use," March 1990.
- [7] E. Groen, M. Wentink, A. Valente Pais, M. Mulder, and M. van Paassen, "Motion perception thresholds in flight simulation," in *AIAA Modeling and Simulation Technologies Conference and Exhibit*, (Reston, Virginia), p. 1088, American Institute of Aeronautics and Astronautics, August 2006.
- [8] P. R. Grant and L. D. Reid, "Motion washout filter tuning: Rules and requirements," *Journal of Aircraft*, vol. 34, no. 2, pp. 145–151, 1997.
- [9] International Civil Aviation Organization, "Manual of criteria for the qualification of flight simulation training devices: Doc 9625," 2015.

- [10] M. Jones, "Enhancing motion cueing using an optimisation technique," *The Aeronautical Journal*, vol. 122, no. 1249, pp. 487–518, 2018.
- [11] Federal Aviation Administration, U.S. Department of Transportation, "Advisory circular: Certification of transport category rotorcraft," January 2014.
- [12] Anon, "Helicopter/ship qualification testing," February 2003.
- [13] S. J. Hodge, J. S. Forrest, G. D. Padfield, and I. Owen, "Simulating the environment at the helicopter-ship dynamic interface: research, development and application," *The Aeronautical Journal*, vol. 116, no. 1185, pp. 1155–1184, 2012.
- [14] W. A. Memon, I. Owen, and M. D. White, "Motion fidelity requirements for helicopter-ship operations in maritime rotorcraft flight simulators," *Journal of Aircraft*, vol. 56, no. 6, pp. 2189–2209, 2019.
- [15] S. Casas-Yrurzum, C. Portales-Ricart, P. Morillo-Tena, and C. Cruz-Neira, "On the objective evaluation of motion cueing in vehicle simulations," *IEEE Transactions on Intelligent Transportation Systems*, pp. 1–13, 2020.
- [16] M. Jones, "The suitability of objective motion criteria for rotorcraft manoeuvres," in *AIAA Scitech 2019 Forum*, (Reston, Virginia), American Institute of Aeronautics and Astronautics, July 2019.
- [17] W. Dalmeijer, I. Miletovic, O. Stroosma, and M. Pavel, "Extending the objective motion cueing test to measure rotorcraft simulator motion characteristics," in *AHS 73rd Annual Forum*, 2017.
- [18] North Atlantic Treaty Organisation, "Helicopter operations from ships other than aircraft carriers (hostac): Edition h," April 2017.
- [19] "Ads-33e-prf aeronautical design standard, performance specification, handling qualities requirements for military rotorcraft," March 2000.
- [20] R. Hosman, F. Cardullo, and J. Bos, "Visual-vestibular interaction in motion perception," in *AIAA Modeling and Simulation Technologies Conference*, (Reston, Virginia), p. 163, American Institute of Aeronautics and Astronautics, 2011.
- [21] R. J. Telban and F. M. Cardullo, "Motion cueing algorithm development: Human-centered linear and nonlinear approaches," May 2005.

- [22] H. Heerspink, W. Berkouwer, O. Stroosma, R. van Paassen, M. Mulder, and B. Mulder, "Evaluation of vestibular thresholds for motion detection in the simona research simulator," in *AIAA Modeling and Simulation Technologies Conference and Exhibit*, (Reston, Virginia), p. 205, American Institute of Aeronautics and Astronautics, August 2005.
- [23] D. Stewart, "A platform with six degrees of freedom," *Proceedings of the Institution of Mechanical Engineers*, vol. 180, no. 1, pp. 371–386, 1965.
- [24] S. J. Hodge, P. Perfect, G. D. Padfield, and M. D. White, "Optimising the vestibular cues available from a short stroke hexapod motion platform," in *AHS 67th Annual Forum*, 2011.
- [25] P. R. Grant and L. D. Reid, "Protest: An expert system for tuning simulator washout filters," *Journal of Aircraft*, vol. 34, no. 2, pp. 152–159, 1997.
- [26] J. B. Sinacori, "The determination of some requirements for a helicopter flight research simulation facility," September 1977.
- [27] J. A. Schroeder, "Helicopter flight simulation motion platform requirements," July 1999.
- [28] S. J. Hodge, *Dynamic Interface Modelling and Simulation Fidelity Criteria*. Dissertation, University of Liverpool, Liverpool, September 2010.
- [29] R. Hosman and S. Advani, "Design and evaluation of the objective motion cueing test and criterion," *The Aeronautical Journal*, vol. 120, no. 1227, pp. 873–891, 2016.
- [30] O. Stroosma, M. van Paassen, M. Mulder, R. J. Hosman, and S. K. Advani, "Applying the objective motion cueing test to a classical washout algorithm," in *AIAA Modeling and Simulation Technologies (MST) Conference*, (Reston, Virginia), American Institute of Aeronautics and Astronautics, 2013.
- [31] P. Zaal, J. A. Schroeder, and W. W. Chung, "Objective motion cueing criteria investigation based on three flight tasks," *The Aeronautical Journal*, vol. 121, no. 1236, pp. 163–190, 2017.
- [32] G. E. Cooper and R. P. Harper, "The use of pilot rating in the evaluation of aircraft handling qualities," April 1969.
- [33] H. Duda, S. K. Advani, and M. Potter, "Design of the dlr aves research flight sim-

- ulator," in *AIAA Modeling and Simulation Technologies (MST) Conference*, (Reston, Virginia), p. y2011, American Institute of Aeronautics and Astronautics, 2013.
- [34] J. Gotschlich, T. Gerlach, and U. Durak, "2simulate: A distributed real-time simulation framework," 2014.
- [35] M. Hamers, R. Lantzsch, and J. Wolfram, "First control system evaluation of the research helicopter fhs," in *33rd European Rotorcraft Forum*, 2007.
- [36] J. Kaletka, H. Kurscheid, and U. Butter, "Fhs, the new research helicopter: Ready for service," *Aerospace Science and Technology*, vol. 9, no. 5, pp. 456–467, 2005.
- [37] M. Rohlfs, W. von Grünhagen, and J. Kaletka, "Nonlinear rotorcraft modeling and identification," in *RTO SCI Symposium*, 1998.
- [38] D. M. Pitt and D. A. Peters, "Theoretical prediction of dynamic-inflow derivatives," in *6th European Rotorcraft Forum*, 1980.
- [39] A. Štrbac, T. Martini, D. H. Greiwe, F. Hoffmann, and M. Jones, "Analysis of rotorcraft wind turbine wake encounters using piloted simulation," *CEAS Aeronautical Journal*, vol. 39, no. 1, p. 31, 2021.
- [40] A. Strbac, T. Martini, D. Greiwe, F. Hoffmann, and M. Jones, "Analysis of rotorcraft wind turbine wake encounters using piloted simulation," in *45th European Rotorcraft Forum*, 2019.
- [41] T. Perez, Ø. N. Smogeli, T. I. Fossen, and A. J. Sørensen, "An overview of the marine systems simulator (mss): A simulink toolbox for marine control systems," *Modeling, Identification and Control: A Norwegian Research Bulletin*, vol. 27, no. 4, pp. 259–275, 2006.
- [42] S. J. Carignan, A. W. Gubbels, and K. Ellis, "Assessment of handling qualities for the shipborne recovery task - ads 33 (maritime)," in *AHS 56th Annual Forum*, 2000.
- [43] European Aviation Safety Agency, "Equipment & furnishings - emergency flotation system - rotorcraft flight manual (supplement): Ad no.: 2014-0188r4," July 2015.
- [44] C. B. Hasager, A. N. Hahmann, T. Ahsbahs, I. Karagali, T. Sile, M. Badger, and J. Mann, "Europe's offshore winds assessed with synthetic aperture radar, ascats and wrf," *Wind Energy Science*, vol. 5, no. 1, pp. 375–390, 2020.

-
- [45] Ministry of Defence, "Design and airworthiness requirements for service aircraft: Part 7 - rotorcraft - section 9," December 2007.
- [46] M. Jones, M. D. White, T. Fell, and M. Barnett, "Analysis of motion parameter variations for rotorcraft flight simulators," in *AHS 73rd Annual Forum*, 2017.
- [47] P. Scott, M. D. White, and I. Owen, "The effect of ship size on airwake aerodynamics and maritime helicopter operations," in *41st European Rotorcraft Forum*, 2015.